Murky waters: discerning among sources of natural variation under high uncertainty and at multiple scales

Michael Vlah

A thesis
Submitted in partial fulfillment of the
Requirements for the degree of

Master of Science

University of Washington
2017

Committee
Gordon Holtgrieve
Daniel Schindler
Michael Brett

Program authorized to offer degree:
School of Aquatic and Fishery Sciences

University of Washington

Abstract

Murky Waters: Discerning Among Sources of Natural Variation
under High Uncertainty and at Multiple Scales

Michael Vlah

Chair of the Supervisory Committee:
Assistant Professor Gordon W. Holtgrieve
School of Aquatic and Fishery Sciences

Fresh waters account for an inordinately large portion of Earth's carbon burial and methane production. As such, they are major components of energy flow within and between ecosystems. Yet, the roles of lakes and rivers as sources, conduits, and sinks of energy, and as providers of ecosystem services are incompletely understood. High elevation aquatic systems are of particular concern due their high susceptibility to variation under changing regional climates. I investigated the proportion of consumer biomass derived from terrestrial sources, allochthony, in three metabolic classes of high elevation lakes using a modular, Bayesian, stable isotope mixing model. Additionally, I quantified the influence of local- and regional-scale environmental drivers on flow and thermal regime across three flow-source classes of

rivers using dynamic factor analysis. The most probable estimate of allochthony across consumer taxa was 41% in small-montane lakes. For large-montane and alpine lakes, allochthony was just 4 and 3%, respectively. These results corroborate previous findings that lake size, depth, and light penetration are dominant physical controls on allochthony, but add that it sharply declines at high elevation due to changes in terrestrial primary production near or above tree line. I also found that primarily rain-fed rivers undergo large seasonal temperature fluctuations that closely track air temperature – high coupling – while snow-fed rivers tend to be more weakly, and in some cases inversely, coupled with air temperature fluctuation due to influx of meltwater. However, variation in coupling among snow-fed rivers is high and disproportionately influenced by artificial reservoirs, which appear to magnify the buffering effect of melting snow and glacial ice on riverine thermal regimes in summer.

Preface

Representing nature

Even the most mundane phenomena conceal overwhelming complexity. Flowing water, vegetal growth, the passage of time—each is a component of a vast network spanning the sciences, as well as a network unto itself. However powerful our instruments, there will always be aspects of these phenomena that we cannot see. Yet, we desire to know their inner workings and interconnections.

Human nature affords a certain power to all those who possess it, with or without intention, malicious or benign. It is a power to modify our environment in profound ways, and we exercise it at minimum by participating in a global society that grows unrestrained. The more we come to understand, the more we realize this power can be wielded to exploit, or to preserve. As ecologists, we recognize the potential value in natural complexity itself, and also the blatant truth of our ignorance: we can barely guess at the spiraling implications of most human decisions, or what we might be missing each time a node of the network is lost.

Unfortunately for ecologists, understanding must proceed from simplification. The network must be compartmentalized and rendered in comprehensible terms, which requires the use of models. Often, the programmed goal of a model is to discern among many forces those primarily responsible for driving a phenomenon. From the perspective of the ecologist, these forces may be biological or chemical processes, or human activities, and the phenomenon may be fluctuations of an animal population. In a sense, each force is a lever, placed in its current position by the combined influence of humans and greater nature up to the present moment. The goal is to find the levers that control the phenomenon, so that they may be set according to our ethics and needs, in the context of everything else we know.

Concretely, such a model can be, and often is, very simple. Any system that can be reduced to driving forces (predictors) and resulting phenomena (responses) can be represented as a regression. However, such reduction often belies critical detail, and thus precludes deep understanding. With high uncertainty surrounding predictor or response data, for example, patterns may be submerged that are nonetheless real and consequential. The same may occur if predictors reflect forces acting with different strengths at multiple scales. Luckily, ecologists have access to a rich and burgeoning collection of

computational tools for *reducing* reductionism. The power laws of technological progress yield ever greater capacity to map nature onto 2D surfaces in colorblind-friendly hues.

Of course, reality can be missed just as well through overly intricate representation. Models may attempt to account for phenomena with finer detail than their data justify, as is the case with "overfitting." Modeling is therefore a practice of checking the power of our tools against both our confidence in the information we feed them, and our ability to verify that they are working as we intend. The consummation of the process occurs when model output is transduced into image, sound, or speech, and information is conveyed. This thesis details two such processes, and resulting contributions to the corpus of ecological endeavor. It forwards the idea that many questions of significance are prime for the answering, with no need for elaborate experiments or expenditure. The data have already been collected in many cases, and only need to be organized and analyzed in the right ways to reveal their secrets. As a corollary, it cautions the analyst to increase critical examination, or else skepticism, as a function of model complexity.

Signals in the muck

The first problem is motivated by a decades-old struggle to trace the flow of organic material into and within lacustrine ecosystems. This material can be thought of abstractly as "energy" in the form of organic molecules, which fuel the work of fabricating new organisms. Its major sources are terrestrial plants and aquatic algae, which fix elemental carbon from atmospheric CO_2 into metabolically active forms. For any lake, determining the degree to which the possible sources of energy actually contribute to the metabolism, growth, and makeup of heterotrophic taxa involves identifying source signatures amid the molecular slurry of a consumer's tissue. In this case, that means comparing ratios of molecular markers in the sources with those in the consumer, attempting to correct for changes in those ratios that may have occurred during assimilation, or during transit through bacteria or other organisms on the way to the consumer, and acknowledging that samples represent only snapshots of each organism's molecular makeup in time, often only from selected tissues, tainted with traces of microbial or inorganic matter, and that a whole spectrum of source signatures is represented by a handful of assumed "key players." In short, uncertainty is high.

The complexity of this system is herein harnessed through a Bayesian approach, where parameters governing the transformations and uncertainties described above are randomly drawn, along with source proportions to the final consumer mixture, from distributions specified on prior assumption. Through thousands of iterations, an algorithm hones in on the set of parameters that generate the best approximation of the observed data, and proportional contributions of each source to the consumer mixture are expressed as probability distributions of the true values.

Here, the molecular bioreactors within various algae and plants are the "forces," and the resultant composition of a given consumer is the "phenomenon." By providing a computationally tractable solution to a historically unwieldy problem, Bayesian statistics allow for the dominant forces to be ascertained, and for recommendations to be made regarding management of lacustrine resources. When examined closely, they also alert us to the pitfalls of relying on methods engineered to cut through uncertainty—in other words, some of these methods can deliver an answer to the question posed no matter the degree of support. With greater computational power comes greater need for scrutiny.

This chapter is an attempt to resolve part of the "allochthony problem," by disambiguating the roles of elevation and terrestrial organic matter loading in structuring energy flow through lake food webs. By adding a relatively unrepresented biome to the existing literature, it fills two important gaps in the understanding of allochthony dynamics, namely 1) what happens near and above tree line, where terrestrial loading is at a minimum, and 2) how do loading and other known drivers of allochthony interact? As the density and geographic coverage of our data increase, so does the potential to "solve" the allochthony problem, insofar as *predicting* consumer assimilation of terrestrial resources based on lake features is a solution. This predictive power could be achieved through the synthesis of a single dataset, comprising all reported measurements of terrestrial vs. aquatic resource use in lacustrine consumers, and all available data on the hydrology, geography, and chemistry of their environments. In a machine learning context, using lake traits as features, a system for predicting the relevance of terrestrial plant material to target consumers could be devised, and several main drivers identified. At present, this may only prove successful for temperate and boreal systems, where data density is highest, but in time it could encompass lakes more generally, and facilitate management of lake resources based on knowledge of energetic sources.

Managing scale

The phenomenon of pattern in river temperature is driven by climatic forces, including atmospheric temperature (a proxy for solar heating) and precipitation. Because of the influential role of a river's temperature in dictating its physical properties and available niche space, understanding how these forces act across space and time is of high value. However, the apparent simplicity of the system is broken by the fact that the driving forces are mediated by features of the landscape, including slope and soil permeability, and such features vary widely among rivers and their watersheds. Therefore, modeling temperature across many rivers is not a straightforward matter of weighting predictors and their effects. It demands a more multifaceted approach. In addition, it must be one that can take advantage of the autocorrelated structure of sequential samples in time.

The chosen solution to the problem involved a modular approach, wherein temperature was modeled as a linear combination of known predictors at a regional scale, namely those related to the climate, and additional watershed-scale forces, which were not specified *a priori*, but instead generated by the model. Subsequently, the primary sources of geographic and land-use variation across watersheds were correlated with these unknown forces, allowing their identities to be inferred. This analysis sifted from among dozens of interacting forces a few dominant variables to consider in planning management strategies under projected climate scenarios.

Here too, pitfalls were uncovered. Allowing the model to generate its own information was necessary for determining the identities of watershed-scale scale temperature drivers, but it also meant model-derived trends could be made to fit the data better than known predictors, leading to a problem of model selection in which the most accurate representation of reality was not the one straightforwardly identified by information criteria.

All river, landscape, and climate data used in this chapter were gathered from existing databases. The temperature series come from a one of the longest and broadest collections of temporally explicit river data ever compiled for the Puget Sound region. Coupled with land cover and use metrics, it could be used to decipher countless further relationships between human action and the physical and chemical properties of fresh waters through time.

Moving forward

There are no silver bullets in quantitative analysis. The landscape of statistical (and other mathematical) problems is vast and its topology uncertain. We traverse it with makeshift tools that are continually updated and discarded. Yet, to ask any scientific question, verify any assumption, and ultimately convey information reliably, requires proficient use of those tools. Meanwhile, the body of scientific knowledge expands into ever more esoteric territory, demanding greater expertise on the part of the individual scientist, and inviting the use of more powerful, and less scrutable technologies.

Relative to its more fundamental counterparts, the field of ecology has been dealt a difficult card. It emerges from the noise of forces moving within and between life forms, on and in the earth and air—biological, chemical, physical—a cacophony of statistical fluctuations. Meanwhile, alongside the rest of science, ecology is taking on the colors of a new era in thought, a revised organon, driven by tools that are outstripping even their creators in many areas of problem solving. These tools include machine and deep learning algorithms such as artificial neural networks, the grandest of which currently optimizes 10^{11} parameters. In the face of a skyrocketing capacity to manage complexity, even the most tangled webs of ecological mystery may yield information that is useful to us, possibly at the cost of our simian comprehension of the procedures by which it is derived.

And then again there is the vast web of life, laws, and forces linking the disciplines, and the uneasy human leadership searching it for clues to desired outcomes. In the following chapters, those outcomes relate to freshwater ecosystems and their resources. This thesis offers suggestions about where and where not to prod so that our waters continue to support the living things we cherish and the services we need. It also attempts to convey the necessity of questioning our mathematical tools, however miraculous they may seem, and striving to understand their mechanisms and inherent assumptions. Finally, it marks a jumping-off point in the path of one scientist who recognizes that some such tools pose greater dangers than just false assumptions, and who now aims to discover which levers need to be pulled to keep them from deciding not to work for us anymore.

Chapter 1

Low levels of allochthony in consumers across three high elevation lake types

Introduction

The movement of energy among habitats and within food webs is a central theme in ecology (Lindeman 1942). Primary producers harness solar energy within organic carbon molecules, which then flow through the environment as living tissue and decomposing detritus before returning to inorganic forms. There has been substantial effort to create whole-watershed budgets for the processing of carbon that explicitly consider the role of inland waters in focusing organic material fluxes within the landscape (Richey et al. 2002, Cole et al. 2007, Butman et al. 2011). This has spawned a parallel inquiry into the degree to which exogenous carbon provides a source of energy to aquatic food webs. Energy sources to aquatic food webs can therefore include terrestrial organic matter (t-OM), as well as aquatic algae and vegetation.

Except for those of large, regulated rivers, lotic consumers have long been understood to derive carbon primarily from external, terrestrial production, or allochthony (Vannote et al. 1980, Junk et al. 1989, Thorp & Delong 1994), though this conclusion has recently been challenged (Brett et al. in review). Whether lake and pond (hereinafter simply "lake") consumers also rely on allochthonous carbon has been the subject of debate for more than a decade (Pace et al. 2004; Brett et al. 2009; Cole et al. 2011, Francis et al. 2011). Estimates of allochthony in lake consumers have differed enormously, with zooplankton biomass in particular ranging from 0 to 100% terrestrial derivation across systems (Rautio et al. 2011; Francis et al. 2011). Yet, the drivers of such variation are poorly understood. Lake size, nutrient availability, and the ratio of bacterial to primary production have been shown to contribute to variation in consumer utilization of t-OM (respectively, Wilkinson et al. 2013; Pace et al. 2007; Karlsson et al. 2003), but these alone do not permit accurate prediction of allochthony, even in well-studied ecoregions. Furthermore, nearly all allochthony studies in lakes have been conducted in a handful of locations across the American Midwest, Southern Canada, and Northern Europe. As a result, only northern temperate and boreal ecosystems are well represented in the literature (see review in Appendix C of Berggren et al. 2014). Thus far tropical and sub-tropical lake ecosystems are unrepresented, while high-elevation and

reservoir systems have seen little attention (but see Pulido-Villena et al. 2005, Rose et al. 2015, Emery et al. 2015).

Beyond augmented geographic scope and representation of lake types, a generalizable framework for understanding the factors driving allochthony also requires an expanded set of experimental approaches. Manipulative investigations of one or a few lakes (*sensu* Pace et al. 2007, Cole et al. 2011) can identify elements of local food web structure, but may not suffice to forward general principles, such as those characterizing the energetic base of aquatic food webs along natural gradients in lake trophic status, climate, landscape position, and t-OM loading.

We sought to advance understanding of allochthony in lake food webs by considering high-elevation systems of western North America that span tree-line, and as a result vary greatly in watershed vegetation cover (and thus t-OM loading). We also examined both benthic and pelagic consumer taxa. Using stable isotopes of carbon (C), nitrogen (N), and hydrogen (H) within a custom Bayesian mixing model, and coupled with a qualitative evaluation of consumer fatty acid (FA) profiles, we sought to determine source contributions to consumers across three lake classes: Montane-Small (MS), Montane-Large (ML), and Alpine (AP; above tree-line). These classes occupy extremes along a gradient of terrestrial vegetative cover, the alpine end of which contains only sparse ground plants and shrubs, allowing us to characterize allochthony at the lower limit of t-OM loading. High variation in lake volume and area within the montane lake classes allows comparison of lake size and t-OM loading as drivers of allochthony.

We hypothesized that allochthony in all consumer taxa (calanoid copepods, Cladocera, and caddisflies [Trichoptera *spp.*]) would be most apparent in MS, due to fully forested catchments and a low ratio of lake surface area to volume (Wilkinson et al. 2013). We expected to see little allochthony in AP because of relatively low t-OM loading and thus a reliance on internal production, while ML was expected to fall between these two extremes. Between consumer taxa, Trichoptera were expected to assimilate primarily t-OM and periphyton, given their status as (facultative) grazers of benthic/littoral terrestrial detritus.

Methods

Study site

This study was conducted in 11 lakes and ponds of the Olympic Mountains of western Washington State, U.S.A. Ten lakes were within the Seven Lakes Basin, a region of about 4 km^2, ranging in elevation from approximately 1,200 to 1,500 m. The eleventh site is Milk Lake on the eastern edge of the Olympics (Figure 1.). We grouped lakes into three classes based on chemical and physical characteristics (Table 1).

Table 1 Site data and categorical groupings for the 11 lakes of the study set. "DOC" = dissolved organic carbon; O_2:Ar = the ratio of dissolved oxygen to argon; "Veg" = vegetated area of watershed in hectares.

Lake Name	Lake Class	DOC (mgL^{-1})	Lake Area (ha)	Elevation (m)	Chlorophyll-a (μgL^{-1})	O_2:Ar	Veg:Lake Area
C	MS	2.44	0.068	1305.8	1.70	17.96	71.7
O	MS	4.53	0.070	1285.0	3.67	17.90	81.7
Z	MS	7.02	0.003	1293.6	12.63	16.01	157.9
L	MS	10.08	0.028	1295.1	4.85	12.74	169.3
Morgenroth	ML	0.49	10.979	1320.7	0.55	19.00	20.1
No Name	ML	0.52	3.463	1293.6	1.11	19.52	51.0
Clear	ML	1.15	5.153	1288.7	2.01	19.94	25.5
Mirror	AP	0.26	1.854	1439.0	1.33	19.95	4.3
Y-015	AP	0.43	0.825	1461.5	1.35	19.93	2.2
Y-025	AP	0.49	1.855	1455.1	0.75	20.39	7.5
Milk	AP	0.53	2.300	1435.0	0.76	19.70	11.4

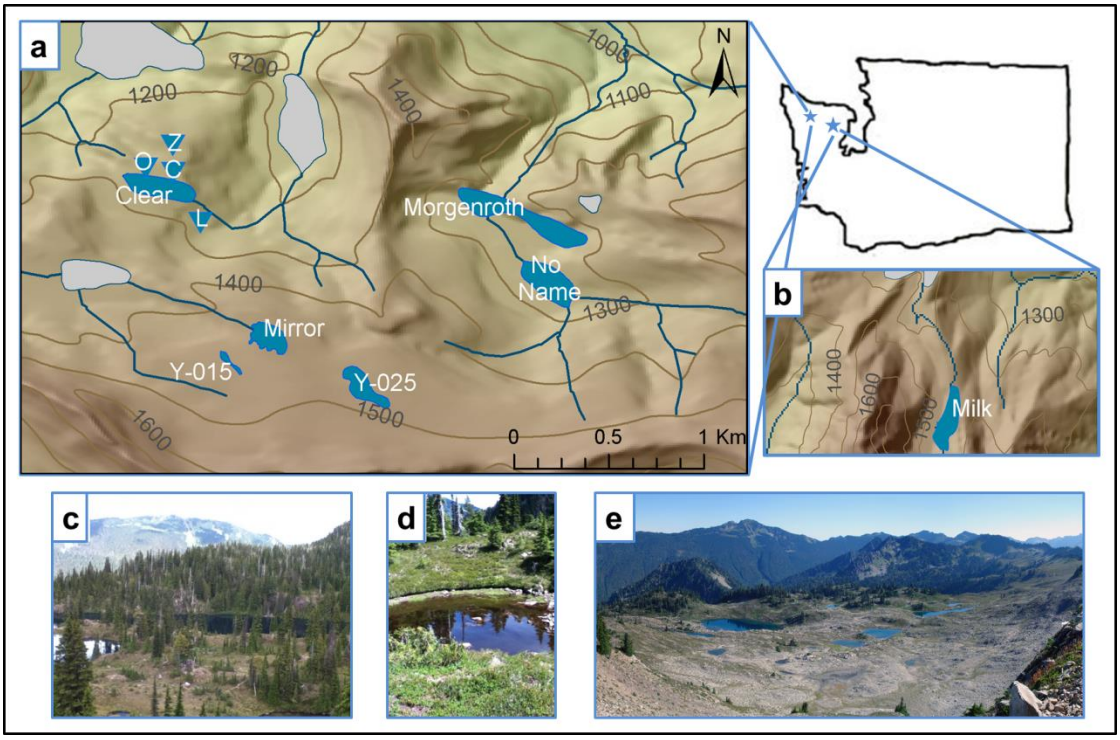

Figure 1 Study lakes within Olympic National Park, western Washington, USA. Panels depict (a) Seven Lakes Basin and (b) Milk Lake. Blue X's mark ponds smaller than 0.1 ha. (c-e) provide examples of ML, MS, and AP lakes, respectively.

Field sample collection

All Seven Lakes Basin samples were collected between 2 and 7 August, 2014. Milk Lake was sampled on 17 August 2014. Targets of SI and FA analysis included three producer categories: phytoplankton, algal periphyton (hereinafter simply "periphyton", unless specified as "total periphyton," which includes bacteria and other microbes), and terrestrial plants, in addition to five consumers: zooplankton (Cladocera, Calanoida, *Chaoborus sp.*), macroinvertebrates (Trichoptera) and fish (*Salvelinus fontinalis*). Phytoplankton were filtered along with other suspended particulate organic matter (POM), from water drawn at 0.5 m depth in the approximate center of each lake, and total periphyton was scrubbed from the upper surfaces of littoral substrates. Both were collected on pre-ashed, 0.7 micron Whatman quartz fiber (QM-A) filters. Plant samples were collected as partly decomposed leaves, bark, and cone material (duff) from beneath trees and shrubs, and combined in approximate proportion to the species assemblages found in each region of the basin. For the montane lake types, we used a mixture of 75% western

hemlock (*Tsuga heterophylla),* 12.5% western red cedar (*Thuja plicata*), and 12.5% subalpine fir (*Abies lasiocarpa*). For the alpine lake type, we used 75% red mountain heather (*Phyllodoce empetriformis*) and 25% blueberry (*Vaccinium sp.*). All zooplankton were collected with a conical 150 µm mesh plankton net and separated into 63 µm < *x* < 500 µm and > 500 µm size classes (roughly delineating Cladocera and copepods + *Chaoborus sp.*) and later sorted by major taxon. Trichoptera were collected by hand, 10-15 from each lake, and *S. fontinalis* were caught via fly rod (IACUC Protocol #4332-02). All samples were frozen in the field on dry ice, then later freeze-dried and homogenized with a ball mill prior to analysis.

Water samples for DOC concentration and chlorophyll-a concentration were collected from a depth of 0.5 m using a Niskin sampler. These were subsampled with 25 mL for DOC and preserved by acidifying to pH 2 with phosphoric acid. An additional 400-1000 mL was filtered through 0.7 micron Whatman GF/F filters; filters were wrapped in foil, and immediately frozen on dry ice for chlorophyll-a analysis at the University of Washington. Samples for the ratio of dissolved O_2 to argon gas (O_2:Ar), used to compare relative heterotrophy among lakes, were collected in 12 mL glass sample vials with butyl septa (Exetainers, Labco) that had been washed with soap and water, ashed at 500 °C, coated with 80 µL saturated zinc chloride as a preservative, and flushed with helium to remove atmospheric O_2. In the field, these were opened, filled, and capped while fully submerged at 0.5 m depth. The caps were sealed with silicone grease and kept cool until analysis.

Daphnia magna rearing

To compare growth, mortality, and reproduction of *Daphnia magna* reared on the available C sources (sensu Brett 2009), we fed individual neonates for three weeks on treatments containing the duff mixtures described above, in both microbially primed and “raw” forms, as well as a pure algal treatment containing *Cryptomonas ozolinii*. For both forms of treatment, duff material was oven dried for 48 hours at 60°C, ground, and sieved through 106 µm mesh. Each treatment then consisted of 10 mg/L of duff in 25 replicates of 40 mL vials containing L16 growth medium (Lindström 1991). Every two days, two-thirds of the solution in each vial was replaced with new solution containing the same concentration of suspended duff. For the microbially primed treatments, replacement solution was obtained from a stock mixture that consisted of 950 mL duff in L16, and 50 mL water from Lake Washington, Seattle, WA, which was first

strained through a 63µm screen in order to exclude most dinoflagellates and larger organisms. Stock mixtures were given two weeks to microbially mature before the experiment began, and were stored on a shake-table in the dark, to prevent cementing of fine sediment and algal growth.

D. magna were harvested for FA analysis following successful parthenogenic reproduction in the *C. ozolinii* treatments. After seven days and complete mortality in the duff treatments, we removed the requirement for reproductive maturity and began harvesting neonates after 6 days of growth, assuming some lipid assimilation would occur. Individuals were replaced following mortality or successful harvest.

A bulk rearing method was also employed in order to obtain FA profiles for *D. magna* raised on terrestrial plant diets. We fed approximately 250 neonates *ad libitum* diets of microbially primed montane duff in a ratio of 1mg to 1mL. Individuals were harvested after the appearance of eggs visible to the naked eye and analyzed for SI and FA. All treatments containing terrestrial material were kept in the dark to prevent algal contamination. Once daily, each vial or beaker was lightly shaken in order to re-suspend settled food particles.

Lab analyses for DOC, chl-a, and O_2:Ar

Samples for dissolved organic carbon (DOC) were kept cool until analysis on a Shimadzu TOC-Vcsh DOC analyzer (Shimadzu, Kyoto, Japan) at the University of Washington's Marine Chemistry Lab. Chlorophyll-a concentration was analyzed via fluorometry after methanol extraction, as described in Holtgrieve et al. (2010). Dissolved O_2:Ar analysis was performed in the University of Washington's Oceanography Stable Isotope Lab. One day before O_2:Ar analysis, roughly half of the water was displaced from each Exetainer with helium. Headspace gas was analyzed on a Finnegan Delta XL continuous-flow isotope ratio mass spectrometer (Thermo Electron). O_2 and Ar were measured at m/z 32 and 40, respectively, and dissolved Ar concentration was calculated as a function of water temperature following Weiss (1970).

Fatty acid profiles

FA extraction and analyses of all consumers and producers (i.e. sources) were performed according to the procedure in Strandberg et al. (2014). Total lipids were extracted from freeze-dried and homogenized

samples (1-1.5 mg for animal tissue, 5 mg for plant) in a chloroform-methanol-water solution (2:1:0.8, by volume) and dissolved in toluene. FA were trans-methylated in 1% H_2SO_4 and methanol at 50 °C for 16 h, to produce fatty acid methyl esters (FAMEs), which were analyzed at the University of Washington on a HP6890 gas chromatograph with flame ionization detection (GC-FID). We used a DB-23 capillary column (length 30 m, inner diameter 0.25 mm, film thickness 0.25 mm; Agilent Technologies, Santa Clara, California, USA) with splitless injection.

FAME peaks were initially identified by visual comparison to known standards (37-component FAME mix; Supelco, St. Louis, Missouri, USA), and subsequently verified by gas chromatography/mass spectrometry (Shimadzu GCMS QP2010 plus; Agilent DB-23 column) with splitless injection. The locations of double bonds in the carbon chains of monounsaturated FAs were determined by analysis of dimethyl disulfide adducts (Nichols et al. 1986). We identified 57 peaks in all, from which we determined the proportional FA composition of all consumers. FA were grouped into categories by probable taxonomic origin where applicable, or by chemical structure otherwise (see Appendix B), and then used to infer pathways of energy flow among sources and consumers via Principal Component Analysis. We arcsine-square-root transformed each FA proportion prior to ordination.

Stable Isotope and mass ratios

Isotope ratio mass spectrometry (irMS) of ^{13}C:^{12}C and ^{15}N:^{14}N of bulk tissues, and determination of C:N mass ratios, were carried out at the University of Washington's IsoLab on a Finnigan MAT253 connected to a Costech elemental analyzer in continuous flow mode. Determination of ^{2}H:^{1}H of bulk tissues took place at the Colorado Plateau Stable Isotope Laboratory, Northern Arizona University, where samples were equilibrated with local water vapor to correct for exchangeable H. Analysis then proceeded by pyrolysis and irMS (Doucett et al. 2007). High temperatures associated with this process preclude the use of samples that include filter material. We were therefore unable to directly analyze POM samples for ^{2}H:^{1}H. All other field samples were analyzed for isotopes of C, N, and H, including total periphyton, which was collected in large enough quantities that we were able to scrape it from the surface of the filters.

Water samples were analyzed for ^{2}H:^{1}H of H_2O via cavity ring-down laser absorption spectroscopy at the University of Washington's IsoLab. Isotope signatures are expressed in standard

delta notation relative to Vienna PeeDee Belemnite (VPDB) for $\delta^{13}C$, atmospheric nitrogen for $\delta^{15}N$, and Vienna Standard Mean Ocean Water (VSMOW) for ($\delta^{2}H$).

Stable isotope mixing model

Consumer assimilation of t-OM (allochthony), and aquatic resources was estimated individually for 31 consumers using a system of three Bayesian models, one each for the determination of source and consumer isotope ratios and one for isotopic mixing. Models were written in the JAGS programming language (Plummer, 2003), and implemented in R (R Development Core Team 2016) using the "rjags" package (Plummer, 2016).

Both POM and total periphyton are complex mixtures of organic matter from multiple sources, making it impractical to directly measure the isotopic signature of autotrophs in isolation. We therefore estimated the $\delta^{2}H$, $\delta^{13}C$, and $\delta^{15}N$ of the algal component of POM and total periphyton using a combination of measured parameters and relationships from the literature.

The $\delta^{2}H$ of algae was estimated from the measured $\delta^{2}H$ of lake water and literature values of photosynthetic discrimination against ^{2}H over ^{1}H (ε_H), using the following equation:

$$\delta^2 H_{corr} = \delta^2 H\text{-}H_2O + \epsilon_H \quad (1)$$

where ε_H has a mean of -150 ± 27 (1 SD) based on the most current review of 86 published measurements (Brett et al. in review).

The isotopic signatures of phytoplankton ($\delta^{13}C$, and $\delta^{15}N$) and periphyton ($\delta^{2}H$, $\delta^{13}C$ and $\delta^{15}N$), designated generically below as δ, were estimated from the measured values of POM and total periphyton after removing the contribution of the terrestrial fraction (Φ_T), based on the expected differences in the C:N of algae versus terrestrial organic matter (Francis et al. 2011):

$$\delta_{corr} = \frac{\delta_P - (\delta_T \Phi_T)}{1 - \Phi_T} \quad (2)$$

where:

$$\Phi_T = \frac{C{:}N_P - C{:}N_A}{C{:}N_T - C{:}N_A} \quad (3)$$

and where P = POM/total periphyton, T = terrestrial, and A = aquatic. $C{:}N_A$ was assigned a normally distributed prior of mean=6.70 and SD=1.51 (n=151), determined by averaging the results of Table 3 in

Vuorio et al. (2006), while $C:N_P$ and $C:N_T$ were assigned normally distributed priors parameterized by the means and SDs of our measured field samples (means ± SD: $C:N_{POM}$ = 10.7 ± 1.8; $C:N_{Peri}$ = 15.4 ± 5.5; $C:N_T$ = 59.9 ± 25.0).

Trophic enrichments of C and N isotope ratios ($\Delta^{13}C$ and $\Delta^{15}N$) were given normal priors based on the means and standard deviations ($\Delta^{13}C$ = 0.39 ± 1.14, $\Delta^{15}N$ = 3.4 ± 0.99) recommended by Post (2002) and applied using $\delta X_{corr} = \delta X_{raw} - \Delta X$.

Consumer δ^2H was corrected for environmental water (ω) as a fraction of consumer tissue in the manner of Solomon et al. (2009):

$$\delta^2 H_{corr} = \frac{\delta^2 H_{raw} - (\omega \delta^2 H\text{-}H_2O)}{1-\omega} \quad (4)$$

where ω accounts for total environmental water, including the proportion accumulated during a single trophic transfer (ω_0) and the trophic level of the consumer (t), which was assumed to be 1.5 for Calanoida, Clacodera, and Trichoptera.

$$\omega = 1 - (1 - \omega_0)^t \quad (5)$$

We estimated ω_0 using the distribution of directly measured values across 11 published experiments (mean=0.28, sd=0.12; Brett et al. in review).

We constructed our models as a two-phase, modular procedure, wherein the estimations and adjustments described above (the endmember determination phase) were performed first, followed by isotopic mixing (the mixing phase). This was to prevent the joint likelihood surface of the mixing parameters from modifying that of the endmember determination parameters, which can be unjustifiably driven to the extremes of their empirical ranges by the Bayesian requirement that isotopic mass balance be preserved during mixing (Brett et al. in review). Adjustments to source signatures were made hierarchically by lake class, while consumers were adjusted independently. After estimating the isotopic signatures of OM sources and correcting consumers for environmental water and trophic fractionation using the above methods, these values were passed into a mixing model of the form:

$$\delta_{t,c} = \delta_{t,1:s} \circ \Phi_{1:s} \quad (6)$$

where $\delta_{t,c}$ is the isotopic signature of each consumer (c) with respect to each tracer (t), $\delta_{t,1:s}$ is the vector of isotopic signatures for each of its potential food sources (1:s), and Φ is a vector of source proportions

(drawn from a Dirichlet distribution with alpha set to a vector of ones). The symbol ∘ represents the scalar product. Normal priors on source signatures were parameterized with the mean and precision values of the posteriors from the endmember determination phase. The likelihoods of source draws were evaluated against the same distributions, thus allowing for error to be incorporated into source signatures. Posterior consumer means from the endmember determination phase were used as consumer "data" in the mixing model, and variance on estimated consumer signatures ($\delta_{t,c}$ in Equation 6) was modeled as:

$$\sigma_{t,c} = \sigma_{t,1:s} \circ \Phi_{1:s}^2 + \epsilon_{t,s} \quad (7)$$

where ϵ represents additional, or residual, error (Jackson et al. 2008). Each model run included all sources and isotopic tracers.

MCMC sampling of posteriors was performed with three chains and 100,000 iterations, post burn-in. Chains were thinned at intervals of 100 samples to achieve independence of posterior draws, and convergence was assessed using the Gelman-Rubin diagnostic (with attention to the selection of initial values; Gelman & Rubin 1992), along with visual examination of posterior traces.

Sensitivity analysis

Food web mixing models frequently combine endmember determination and mixing of measured tracer values into one analytical process, allowing influential *correction* and *estimation* parameters to be shifted to the extremes of their known ranges by the topology of the theoretically distinct *mixing* likelihood space. These shifts can have considerable effects on model estimations of source contributions to the consumer. Our models contain five estimated parameters that influence source and consumer isotope signatures during the endmember determination phase. These are environmental H_2O-H as proportion of consumer H (ω), isotopic fractionation of H by phytoplankton during photosynthesis (ε_H), isotopic fractionation of C and N with each trophic transfer ($\Delta^{13}C$, $\Delta^{15}N$), and the molar carbon-to-nitrogen ratio of aquatic algae ($C:N_A$). Estimation of each parameter was informed through Bayesian priors based on empirical distributions reported in the literature. To understand the power of each estimated parameter to influence resulting allochthony estimates, we performed a sensitivity analysis where each parameter was individually fixed at the prior mean, and at mean ± 2 standard deviations (Table 2). The full model,

including endmember determination and mixing phases, was rerun under each condition with the remaining parameters estimated normally.

Results

Physical and chemical patterns among lake types

The 11 lakes included in this study were separated into three classes based on physical and chemical attributes related to nutrient input and availability (Table 1). MS was distinguished from ML and AP by relatively high DOC (means = 6.02 vs. 0.55 mg L^{-1}, respectively) and chlorophyll-a (5.71 vs. 1.12 µg L^{-1}), but low O_2:Ar (16.15 vs. 19.78). ML and AP were further discriminated by the ratio of vegetated watershed area to lake surface area (32.2 vs. 6.35), and all three categories were distinct in terms of surface area alone (MS = 0.04 ha, AP = 1.70 ha, ML = 6.53 ha). Elevation and watershed vegetation type further distinguished AP from the rest of the lakes, which should affect levels of allochthony, as these variables relate to wind and sun exposure, duration of ice-cover, and the composition and amount of organic material entering the lakes.

Estimates of model parameters

Isotope biplots (Figure 2) illustrate the isotopic position of each consumer type relative to phytoplankton, periphyton, and t-OM (sources), after accounting for environmental water, trophic fractionation, and terrestrial material in total periphyton and POM. With respect to δ^2H, phytoplankton differed among lake classes, and MS phytoplankton were more enriched than those of either ML or AP (Table 2). The same was true for periphyton and water. No source or consumer differed between ML and AP for δ^2H, and terrestrial δ^2H was uniform across lake classes. AP stood out in terms of terrestrial OM, being most depleted in ^{15}N and most enriched in ^{13}C.

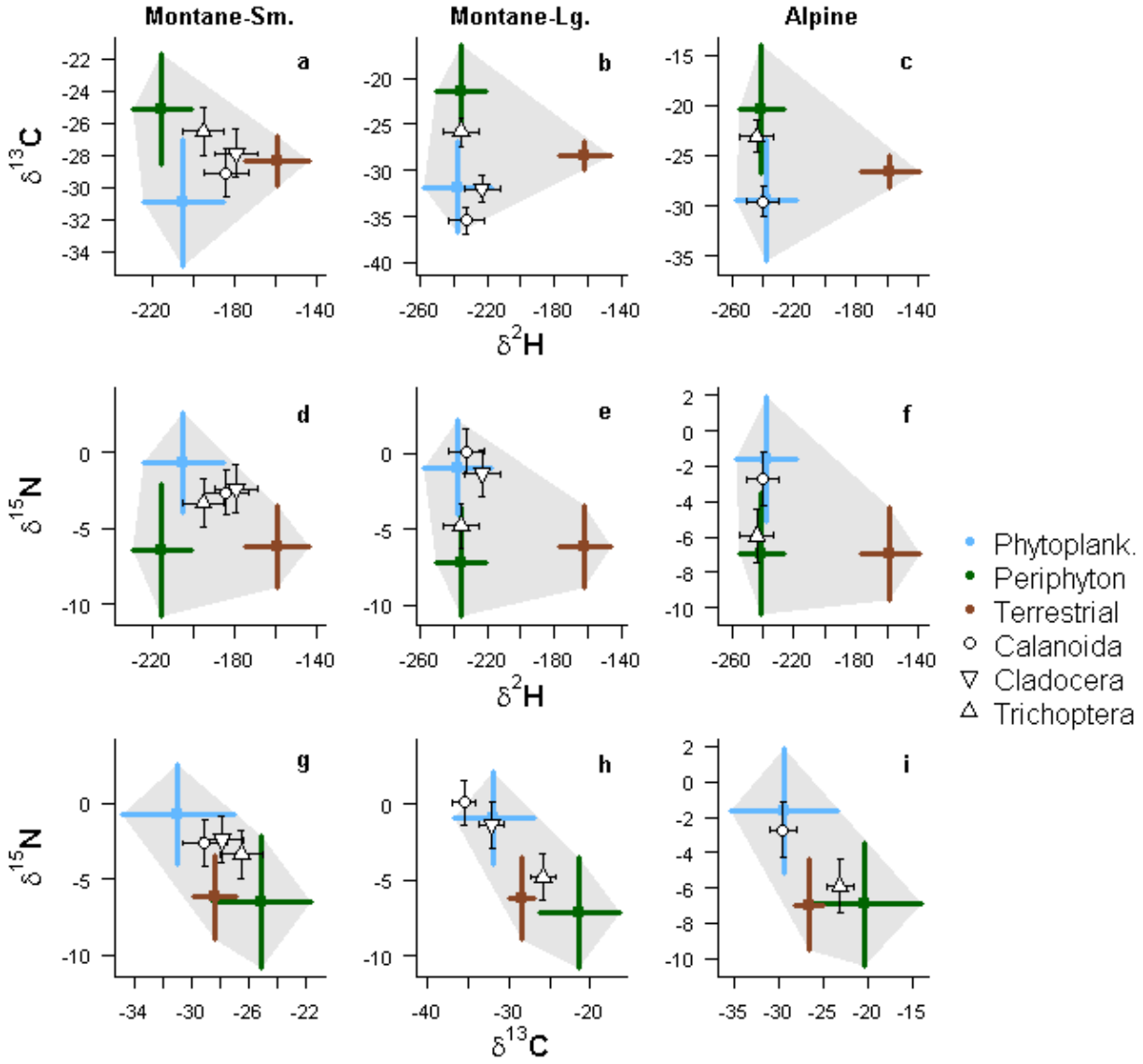

Figure 2 Two-dimensional cross-sections of consumer signatures relative to source polygons in three-dimensional isotope space, after endmember determination. Mean values are shown for the consumers and sources across all lakes in each class. Error bars represent 1 pooled standard deviation based on model estimates from the endmember tuning phase. Shaded area designates the outer limits of the region encompassed by 1 SD of the source signatures, which conservatively represents the region of correct model specification. All units are reported in per mil relative to international standards.

Table 2 Comparison of isotopic composition of source and consumer taxa with respect to each elemental tracer, as well as δ^2H of water, across lake types. Omnibus *F* and *p* represent the results of one-way, two-tailed ANOVA by lake class. Pairwise comparisons were performed using Tukey's HSD. Phyto = phytoplankton.

Tracer	Result	Phyto.	Periphyton	t-OM	Calanoida	Cladocera	Trichoptera	H_2O
$\delta^{13}C$	omnibus *F*	2.12	12.65	90.52	2.48	2.48	7.10	NA
	omnibus *p*	0.18	< 0.01	< 0.01	0.15	0.15	0.02	NA
	MS-ML *p*	0.83	0.03	0.28	0.07	< 0.01	0.48	NA
	MS-AP *p*	0.35	< 0.01	< 0.01	0.85	NA	< 0.01	NA
	ML-AP *p*	0.19	0.41	< 0.01	0.09	NA	0.02	NA
$\delta^{15}N$	omnibus *F*	11.94	0.22	6.34	22.34	12.90	155.17	NA
	omnibus *p*	< 0.01	0.81	0.02	< 0.01	0.02	< 0.01	NA
	MS-ML *p*	0.25	0.83	0.88	< 0.01	0.02	< 0.01	NA
	MS-AP *p*	< 0.01	0.85	0.02	0.81	NA	< 0.01	NA
	ML-AP *p*	0.06	1.00	0.07	< 0.01	NA	< 0.01	NA
δ^2H	omnibus *F*	62.89	31.37	0.39	48.74	495.18	7.36	28.73
	omnibus *p*	< 0.01	< 0.01	0.69	< 0.01	< 0.01	0.02	< 0.01
	MS-ML *p*	< 0.01	< 0.01	0.77	< 0.01	< 0.01	0.02	< 0.01
	MS-AP *p*	< 0.01	< 0.01	0.99	< 0.01	NA	< 0.01	< 0.01
	ML-AP *p*	0.88	0.52	0.69	0.35	NA	0.51	0.71

Comparison of consumer taxa revealed a similar δ^2H pattern to that of the sources, namely enrichment of MS relative to ML and AP. There was also a consistent trend across lake classes of relatively ^{13}C-enriched Trichoptera (mean and SD across classes = -25.0 ± 1.9), and relatively depleted Calanoida (-30.6 ± 4.0). This trend was reversed with respect to $\delta^{15}N$ (Trichoptera: -4.8 ± 1.1; Calanoida: -2.1 ± 1.3). Both trends were more pronounced in ML and AP than in MS. Trichoptera in ML and AP tended to be more isotopically similar to periphyton than to either phytoplankton or t-OM, and both zooplankton taxa were consistently similar to phytoplankton in these lake classes. The mean position of ML Calanoida fell slightly outside its source triangle's region of error (± 1 SD) with respect to $\delta^{13}C$ and $\delta^{15}N$ (Figure 2, panel h), reflecting greater $\delta^{13}C$ depletion (marginal significance) and greater $\delta^{15}N$ enrichment than those of MS and AP (Table 2).

Estimates of allochthony

After endmember determination, model-adjusted means and variances were passed as priors into the mixing phase of the model. MS consumers exhibited considerably greater t-OM assimilation as a proportion of total, (mode=0.41, mean=0.39, 95% CL [0.03,0.80])

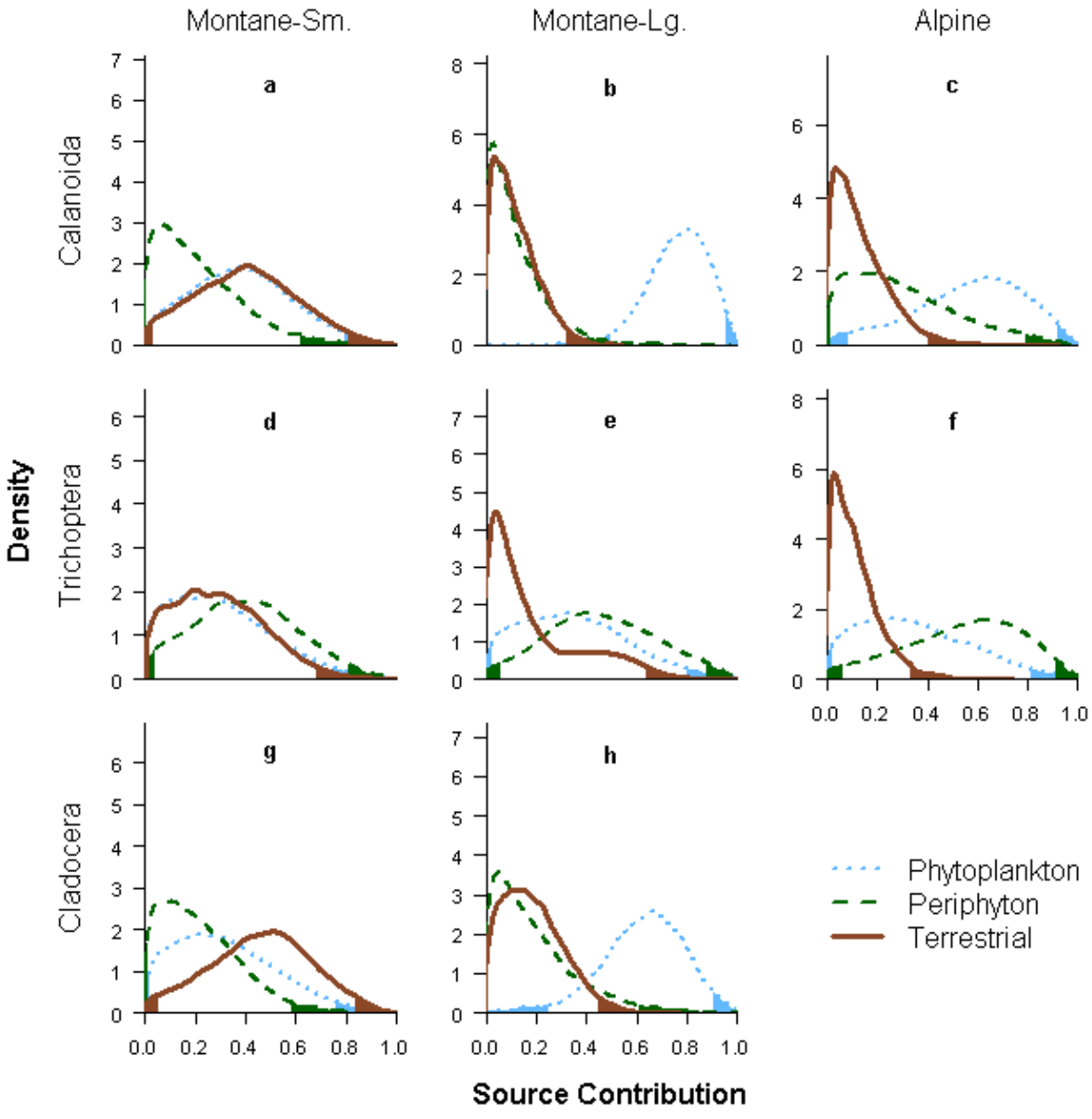

Figure 3 Posterior probability density of proportional source contributions by lake class and consumer taxon. Peak height represents density of 3000 posterior draws after burn-in and thinning. The unshaded region under each peak corresponds to the 95% credible interval.

than those of either ML (mode=0.04, mean=0.18, 95% CL [0.01,0.57]) or AP (mode=0.03, mean=0.16, 95% CL [0.01,0.48]). Zooplankton were particularly high in t-OM in MS (Calanoida mode=0.41, mean=0.40, 95% CL [0.04,0.81]; Cladocera mode=0.51, mean=0.50, 95% CL [0.06,0.83]), while phytoplankton dominated the diets of both zooplankton taxa in ML (Calanoida mode=0.81, mean=0.76, 95% CL [0.50,0.95]; Cladocera mode=0.66, mean=0.63, 95% CL [0.24,0.90]). ML Cladocera assimilated the greatest proportion of t-OM out of all consumers in the ML or AP classes (mode=0.12, mean=0.18, CL [0.01,0.45]). MS Trichoptera exhibited relatively low t-OM assimilation compared with MS zooplankton (mode=0.20, mean=0.30, CL [0.02,0.68]). Different source contributions were estimated for ML Trichoptera along the three axes of its mixing polygon (compare Figure 2, panel h with panels b and e), resulting in a small posterior density bulge around 50% t-OM assimilation and a tall peak at 4% (Figure 3, panel e).

Parameter sensitivity

Five estimated parameters (ω, $\Delta^{13}C$, $\Delta^{15}N$, $C:N_a$, ε_H) had the potential to influence mixing results. We fixed each of these in turn at its mean and at ± 2 SD (Table 3) to explore the resulting influence on model estimated allochthony, which was aggregated across all consumer taxa by combining posterior distributions. Predictions varied substantially with variation in ω and $C:N_a$, particularly in MS (Figure 4).

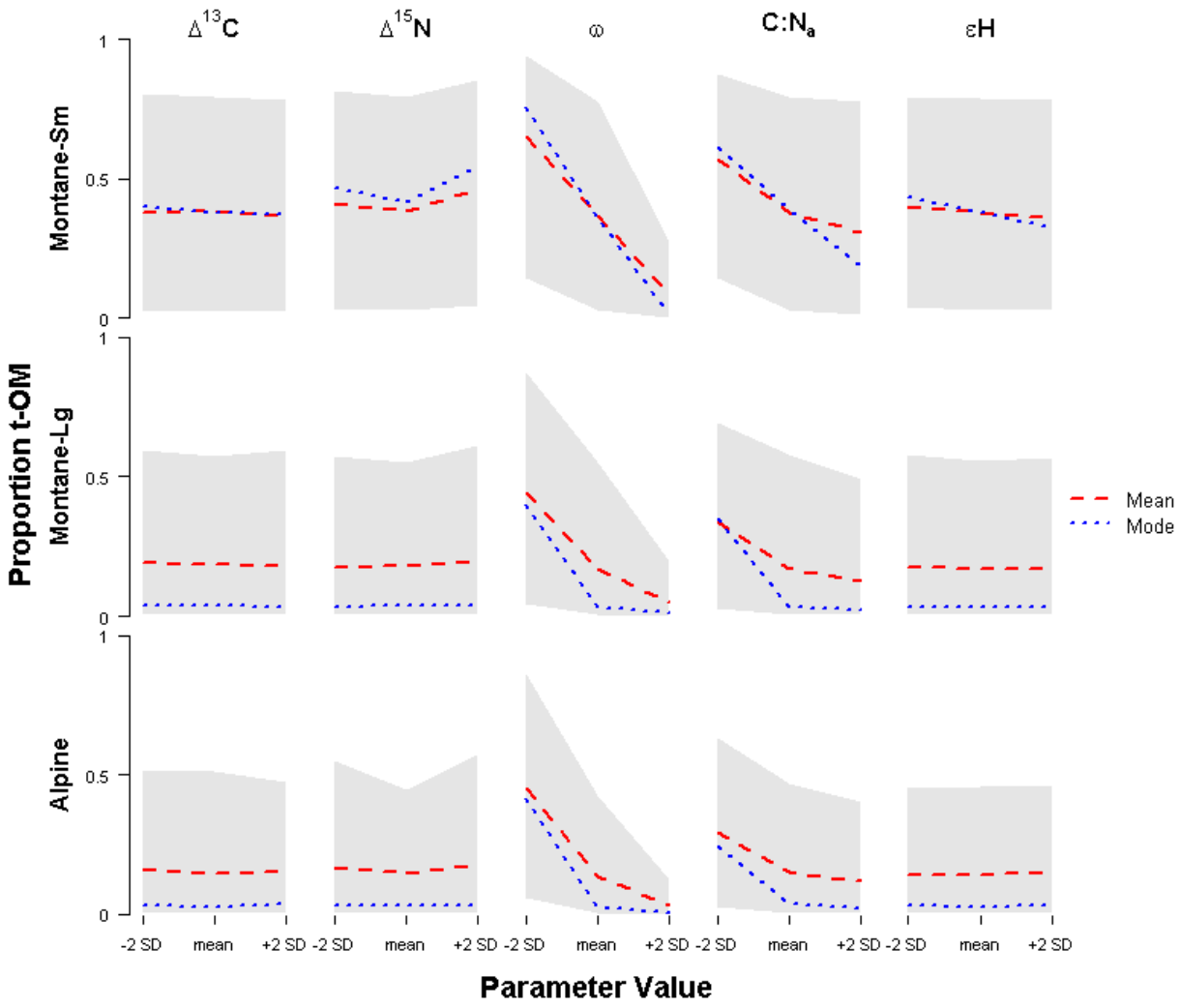

Figure 4 Estimates of t-OM proportion resulting from parameters fixed at mean and ± 2 standard deviations. Gray regions represent 95% credibile intervals based on 3000 posterior draws after burn-in and thinning.

Compared with the full model run, in which each of the five influential parameters was allowed to vary along empirical distributions, some fixed-parameter model runs produced large variations in estimates of t-OM assimilation. Unless specified, we here report pooled mean, mode, and 95% credible intervals across lake classes. Varying trophic enrichment of ^{13}C and ^{15}N, and photosynthetic ^{2}H discrimination, from +2 SD to -2 SD of mean literature reported values had relatively little effect on proportion t-OM estimates from our model. In contrast, substantial differences in model estimated t-OM

occurred when varying proportion dietary water (ω) and the C:N of algae. Overall proportion t-OM was highest when assuming minimal influence of dietary water (ω = 0.04; t-OM mode=0.52, mean=0.52, CL [0.08,0.89]), and lowest at high proportion dietary water (ω = 0.52; mode=0.05, mean=0.01, CL [0.00,0.20]). Further information on the influence of ω can be found in Appendix A. $C:N_a$ produced moderate increases in proportion t-OM at its lower extreme of 3.68 (mode=0.40, mean=0.40, CL [0.07,0.73]), but was fairly uninfluential at its upper extreme of 9.72 (mode=0.18, mean=0.08, CL [0.01,0.56]), yielding t-OM estimates similar to those of varying-parameter conditions (0.24, 0.16, [0.01,0.62]). Similar values to these were estimated across values of the other three parameters.

Table 3 Distributions of influential parameters for correction and estimation of sources and consumers.

Parameter	Model Mean	Model SD	Lit. Mean	Lit. SD	Lit. n	Source
ω	0.3	0.02	0.28	0.12	11	Brett et al. in review
ϵ_H	-150.7	4	-150	27	99	Brett et al. in review
$C:N_a$	6.7	0.27	6.7	1.51	151	Vuorio et al. 2006
$\Delta^{13}C$	0.45	0.1	0.39	1.3	107	Post et al. 2002
$\Delta^{15}N$	3.4	0.16	3.4	0.98	56	Post et al. 2002

Fatty acid tracers of allochthony

The first principal component explained 47.0% of the variation in FA among consumers, and separated FA indicative of algal synthesis (e.g., eicosapentaenoic acid, docosahexaenoic acid, alpha-linolenic acid) from generally abundant FAs that are widely synthesized by many diverse taxonomic groups (e.g., short saturated fatty acids [SAFA], oleic acid; Figure 5). Calanoida and *Chaoborus sp.* from ML and AP lakes loaded toward algal FA, while Trichoptera from these lakes and all Cladocera loaded away from algal FA. Trichoptera and Calanoida from MS occupied the midrange of this axis.

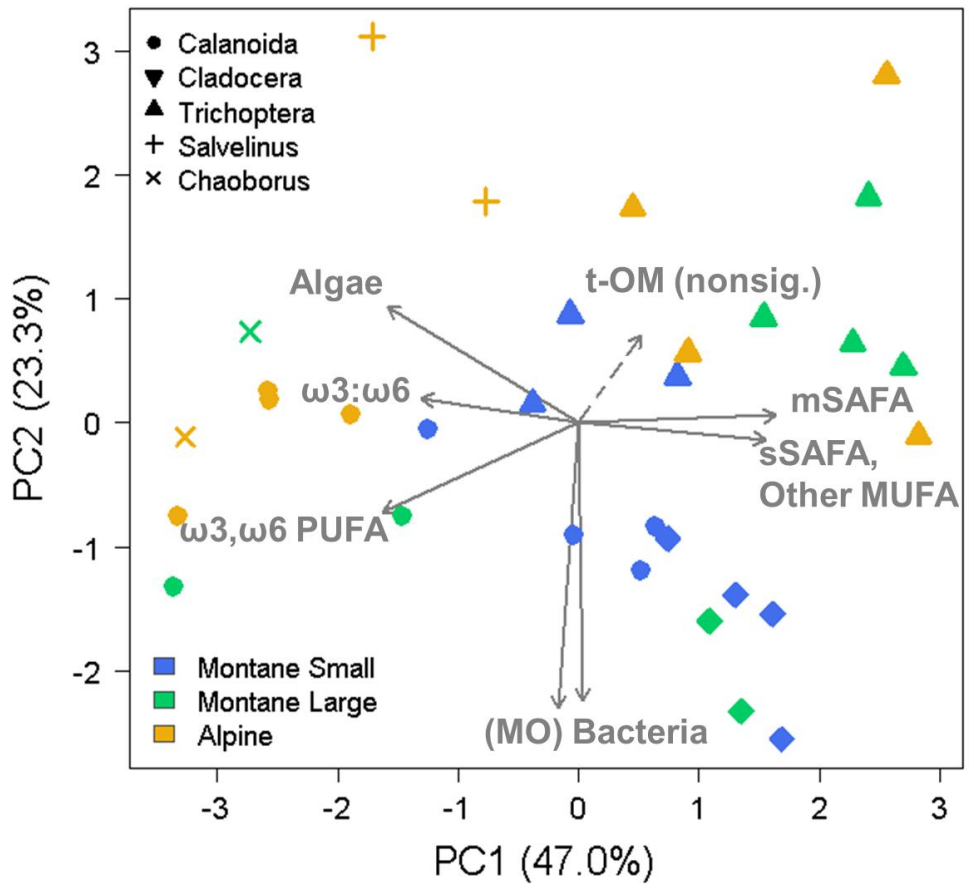

Figure 5 Principal Component Analysis of consumers based on concentrations of 57 fatty acids (FA). Arrows represent source-diagnostic and other major FA groupings, as well as the ratio of ω-3 to ω-6 FA, high values of which typically indicate algal synthesis. mSAFA and sSAFA refer to medium- and short-length saturated FA. MUFA and PUFA stand for mono- and polyunsaturated FA. MO = "methane oxidizing".

Along the second principal component axis, which carried 23.3% of overall variation, bacterial FA (e.g., branched chain, 15:0) played a strong role. This axis was responsible for the separation of Cladocera (high relative content of bacterial FA) from Trichoptera and *Salvelinus* (low relative content). FA diagnostic of terrestrial plant synthesis loaded positively, though not significantly onto both principal axes (loadings < 0.3, 15% of variance in lSAFA explained by first two principal components), along with ML and AP Trichoptera.

The strong grouping of MS consumers across taxa contrasted with much greater dispersal of taxonomic groups in the other lake classes. MS consumers generally plotted centrally with respect to both principal axes, or loaded positively onto PC1 and negatively onto PC2. Trichoptera and Cladocera represented the rough extremes of this spectrum of variation. For details on all FA used in this analysis, including source attribution, see Appendix B.

Daphnia magna survival on t-OM

We compared *Daphia magna* fitness on simulated terrestrial and aquatic diets using four treatments of terrestrial duff feed: Montane, Montane-primed, Alpine, Alpine-primed, and *C. ozolinii* as an algal reference (Figure 6). In the *C. ozolinii* treatment, parthenogenic reproduction occurred at a mean of 12.8 ± 1.9 (SD; n=24) days after introduction of the neonate. Only 2% of 25 individuals died before reproducing. In the duff treatments, even after we removed the requirement for reproductive maturity, only microbially primed duff produced harvestable individuals, and the unprimed treatments were abandoned after 14 days. In the Montane-primed treatment, 83.1% of 71 individuals did not reach the 6-day survival threshold, compared with 97.4% of 76 individuals in Alpine-primed.

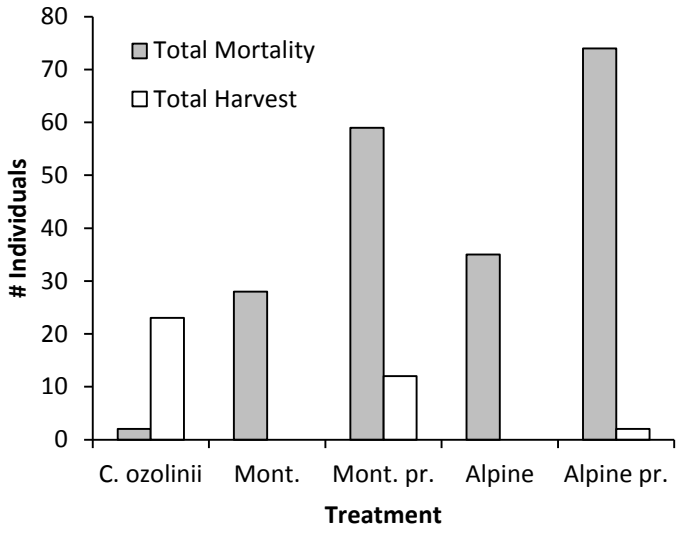

Figure 6 *D. magna* mortality and reproduction over three weeks. "Mont. pr." stands for Montane-primed.

None of the duff treatments produced enough biomass for FA analysis. The individual treatments were therefore replaced with 500mL beakers for *ad libitum*, bulk rearing. Of these, only the Montane-primed treatment generated mature adults, which were analyzed via gas chromatography—flame ionization detection (GC-FID) to catalogue FA composition.

Discussion

We here define allochthony as the assimilation of OM of terrestrial origin by lacustrine consumers, represented by proportional composition of elemental carbon, hydrogen, and nitrogen from terrestrial sources (t-OM). We evaluated allochthony across three consumer taxa using a mixing model with stable isotope tracers, and two additional taxa by comparing fatty acid concentration profiles of consumers and their potential food sources.

Allochthony patterns among lakes

We estimated proportional resource assimilation for three consumer taxa across three lake classes to assess the relative influence of allochthony on consumer biomass under different conditions of lake morphology and watershed ecosystem development. Our separation of lakes into Montane-Small, Montane-Large, and Alpine classes according to physical and chemical attributes correlates with strong differences in model-estimated resource use between classes, and indicated appreciable allochthony in consumers in only the most terrestrially connected systems (i.e., MS systems). These four lakes (technically ponds; Figure 1) were very small, each less than 0.1 hectare when fully filled, and occupied forested watersheds. They had shrunken considerably when we sampled in early August, thereby further concentrating their already solute- and particulate-rich waters. The relative ^{2}H enrichment of MS consumers (Figure 3) probably corresponds to the relative enrichment of their dominant food sources, phytoplankton and periphyton, which is a direct result of ^{2}H enrichment in the water of the MS lakes. Consumers in lakes of this kind, both pelagic and littoral/benthic, are presented with high concentrations of both t-OM and algal resources, as evidenced by DOC and chlorophyll-a concentrations far exceeding those of the other lake classes (Table 1). By selecting among more energetically efficient algal food particles, a consumer could conceivably exhibit low allochthony even in such a setting (Demott 1982;

Hadas et al. 1982), but this is not what we observed. Among lakes of the MS class, the most probable level of allochthony across taxa was estimated at 41% (Figure 3). Thus, we conclude that the combination of low lake volume and high terrestrial loading — for which watershed vegetation and DOC concentration are proxies — results in relatively high allochthony. Despite the very small volume and high t-OM concentration of the MS lakes, the highest mode estimate of allochthony for any taxon in these systems was only 51% (Cladocera). This is substantially less than a number of recently reported values for zooplankton in much larger lakes, including 77% (Karlsson et al. 2003), 82% (Wilkinson et al. 2013), and 89% (Grey et al. 2001). However, the 95% credible interval of the posterior distribution ranged from 6% to 83%, indicating many highly probable values.

The AP class, with its barren, rocky catchments, silty sediments, and extremely dilute waters, was expected to provide a lower limit on terrestrial support of aquatic food webs, given the near complete lack of terrestrial material available in the watershed. In support of our hypothesis, the most probable allochthony estimate for AP consumers was a mere 3% across taxa. This value is relatively well constrained in our model with a 95% credible interval ranging from 0 to 48%. The most probable autochthonous energy source differed by taxon in AP, with Calanoida assimilating primarily phytoplankton (64%), and Trichoptera preferring periphyton (63%).

In contrast to the shallow and concentrated MS systems and the clear AP systems with near complete absence of watershed OM, the ML systems represent the most “conventional” of the lakes in our study set, as well as the most analogous to previous lake allochthony studies (Carpenter et al. 2005, Francis et al. 2011, Karlsson et al. 2012). Lakes in this class have surface areas over three hectares, maximum depths greater than seven meters, and OM-rich sediments. Two of the three (neighbors Morgenroth and No Name) were partly stratified at the time of sampling. ML and MS catchments are very similar to each other, but for areal coverage. All are fully forested and situated at approximately 1,300 m in elevation, with visually homogeneous forest composition across their watersheds (Figure 1). Contrary to our original expectations, allochthony of ML consumers was near zero and very similar to the AP lakes. The most probable value of allochthony was just 4% across taxa, which is substantially lower than minimum values reported in several previous studies, such as 20% (Cole et al. 2011), 22% (Pace et al. 2004), and 23% (Karlsson et al. 2012).

One potential explanation for the extremely low allochthony is that terrestrial organic material entering these lakes is diluted into vastly more water than in the MS systems. In this way our results support previous work by Wilkinson et al. (2013) demonstrating an inverse relationship between lake surface area and allochthony. However, [DOC] and [chl-a]:[DOC] for the ML lakes are similar to other studies yet have overall substantially lower allochthony estimates (Cole et al. 2011, Rautio et al. 2011). This may relate to the nutrient quality of high elevation conifers and shrubs relative to lowland plants, or to the influence of deep autotrophic production on zooplankton diets, which we did not quantify (Francis et al. 2011).

In addition to receiving very little terrestrial loading, AP lakes also receive t-OM of particularly low energetic and nutritional quality. Terrestrial duff material collected from AP plants resulted in higher mortality and lower growth and reproduction than montane duff when fed to *Daphnia magna* (Figure 6). It also had higher C:N (mean=46 ± 0.2 vs. 38 ± 0.2), corresponding to greater recalcitrance. An examination of the FA profiles of dominant plants from each region reveals that alpine plants (*P. empetriformis* and *Vaccinium sp*.) have lower relative concentrations of linoleic acid and α-linolenic acid, both essential PUFA, than those of the montane region. In short, the structural demands of AP plants, subjected to high winds and snowpack, seem to render them poor food resources, diminishing the effect of AP allochthony beyond vegetation sparseness alone.

Ordination of MS consumers by FA composition also reveals strong grouping, which suggests a high degree of similarity in utilization of basal resources across consumer taxa (Figure 5). The identity of these resources is further illuminated by the most abundant FAs within consumer tissues. For MS consumers, these tend to be SAFA more so than PUFA, and low concentrations of ω-3 PUFA relative to ω-6 PUFA, all characteristic of terrestrial plants, as the mixing model predicts. Consumers of this class also contain high concentrations of branched-chain FA and medium-length, odd-numbered-carbon SAFA, both indicative of bacterial origin. Strong bacterial influence on the MS food web may also relate to mixing model results in that decomposers are largely responsible for liberating nutrients from recalcitrant plant material (Moore, 2004), thus higher representation of bacterial matter would be expected in allochthonous consumer tissues. Our feeding experiment suggests microbial priming is likely essential to

consumers of t-OM in the Seven Lakes Basin, as *D. magna* mortality was complete in the absence of microbial inoculation of feed (Figure 6).

Allochthony patterns among consumer taxa

The lentic allochthony literature is dominated by studies of zooplankton. As consumers of primary production, and prey for large and small predators, zooplankton often play the role of a fulcrum in structuring the trophic distribution of energy between producers and higher consumers (Carpenter et al. 1996). However, other functional groups, including detritivores and top predators, may refine our understanding of trophic pathways, or even suggest new ones. In addition to zooplankton, we included in our model larvae of case-building caddisflies (Trichoptera), which are littoral/benthic macroinvertebrates and facultative grazers. We have also included eastern brook trout (*S. fontinalis*) and *Chaoborus sp*. in the FA portion of our analysis.

Large, consistent differences in allochthony were not observed across the three taxa included in the mixing model (Figure 3). Rather, lake class appears to be the most important determinant of the degree of terrestrial resource use by all consumers. However, our model reveals several trophic dynamics stemming from aquatic production. As the presence of t-OM declines (i.e., moving from MS to either ML or AP), the prevalence of aquatic resources in a consumer's diet may increase in multiple ways. For zooplankton, this corresponds directly to an increase in phytoplankton consumption in the ML lakes, while there may also be a mild increase in consumption of periphyton by AP Calanoida. We are unaware of documented benthic grazing by copepods, but our results suggest it may occur under highly oligotrophic conditions. The increased utilization of periphyton by multiple consumers in AP may relate to the low depth ratio and high light penetration of these lakes, which yields greater primary production by attached, relative to free-floating, algae (Vadeboncoeur et al. 2008). ML Cladocera were the most allochthonous taxon in both lake classes where they were collected. Unlike copepods, which exhibit directed, linear locomotion and semi-raptorial feeding, *Daphnia spp.* and *Bosmina spp.* (the two cladoceran genera observed in our lake set) are filter-feeders (Demott 1982). As such, they have little ability to discriminate among food particles. This probably explains why cladoceran assimilation of t-OM is higher than that of Calanoida. Given the low palatability of AP t-OM (Figure 6), it may also partly explain the lack of

Cladocera we observed in the AP lakes. However, the primary reason for this absence probably relates to the nutrient quality (i.e. carbon:phosphorus ratio) of algae in very clear lakes, which can be too high to sustain phosphorus-rich Cladocera (Sterner et al. 1997).

For Trichoptera, the absence of available t-OM corresponds to increased consumption of both phytoplankton and periphyton, the latter dominating in the AP class. The bulge in posterior density around 0.5 for ML Trichoptera is a result of contradicting mixing configurations given by different tracers. With respect to δ^2H and $\delta^{13}C$, or δ^2H and $\delta^{15}N$, Trichoptera plot far from t-OM (Figure 2, panels b and e), while they are much closer with respect to $\delta^{13}C$ and $\delta^{15}N$ (Figure 2, panel h). Although the Trichoptera mean in each case falls directly between the means for periphyton and phytoplankton, the error around each is such that some Trichoptera posterior draws suggest 50% t-OM contribution. Although the likelihood density is low for this particular outcome, we cannot rule out the possibility that t-OM contributes 50-60% of the diet of ML Trichoptera.

A considerable portion of ML Calanoida posterior composition estimates exceeded their mixing polygons (e.g., Figure 2, panel h), suggesting potential error either in the measurement and endmember determination of isotopic signatures, or in omission of a relevant source material (i.e., a vertex of the mixing polygon). In the case of the former, a Bayesian approach can allow meaningful estimates of allochthony despite such error. In the case of the latter, Bayesian methods can be highly misleading. We did not include deep POM (comprised of phytoplankton and t-OM found below the mixed layer) as a source in our analysis, and this may play a significant role in calanoid diets within the ML class. Zooplankton were found to assimilate up to 80% of their tissue from deep POM in a separate set of Pacific Northwest lakes with deep chlorophyll maxima (Francis et al. 2011). ML Calanoida were indeed more depleted in ^{13}C than those of either MS or AP, which accounts for their being farther outside their source polygon than any other consumers. It is thus likely that our omission of deep POM explains the poor constraint of ML Calanoida.

Notes on model design and influential parameters

In the classical, algebraic approach to mixing models, *n*-1 tracers are used to determine *n* source contributions to a mixture. Under a Bayesian framework, any number of tracers (in this case, isotopes of

H, C, and N) can be incorporated, and the model produces a range of solutions with associated likelihoods. In the first case, the coordinate position of the mixture with respect to each tracer in *n*-dimensional space must lie within the polygon formed by its sources. Otherwise, the predicted proportional contributions of each source will not fall within meaningful limits, i.e. [0,1], signifying that the model is misspecified. Under the Bayesian approach, possible source proportions are drawn from a Dirichlet prior, which ensures that none exceeds [0,1] and that all sum to unity. As a result, even the most poorly specified model will still produce an apparently sensible output. This necessitates careful examination of both isotope biplots (e.g., Figure 2) and full posterior densities (e.g., Figure 3).

A second pitfall of some Bayesian approaches arises from the practice of estimating source and mixing parameters concurrently. Because source contributions may only take values between 0 and 1, higher likelihoods are assigned to source and consumer configurations that readily satisfy this constraint. In other words, if by adjusting source parameters like ω and ε_H the model can place a consumer within the source polygon, it will do so. This becomes especially problematic when influential parameters are assigned values from the extremes of their empirically observed ranges. Without experimental corroboration, allowing such model flexibility cannot be justified. Thus, to avoid undesirable model behavior, we estimated or corrected all consumer and source isotope signatures separately from the determination of source contributions to the consumer.

We determined most model-estimated parameters to be of little influence with respect to estimated allochthony, specifically $\Delta^{13}C$, $\Delta^{15}N$, and ε_H. Separation of terrestrial and aquatic sources in isotope space was achieved largely by δ^2H, thereby rendering $\Delta^{13}C$ and $\Delta^{15}N$ uninformative in our particular case. However, $C:N_A$ and ω, critical determinants of consumer and aquatic source position, could have altered overall allochthony estimates considerably by shifting two standard deviations from their known means. Ideally, before any investigation of lacustrine allochthony, parameters like these would be measured or experimentally determined for the systems in question, and incorporated as informative priors. A strong presence of such experimental approaches in the literature would provide model constraints in cases where such scrutiny is infeasible. We advocate close examination of each estimated parameter in future studies, and separate assignment of likelihoods between correction or estimation of tracer values and determination of source proportions, wherever possible.

Fatty acid analysis

FA analysis provided a second line of evidence for the separation of consumer taxa by resource assimilation (Figure 5). It also revealed microbial trophic pathways typically not detectable via SI-based analyses alone. PCA corroborated the predominance of phytoplankton in ML and AP calanoid diets. *Chaoborus sp.* and *S. fontinalis*, both predators of smaller zooplankton, also showed considerable algal FA composition, though with higher relative proportions of long-chain PUFA like DHA, DPA, and EPA corresponding to their relative trophic positions. These essential FA are conserved in the tissues of consumers and accumulate with each trophic transfer (Brett et al. 2006). There are no unique FA biomarkers of total periphyton, as it is a combination of producer and decomposer taxa, as well as assorted detritus. However, consumers of total periphyton would be expected to occupy a region of ordination space distinct from purely algal or bacterial markers. This combination of FA probably loads positively onto PC1 (away from Calanoida and toward Trichoptera), while PC2 may separate it according to bacterial FA content. Of all five taxa, Cladocera contain the highest relative proportion of bacterial FA, likely due to their consumption of bacteria along with t-OM, of which they are the foremost consumers. Terrestrial FA did not load significantly onto either major principal component.

Conclusions

After examining biological and physical markers of resource preference in multiple consumer taxa across 11 mountain lakes and conducting a separate feeding experiment, we conclude that allochthony in these lakes is a function primarily of terrestrial organic matter loading and physical controls, specifically lake size and light penetration. We expect allochthony to decrease along elevational gradients as a result of thinning forests and stouter, less digestible plants. Above tree line, this effect should be very pronounced. Our results suggests previously documented trends in allochthony, primarily derived from studies of zooplankton, may not hold for other taxa, in particular benthic invertebrates, which may be dominant food sources for fish in wetlands and shallow lakes (Vadeboncoeur et al. 2002). Grazers of periphyton, in particular, may be substantially less allochthonous than zooplankton. A complete picture of the transfer of terrestrial energy into lake food webs will require examinations of allochthony in other

macroinvertebrate functional groups, including shredders and piercers. A catalogue of major basal consumers and their propensities toward allochthony will aid our understanding of resource use by higher predators, which incorporate allochthonous material via their prey.

Finally, Bayesian mixing models, ubiquitous in the allochthony literature, are highly sensitive to underlying assumptions, like many statistical tools. We urge caution in ensuring that such models do not artificially assign extreme values to parameters that determine source contributions. This can be accomplished by separating mixing models into multiple modules, where source contributions are determined in isolation from the correction of tracer values.

Acknowledgments

We thank Laura Twardochleb and Rachel Steinmetz for helping with sample collection and processing in the field. Daniel Schindler and Michael Brett provided tremendous logistical, conceptual, and technical advice, as well as lab space. Additional contributors of valuable time and expertise include Eric Ward, Andrew Schauer, Arni Litt, Joshua Gregersen, Ashley Maloney, Sydney Clark, Jon Wittouck, Arielle Ellis, and Frieda Taub.

References

Berggren, M., Ziegler, S. E., St-Gelais, N. F., Beisner, B. E., & del Giorgio, P. A. (2014). Contrasting patterns of allochthony among three major groups of crustacean zooplankton in boreal and temperate lakes. *Ecology*, *95*(7), 1947–1959.

Brett, M. T., Holtgrieve, G. W., & Schindler, D. E. (n.d.). An assessment of assumptions and uncertainty in deuterium-based estimates of trophic interactions in aquatic ecosystems. *In Review*.

Brett, M. T., Kainz, M. J., Taipale, S. J., & Seshan, H. (2009). Phytoplankton, not allochthonous carbon, sustains herbivorous zooplankton production. *Proceedings of the National Academy of Sciences*, *106*(50), 21197–21201.

Brett, M. T., Müller-Navarra, D. C., Ballantyne, A. P., Ravet, J. L., & Goldman, C. R. (2006). Daphnia fatty acid composition reflects that of their diet. *Limnology and Oceanography*, *51*(5), 2428–2437.

Butman, D., & Raymond, P. A. (2011). Significant efflux of carbon dioxide from streams and rivers in the United States. *Nature Geoscience*, *4*(12), 839–842.

Carpenter, S. R., Cole, J. J., Pace, M. L., de Bogert, M., Bade, D. L., Bastviken, D., … Kritzberg, E. S. (2005). Ecosystem subsidies: terrestrial support of aquatic food webs from 13C addition to contrasting lakes. *Ecology*, *86*(10), 2737–2750.

Carpenter, S. R., & Kitchell, J. F. (1996). *The trophic cascade in lakes*. Cambridge University Press.

Cole, J. J., Prairie, Y. T., Caraco, N. F., McDowell, W. H., Tranvik, L. J., Striegl, R. G., … Melack, J. (2007). Plumbing the Global Carbon Cycle: Integrating Inland Waters into the Terrestrial Carbon Budget. *Ecosystems*, *10*(1), 172–185. http://doi.org/10.1007/s10021-006-9013-8

Cole, J. J., Carpenter, S. R., Kitchell, J., Pace, M. L., Solomon, C. T., & Weidel, B. (2011). Strong evidence for terrestrial support of zooplankton in small lakes based on stable isotopes of carbon, nitrogen, and hydrogen. *Proceedings of the National Academy of Sciences*, *108*(5), 1975–1980.

DeMott, W. R. (1988). Discrimination between algae and detritus by freshwater and marine zooplankton. *Bulletin of Marine Science*, *43*(3), 486–499.

Doucett, R. R., Marks, J. C., Blinn, D. W., Caron, M., & Hungate, B. A. (2007). Measuring terrestrial subsidies to aquatic food webs using stable isotopes of hydrogen. *Ecology*, *88*(6), 1587–1592.

Emery, K. A., Wilkinson, G. M., Ballard, F. G., & Pace, M. L. (2015). Use of allochthonous resources by zooplankton in reservoirs. *Hydrobiologia*, *758*(1), 257–269.

Francis, T. B., Schindler, D. E., Holtgrieve, G. W., Larson, E. R., Scheuerell, M. D., Semmens, B. X., & Ward, E. J. (2011). Habitat structure determines resource use by zooplankton in temperate lakes. *Ecology Letters*, *14*(4), 364–372. http://doi.org/10.1111/j.1461-0248.2011.01597.x

Gelman, A., & Rubin, D. B. (1992). Inference from iterative simulation using multiple sequences. *Statistical Science*, 457–472.

Grey, J., Jones, R. I., & Sleep, D. (2001). Seasonal changes in the importance of the source of organic matter to the diet of zooplankton in Loch Ness, as indicated by stable isotope analysis. *Limnology and Oceanography*, *46*(3), 505–513. http://doi.org/10.4319/lo.2001.46.3.0505

Hadas, O., Cavari, B. Z., Kott, Y., & Bachrach, U. (1982). Preferential feeding behaviour of Daphnia magna. *Hydrobiologia*, *89*(1), 49–52.

Holtgrieve, G. W., Schindler, D. E., Gowell, C. P., Ruff, C. P., & Lisi, P. J. (2010). Stream geomorphology regulates the effects on periphyton of ecosystem engineering and nutrient enrichment by Pacific salmon. *Freshwater Biology*, *55*(12), 2598–2611.

Jackson, A. L., & Bearhop, S. (2009). TECHNICAL Erroneous behaviour of MixSIR , a recently published Bayesian isotope mixing model : a discussion of Moore & Semmens (2008), 1–5. http://doi.org/10.1111/j.1461-0248.2008.01233.x

Junk, W. J., Bayley, P. B., Sparks, R. E., & others. (1989). The flood pulse concept in river-floodplain systems. *Canadian Special Publication of Fisheries and Aquatic Sciences*, *106*(1), 110–127.

Karlsson, J., Berggren, M., Ask, J., Byström, P., Jonsson, A., Laudon, H., & Jansson, M. (2012). Terrestrial organic matter support of lake food webs: Evidence from lake metabolism and stable hydrogen isotopes of consumers. *Limnology and Oceanography*, *57*(4), 1042–1048. http://doi.org/10.4319/lo.2012.57.4.1042

Karlsson, J., Jonsson, A., Meili, M., & Jansson, M. (2003). Control of zooplankton dependence on allochthonous organic carbon in humic and clear-water lakes in northern Sweden. *Limnology and Oceanography*, *48*(1), 269–276.

Lindeman, R. L. (1942). The trophic- dynamic aspect of ecology. *Ecology*, *23*(4), 399–417.

Lindström, K. (1991). Nutrient requirements of the dinoflagellate Peridinium gatunense. *Journal of Phycology*, *27*(2), 207–219.
Moore, J. C., Berlow, E. L., Coleman, D. C., Ruiter, P. C., Dong, Q., Hastings, A., … Morin, P. J. (2004). Detritus, trophic dynamics and biodiversity. *Ecology Letters*, *7*(7), 584–600.
Nichols, P. D., Palmisano, A. C., Smith, G. A., & White, D. C. (1986). Lipids of the Antarctic sea ice diatom Nitzschia cylindrus. *Phytochemistry*, *25*(7), 1649–1653.
Pace, M. L., Carpenter, S. R., Cole, J. J., Coloso, J. J., Kitchell, J. F., Hodgson, J. R., … Weidel, B. C. (2007). Does terrestrial organic carbon subsidize the planktonic food web in a clear-water lake? *Limnology and Oceanography*, *52*(5), 2177–2189. http://doi.org/10.4319/lo.2007.52.5.2177
Pace, M. L., Cole, J. J., Carpenter, S. R., Kitchell, J. F., Hodgson, J. R., Van de Bogert, M. C., … Bastviken, D. (2004). Whole-lake carbon-13 additions reveal terrestrial support of aquatic food webs. *Nature*, *427*(6971), 240–243.
Plummer, M. (2016). rjags: Bayesian Graphical Models using MCMC. Retrieved from https://cran.r-project.org/package=rjags
Plummer, M., & others. (2003). JAGS: A program for analysis of Bayesian graphical models using Gibbs sampling. In *Proceedings of the 3rd international workshop on distributed statistical computing* (Vol. 124, p. 125).
Post, D. M. (2002). Using stable isotopes to estimate trophic position: models, methods, and assumptions. *Ecology*, *83*(3), 703–718.
Pulido-Villena, E., Reche, I., & Morales-Baquero, R. (2005). Food web reliance on allochthonous carbon in two high mountain lakes with contrasting catchments: a stable isotope approach. *Canadian Journal of Fisheries and Aquatic Sciences*, *62*(11), 2640–2648.
R Core Team. (2017). R: A Language and Environment for Statistical Computing. Vienna, Austria. Retrieved from https://www.r-project.org/
Rautio, M., Mariash, H., & Forsström, L. (2011). Seasonal shifts between autochthonous and allochthonous carbon contributions to zooplankton diets in a subarctic lake. *Limnology and Oceanography*. Retrieved from http://aslo.info/lo/toc/vol_56/issue_4/1513.pdf
Richey, J. E., Melack, J. M., Aufdenkampe, A. K., Ballester, V. M., & Hess, L. L. (2002). Outgassing from Amazonian rivers and wetlands as a large tropical source of atmospheric CO2. *Nature*, *416*(6881), 617–620.
Rose, K. C., Williamson, C. E., Kissman, C. E. H., & Saros, J. E. (2015). Does allochthony in lakes change across an elevation gradient? *Ecology*, *96*(12), 3281–3291. http://doi.org/10.1890/14-1558.1
Solomon, C. T., Cole, J. J., Doucett, R. R., Pace, M. L., Preston, N. D., Smith, L. E., & Weidel, B. C. (2009). The influence of environmental water on the hydrogen stable isotope ratio in aquatic consumers. *Oecologia*, *161*(2), 313–324. http://doi.org/10.1007/s00442-009-1370-5
Sterner, R. W., Elser, J. J., Fee, E. J., Guildford, S. J., & Chrzanowski, T. H. (1997). The light: nutrient ratio in lakes: the balance of energy and materials affects ecosystem structure and process. *The American Naturalist*, *150*(6), 663–684.
Strandberg, U., Taipale, S. J., Kainz, M. J., & Brett, M. T. (2014). Retroconversion of docosapentaenoic acid (n-6): an alternative pathway for biosynthesis of arachidonic acid in Daphnia magna. *Lipids*, *49*(6), 591–595.
Thorp, J. H., & Delong, M. D. (1994). The riverine productivity model: an heuristic view of carbon sources and organic processing in large river ecosystems. *Oikos*, 305–308.
Vadeboncoeur, Y., Peterson, G., Vander Zanden, M. J., & Kalff, J. (2008). Benthic algal production across lake size gradients: interactions among morphometry, nutrients, and light. *Ecology*, *89*(9), 2542–2552.
Vadeboncoeur, Y., Vander Zanden, M. J., & Lodge, D. M. (2002). Putting the Lake Back Together: Reintegrating Benthic Pathways into Lake Food Web Models: Lake ecologists tend to focus their research on pelagic energy pathways, but, from algae to fish, benthic organisms form an integral part of lake food webs. *Bioscience*, *52*(1), 44–54.
Vannote, R. L., Minshall, G. W., Cummins, K. W., Sedell, J. R., & Cushing, C. E. (1980). The river continuum concept. *Canadian Journal of Fisheries and Aquatic Sciences*, *37*(1), 130–137.
Vuorio, K., Meili, M., & Sarvala, J. (2006). Taxon-specific variation in the stable isotopic signatures (d 13 C and d 15 N) of lake phytoplankton, 807–822. http://doi.org/10.1111/j.1365-2427.2006.01529.x
Weiss, R. F. (1970). The solubility of nitrogen, oxygen and argon in water and seawater. In *Deep Sea Research and Oceanographic Abstracts* (Vol. 17, pp. 721–735). Elsevier.

Wilkinson, G. M., Carpenter, S. R., Cole, J. J., Pace, M. L., & Yang, C. (2013). Terrestrial support of pelagic consumers: Patterns and variability revealed by a multilake study. *Freshwater Biology*, *58*(10), 2037–2049. http://doi.org/10.1111/fwb.12189

Appendix A

When ω is very low (left column in Figure A1), consumers are assumed to be comprised of only 4% environmental water. Removing this small fraction results in very little correction being applied, and raw consumer values are left essentially unchanged, potentially reflecting the highly enriched δ^2H values of lake water (mean=-65.5, SD 19.2 across lakes). When ω is high (right column in Figure A1), measured consumer δ^2H is assumed to reflect mostly lake water (52%), the correction for which leaves consumers highly depleted relative to all sources.

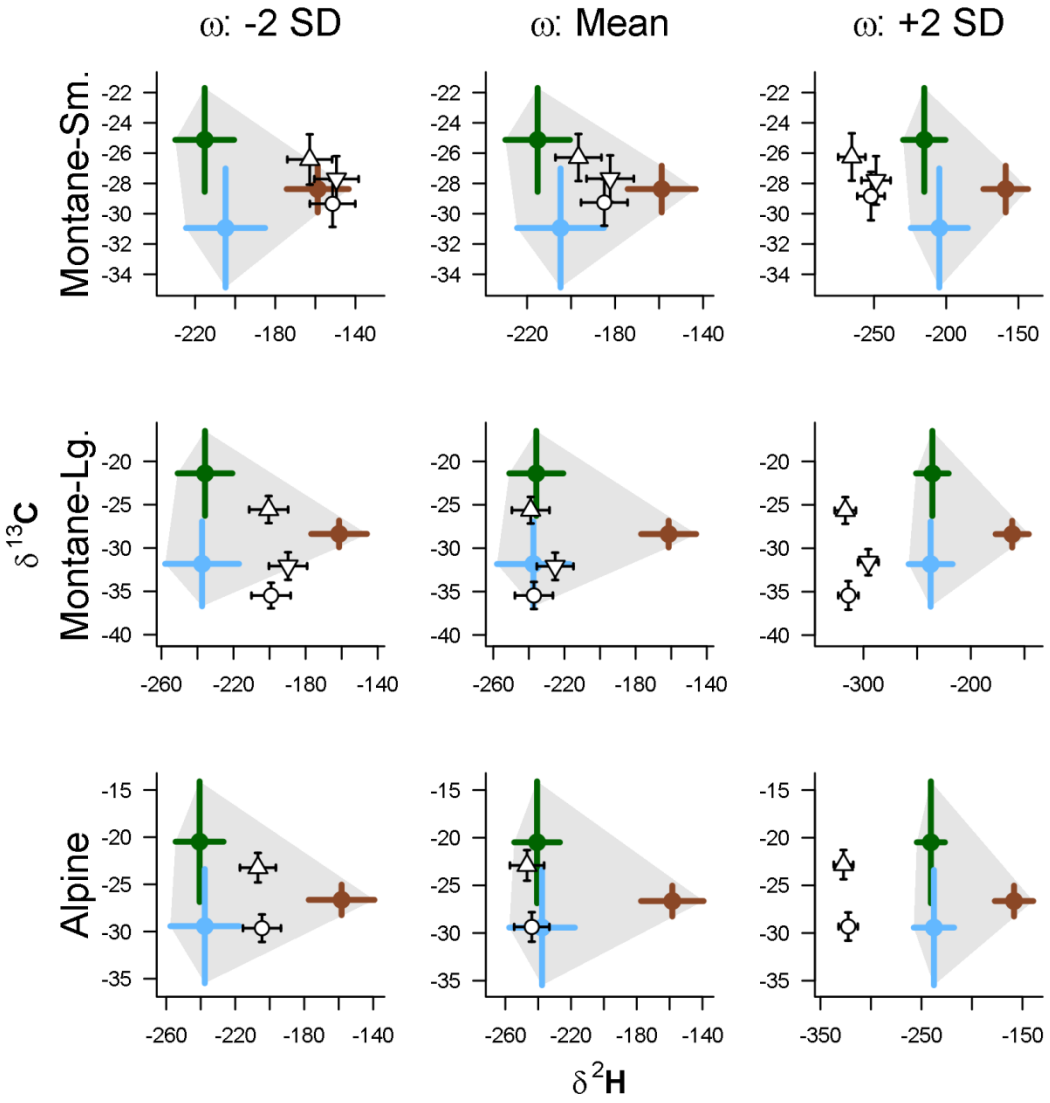

Figure A1 Configuration of consumers and sources with respect to $\delta^{2}H$ and $\delta^{13}C$, after correction. Corrections assume consumer H is comprised of 4% environmental H_2O-H (-2 SD, column 1), 28% (mean, column 2), and 52% (+ 2 SD, column 3).

Appendix B

Table B1 Fatty acids (FA) used in PCA, listed by category. For FA assumed to be synthesized by particular taxonomic groups, sources are also included. Medium-chain SAFA often indicate terrestrial origin, though not to the degree that long-chain SAFA do. ω-3 and ω-6 PUFA are not necessarily synthesized by algae, but are rarely of terrestrial origin. (EPA, DHA, ALA, LIN, etc.)

FA	Synthesizer/ Class	Source	FA	Synthesizer/ Class	Source
16:3ω4	Algae	Smits et al. 2015	13:0	sSAFA	
16:4ω3	Algae	Torres-Ruiz et al. 2007	14:0	sSAFA	
18:2ω6c	Algae	Torres-Ruiz et al. 2007	16:0	mSAFA	Taipale et al. 2013
18:2ω6t	Algae	Torres-Ruiz et al. 2007	18:0	mSAFA	Taipale et al. 2013
18:3ω3	Algae	Torres-Ruiz et al. 2007	18:3ω6	ω-3, ω-6 PUFA	Taipale et al. 2015
20:5ω3	Algae	Brett et al. 2009	18:4ω3	ω-3, ω-6 PUFA	Taipale et al. 2015
22:6ω3	Algae	Brett et al. 2009	18:5ω3	ω-3, ω-6 PUFA	Taipale et al. 2015
16:2?	Algae	Smits et al. 2015	20:3ω3	ω-3, ω-6 PUFA	Taipale et al. 2015
16:2ω4	Algae	Smits et al. 2015	20:2ω6	ω-3, ω-6 PUFA	Taipale et al. 2015
high ω-3:ω-6	Algae	Taipale et al. 2015	20:3ω6	ω-3, ω-6 PUFA	Taipale et al. 2015
20:0	Terrestrial	Taipale et al. 2015	20:4ω6	ω-3, ω-6 PUFA	Taipale et al. 2015
22:0	Terrestrial	Taipale et al. 2015	20:4ω3	ω-3, ω-6 PUFA	Taipale et al. 2015
24:0	Terrestrial	Taipale et al. 2015	21:5ω3	ω-3, ω-6 PUFA	Taipale et al. 2015
i14:0	Bacteria	Kharlamenko et al. 1995	22:4ω6	ω-3, ω-6 PUFA	Taipale et al. 2015
a14:0	Bacteria	Kharlamenko et al. 1995	22:5ω6	ω-3, ω-6 PUFA	Taipale et al. 2015
i15:0	Bacteria	Kharlamenko et al. 1995	22:5ω3	ω-3, ω-6 PUFA	Taipale et al. 2015
a15:0	Bacteria	Kharlamenko et al. 1995	14:1?	Other MUFA	
15:0	Bacteria	Dalsgaard et al. 2003	16:1ω7	Other MUFA	
i16:0	Bacteria	Kharlamenko et al. 1995	17:1?	Other MUFA	
a16:0	Bacteria	Kharlamenko et al. 1995	17:1?	Other MUFA	
i17:0	Bacteria	Kharlamenko et al. 1995	17:1ω7t	Other MUFA	
a17:0	Bacteria	Kharlamenko et al. 1995	17:1ω7c	Other MUFA	
17:0	Bacteria	Dalsgaard et al. 2003	18:1ω9c	Other MUFA	
i18:0	Bacteria	Kharlamenko et al. 1995	18:1ω7	Other MUFA	
16:1ω6c	MOB	Taipale et al. 2015	20:1ω9	Other MUFA	
16:1ω5t	MOB	Elvert et al. 2003	20:1ω7	Other MUFA	
18:1ω6c	MOB	Taipale et al. 2015	24:1ω?	Other MUFA	
18:1ω5c	MOB	Taipale et al. 2015	16:1ω9t	Other MUFA	
12:0	sSAFA		16:1ω9c	Other MUFA	

Chapter 2

Multi-scale controls on river temperature: a multivariate, autoregressive time series approach

Introduction

The biodiversity of a stream or river and the goods and services it provides are strongly influenced by the timing and magnitude of seasonal changes in water temperature (Caissie 2006, Olden & Naiman 2010). Temperature structures the distribution of ectothermic taxa within river networks (Vinson & Hawkins 1998, Huryn & Wallace 2000), including fish, which thermoregulate by occupying cool seeps and confluences (Berman & Quinn 1991) or small, warm tributaries (Peterson & Rabeni 1996) depending on conditions needed for optimal feeding and growth. Modifications to temperature regimes, such as through dam construction, can radically alter species and functional diversity, sometimes yielding near or complete extirpation of native invertebrates and fish (Lehmkuhl 1974, Zhong & Power 1996).

Temperature is also a chief consideration in the management of fisheries, as it affects species distribution (Boisneau et al. 2008), growth and reproduction (McCullough 1999), and migration timing (Boscarino et al. 2007). In particular, In the Puget Sound watershed of the American Pacific Northwest, several salmonid species spawn, migrate, or emerge only within the bounds of a few degrees Celsius, and reproduce optimally under even greater temperature constraints (Carter 2005). Colder water is associated with earlier spawn timing in salmonids (Beechie et al. 2008), while warmer water is associated with a greater incidence of infectious disease (Sanders et al. 1978).

Alongside water temperature, discharge (flow) regime is a major factor in shaping biotic composition, both directly (Rörslett et al. 1989, Munn & Brusven 1991, Bunn & Arthington 2002) and by altering the heat capacity of water; i.e. greater volume absorbs less heat per unit time (Smith 1972). Conversely, temperature can affect discharge by determining the timing and magnitude of flow resulting from melting snow and ice (Wulf et al. 2016). This interdependence implies a complex relationship between thermal regime and climate, which affects both temperature and discharge in rivers and streams.

River networks tend to be fractal in structure, and so are naturally governed by environmental processes at multiple spatial and temporal scales. Seasonal and inter-annual variation in water temperature and discharge are, in part, functions of regional climate, including solar radiation and

precipitation (Eldridge 1967). These large-scale drivers may in turn be mediated or supplemented by several aspects of watershed morphology at finer scales, including slope, elevation, and geology (Poole & Berman 2001, Lisi et al. 2013). Adding to this picture, flow regimes are highly variable across streams and rivers, with timing of peak annual discharge sometimes varying by many months even within relatively small geographic areas (Reidy Liermann et al. 2012).

Taken together, variation and hierarchy complicate our ability to predict impacts, such as those from changing regional and global climate, on riverine systems. Lisi et al. (2015) found that low-elevation watersheds in southwestern Alaska are 5-8 times more sensitive to variation in summer air temperature than high-elevation streams, due to the cooling effect of melting snow. This implies that the temperature regime of any one river sits on a continuum of relative influence by regional versus within-watershed drivers. Effective management plans must therefore integrate a diversity of factors across space and time in order to determine which rivers and watersheds are likely to see consequential changes under projected climate and land use scenarios for the Pacific Northwest (Mote & Salathe 2010, Radeloff et al. 2012), and identify potential mitigating actions. However, the understanding required to do so is limited by knowledge of relationships among temperature drivers at multiple scales.

We sought to determine whether rivers in the Puget Sound region vary in sensitivity to climatic forces, including air temperature (a proxy for the effect of solar radiation), precipitation, and snowmelt. We examined climatic effects on both water temperature and discharge throughout the year. Our second aim was to identify watershed features that correlate with variation in sensitivity, i.e. *coupling* between climatic forces and river temperature/discharge, and thus to provide a more nuanced basis for predicting impacts on aquatic biodiversity and fishery health. In the Puget Sound, watersheds vary with latitude and elevation (Reidy Liermann et al. 2012, Mauger et al. 2015), and can be classified broadly into three categories by flow source and hydrograph shape. Rain-dominated (RD) rivers receive little or no input from snowmelt, and thus peak in discharge (Q) during the rainy season, usually between October and February. Snow-dominated (SD) rivers instead see peak flow during spring snowmelt, often in April, May, or June. Between these extremes lies a third class of rain-and-snow-driven (RS) rivers, which have appreciable peaks at both times. We hypothesized that water temperature (T_{water}) would be most closely coupled with air temperature (T_{air}) in RD rivers (ward1985thermal, garner2014river, Lisi et al. 2015). We

expected deviations from this relationship to correlate with cold-water influx from snow and ice melt (Lisi et al. 2015) and with factors affecting thermal sensitivity of water, including Q and watershed slope (van Vliet et al. 2013). Finally, we expected Q to be most strongly coupled with T_{air} in the SD rivers, potentially serving to lessen the thermal sensitivity of water to changes in T_{air}.

Methods

Water and climate data

We investigated climate and landscape controls on T_{water} and Q, as separate response variables, from January 1978 to December 2015. Time series of water temperature by month were obtained for 24 river sites via the Washington Department of Ecology's River and Stream Water Quality Monitoring program (von Prause 2017). These sites represent 19 separate watersheds across 9 counties, and range from 4 to 775 m in elevation. River order (Strahler number) at mouth ranges from 5 to 8. For at least one site in each watershed, monthly discharge time series were available through the USGS National Water Information System database (USGS 2017), either at the same location as one of the temperature monitoring sites, or within 30 km on the same major reach.

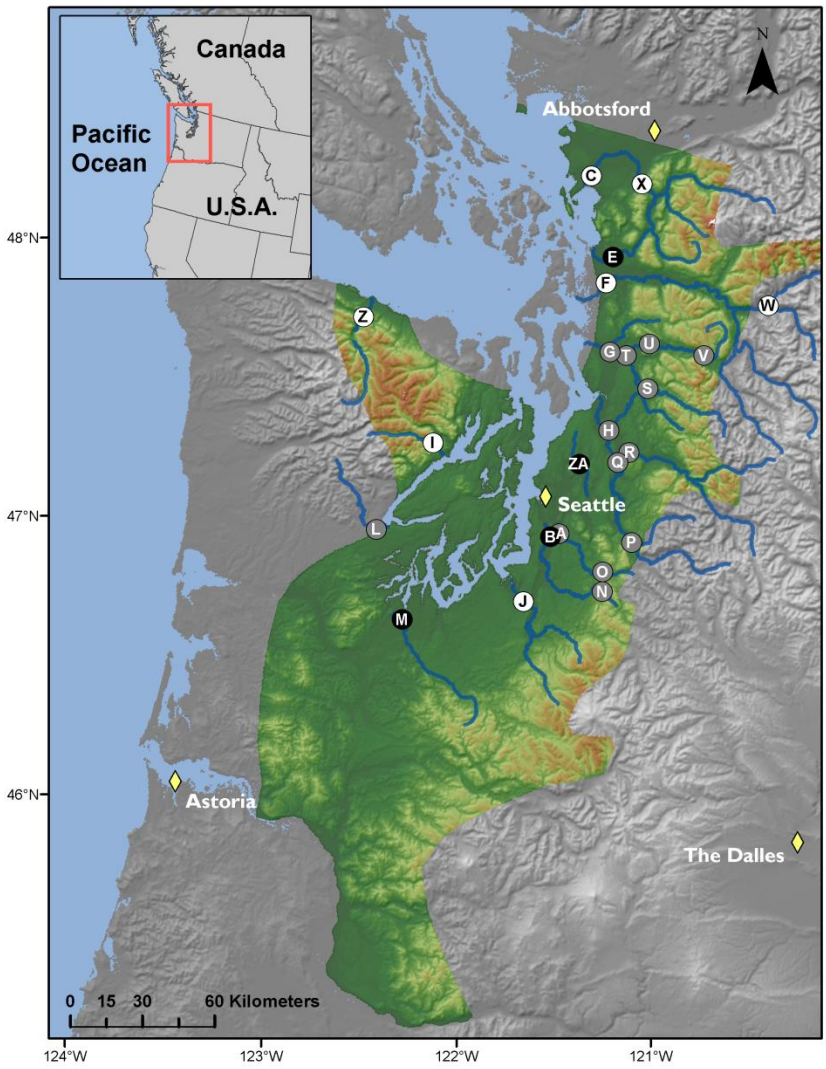

Figure 1 Site locations in relation to combined Washington State climate divisions 3 and 4 (colored topography), the region across which climate data were aggregated. See Appendix C for site information.

Potential climatic predictors of T_{water} and Q included mean and max T_{air} (°C), total precipitation (cm), and snowmelt (cm). All were incorporated as time series matching the span and temporal grain of the T_{water} and Q data. T_{air} and precipitation were available through the U.S. Climate Divisional Dataset, developed by the National Centers for Environmental Information (NCEI; NOAA 2017), and were

aggregated across two Washington State climate divisions (Puget Sound Lowland and East Olympic/Cascade Foothills; colored topography in Figure 1). Snowmelt was derived from snow water equivalent (SWE) data from six SNOTEL sites (Bumping Ridge, Elbow Lake, Mount Crag, Park Creek Ridge, Stevens Pass, White Pass) listed by the USDA's Natural Resources Conservation Service (USDA 2017). We calculated snowmelt for each site as the absolute value of negative differences in cumulative SWE from each time point to the next. The snowmelt time series was assigned zeros for any positive differences (accumulations).

Time series analysis

Response time series (T_{water} and Q) were modeled using dynamic factor analysis (DFA; Zuur et al. 2003b), a multivariate technique partly analogous to principal component analysis in the time domain. In DFA, response time series are fit with a linear combination of predictors (which can exert unique effects on each response series), model-derived latent trends (which represent additional, unspecified but shared sources of variation), and random error. Each latent trend is generated as a random walk, and may explain variation in multiple response series, such that the number of latent, “shared” trends required to model each response is much smaller than the number of responses. In effect this reduces the dimensionality of predictor data required to model a multivariate system.

We chose DFA over a basic state space approach for two reasons. First, it provides advantages in computational efficiency, as a small number of shared trends often adequately capture variation across dozens of responses, and at much lower parameter cost (Zuur et al. 2003a). Second, in terms of identifying what drives the shared trends, having fewer of them allows for greater inferential parsimony. Being a multivariate technique, DFA also provides an advantage over univariate alternatives in that covariance structure among responses can be specified and compared. All models were fit using maximum likelihood estimation by automatic differentiation, with Template Model Builder software (Kristensen et al. 2015), which we called using package TMB in R (R Core Team 2017, Kristensen et al. 2016).

DFA takes the following form:

$$\mathbf{x}_t = \mathbf{x}_{t-1} + \mathbf{w}_t, \text{where } \mathbf{w}_t \sim \text{MVN}(0, \mathbf{Q}) \quad (1)$$

$$\mathbf{y}_t = \mathbf{Z}\mathbf{x}_t + \mathbf{D}\mathbf{d}_t + \mathbf{v}_t, \text{where } \mathbf{v}_t \sim \text{MVN}(0, \mathbf{R}) \quad (2)$$

$$\mathbf{x}_0 \sim \text{MVN}(0, \mathbf{\Lambda}) \quad (3)$$

At time step *t*, the m*1 vector of shared trends (**x**) is a function of **x** in the previous step, plus normal error (**w**; m*1; Eq. 1). This is the definition of a random walk. The n*1 response vector (**y**) at time *t* is a function of the shared trends and their factor loadings (**Z**; n*m), covariates (**d**; q*1) and their river-specific effects (**D**; n*q), and a second normal error term (**v**; n*1; Eq. 2). **R** and **Q** are variance-covariance matrices of order m, and **Q** is set to identity for model identifiability (Harvey 1990). The initial state of the shared trend vector ($\mathbf{x_0}$) is multivariate-normally distributed with a mean of zero and a diagonal variance-covariance matrix with large variance (e.g. 5; $\mathbf{\Lambda}$; Eq. 3). Response and predictor data were standardized to facilitate comparison of effect sizes and avoid error inflation.

Because we were interested in isolating the effects of climatic predictors on T_{water} and Q, we used a fixed factor to account for recurring seasonal variation not related to the predictors, with one factor level for each month. This factor was incorporated into the covariate matrix (**d**). Thus, the coefficient in **D** relating, say, precipitation (predictor) and T_{water} (response), represents the effect size of the former on the latter. In other words, it is the change in water temperature accompanying a unit change in precipitation across the whole time series. We call this relationship “coupling.” We were also interested in coupling by month for T_{air}, which required that it be arranged as twelve separate, monthly time series. Concretely,

$$
\mathbf{d} = \begin{array}{c} \\ 1 \\ 2 \\ 3 \\ \\ 12 \\ 13 \\ 14 \\ 15 \\ 16 \\ 17 \\ \\ 26 \end{array}
\begin{array}{c}
\begin{array}{ccccc} \text{Jan}_{1978} & \text{Feb}_{1978} & \text{Mar}_{1978} & \cdots & \text{Dec}_{2015} \end{array} \\
\begin{pmatrix}
1 & 0 & 0 & \cdots & 0 \\
0 & 1 & 0 & \cdots & 0 \\
0 & 0 & 1 & \cdots & 0 \\
\vdots & \vdots & \vdots & \ddots & \vdots \\
0 & 0 & 0 & \cdots & 1 \\
precip_1 & precip_2 & precip_3 & \cdots & precip_{456} \\
snowmelt_1 & snowmelt_2 & snowmelt_3 & \cdots & snowmelt_{456} \\
air_1 & 0 & 0 & \cdots & 0 \\
0 & air_2 & 0 & \cdots & 0 \\
0 & 0 & air_3 & \cdots & 0 \\
\vdots & \vdots & \vdots & \ddots & \vdots \\
0 & 0 & 0 & \cdots & air_{456}
\end{pmatrix}
\end{array}
$$

is the covariate matrix structure necessary to account for seasonal variation of unknown origin (rows 1-12), and the effects of precipitation (row 13) and snowmelt (row 14), while also yielding the effect of T_{air} by month (rows 15-26) on the response (**y**; Eq. 2). This is the covariate structure of the T_{water} model we used for subsequent analyses, not including those described in Figure 5d-e, and Appendix B. The same form was used for the Q model. We refer to this as the "full" model form, versus the "reduced" form, described in the following section.

Additional variation due to unknown factors manifests in the shared trends, which represent patterns in the response data that are shared among sites but are not attributable to the specified predictors (i.e. T_{air}, precipitation, and snowmelt). Finally, leftover residual variation is absorbed by error matrix **v**.

We used AIC to find the most parsimonious model while varying the number of shared trends and the error structure among responses. We included four alternative error structures (**R** in equation 2) to allow for multiple suites of unknown drivers affecting rivers, namely shared variance with zero covariance, individual variance with zero covariance, shared variance with shared covariance, and individual variance with individual covariance. Details on these structures and their implications can be found in Holmes et al. (Holmes et al. 2012). Under AIC, negligible likelihood improvements can be inflated when multiplied by

thousands of data points, undermining common rules of thumb for admitting additional parameters (Burnham & Anderson 2003). Thus, we had reason to doubt that the "most parsimonious" model according to AIC alone was any better than a much simpler alternative. To manage this, we required that each additional trend, covariate, or seasonal structure improve the median coefficient of determination (R^2) by at least 1% in order to justify accepting its attendant complexity.

Landscape predictors and post-hoc regression

For post-hoc analyses, monitoring sites were separated into three classes based on relative areal coverage of perennial ice and snow (hereinafter "% glaciation") and mean elevation across their watersheds. The three classes are loosely based on the classification schemes and language of Reidy Liermann et al. (2012) and the Climate Impacts Group at the University of Washington (Mauger et al. 2015), and are here delineated according to Table 1.

Table 1 Watershed classification scheme.

Class	Abb.	Glaciation (%)	Mean elev. (m)
Rain-dominated	RD	< 0.7	< 600
Rain-and-snow	RS	< 0.7	≥ 600
Snow-dominated	SD	≥ 0.7	-

After model selection, climatic predictor effect sizes (**D**; Eq. 2) for each river were back-transformed to their original scales and regressed against multiple landscape predictors (Appendix C) in order to identify watershed-scale controls on coupling. Landscape predictors were compiled individually for each of the watersheds corresponding to our 24 river sites, using the EPA's StreamCat (stream-catchment) data library (Hill et al. 2016) and the National Hydrography Dataset (NHDPlusV2; McKay et al. 2012). Each site was mapped to an individual river reach, defined as a segment bounded on each end by a stream or river source, confluence, or mouth. The region contributing flow to this reach (its watershed) was then fetched, along with selected areal data, from the NHDPlusV2 database. Landscape attributes used as predictors were aggregated by watershed mean where applicable, and include elevation (m), total area (km^2), soil permeability (cm hr^{-1}), water table depth (cm), bedrock depth (cm), Base Flow Index (BFI; %), runoff (mm mo^{-1}), percent perennial ice and snow coverage (National Land Cover Database

[NLDC] 2006 and 2011 average), riparian population density (people km^{-2} within 100m of streams; 2010 census), riparian road density (km km^{-2}; 2010 census), and percent riparian urban land (NLCD 2011). Monitoring site elevation (m) and presence of upstream dams (as full/partial/no damming of upstream mainstem and major tributaries) were also included. Finally, we calculated area above 1000 m (as % watershed area), mean slope (% rise), and mean aspect (degree from true north) by delineating and summarizing watersheds from a digital elevation model in ArcMap v. 10.4 (ESRI 2016).

An additional set of post-hoc regressions was performed using factor loadings on shared trends (**Z**; Eq.2) as dependent variables, with landscape predictors again as independent variables. Loadings represent the degree to which each river's temperature fluctuates with an unknown force driving the corresponding shared trend. A landscape feature that varies in proportion to these loadings may therefore be a mediator or correlate of the unknown driver, or the driver itself. To facilitate inference by way of the shared trends we used a “reduced” model form, based on three simplifications to the full model. We removed the monthly factor and the snowmelt predictor from the covariate matrix (**d**, rows 1-12 and 14) so that the trends would be free to express seasonal and elevational variation. Then, we limited the number of trends to between one and three, to avoid “trend specialization.” In other words, we optimized the trends for flexibility while concentrating their explanatory power. Additionally, we ordinated the landscape predictors via principal coordinates analysis (PCoA) in order to reduce dimensionality. Data constrained to irregular, restricted ranges were scaled to [0-1] and arcsine-squareroot transformed, along with all proportional data (The logit transform was avoided to prevent generation of infinite values.). All continuous data were then centered and scaled to unit variance before PCoA was performed. We used the Gower dissimilarity coefficient (Gower's distance) to account for association among both continuous and nominal variables (Gower 1966).

Results

The response of river and stream water temperature to seasonal air temperature changes varied depending on whether rain, snow, or rain and snow dominated hydrology. Mean monthly temperature trends for the three river classes, aggregated across all 38 years of data, deviated by a minimum of 1.0°C in December, and a maximum of 3.9°C in July (Figure 2). SD rivers remained approximately two degrees colder than their RS counterparts through mid-late summer, and 3-4 degrees colder than RD throughout spring and summer. RD rivers were consistently warmest throughout the year. In January, RS reached a minimum of 4.4°C, and did not significantly differ from SD (Student's t: $p<0.01$, $F=11.9$). RD only attained a minimum of 5.6°C. RS reached a peak summer temperature of 16.9°C in July, while RS and SD followed in August with peak temperatures of 15.5 and 13.5°C, respectively.

Seasonal oscillations in T_{water} were smaller than those in T_{air} for all river classes. T_{air} dipped below T_{water} in autumn to a minimum of 3.2°C in December, and rose above RS and SD in March to an August maximum of 17.4°C. T_{air} did not overtake RD T_{water} until August, by which time the latter had begun to decline.

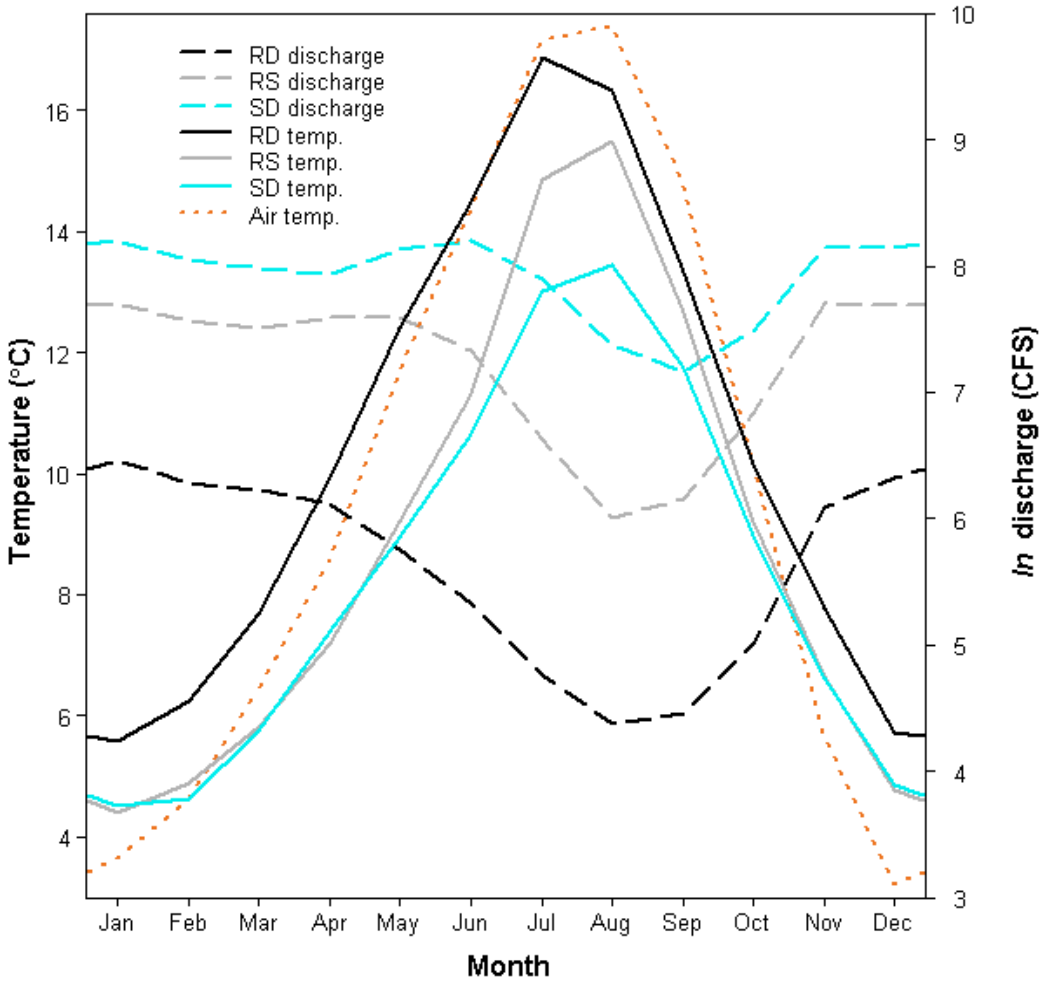

Figure 2 Monthly mean T_{water} and Q by river class, and regional T_{air}, from 1978 to 2015.

Mean absolute discharge for RD, RS, and SD across all 38 years of the time series was 583.7, 2766.9, and 5256.5 CFS, respectively. The discharge peak resulting from melting snow and ice, spanning approximately April to August, was most prominent and persisted longest in the SD rivers.

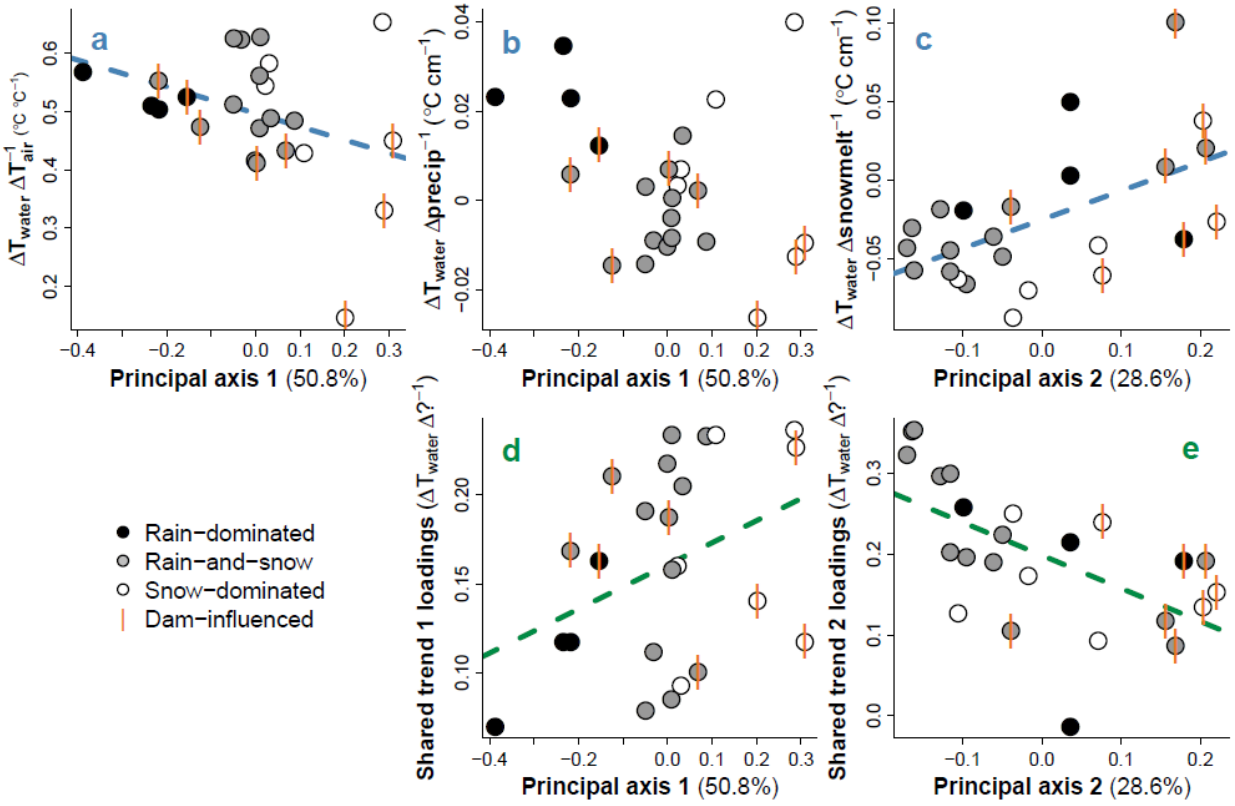
a
b
c
d
e
Principal axis 1 (50.8%)
Principal axis 2 (28.6%)
Rain−dominated
Rain−and−snow
Snow−dominated
Dam−influenced

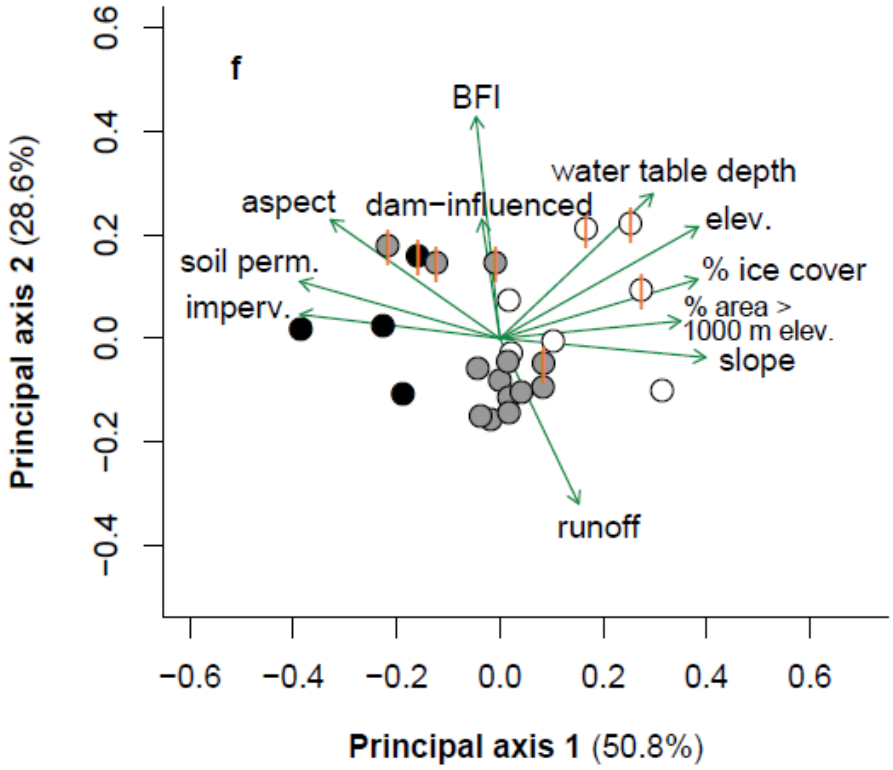
f
BFI
water table depth
aspect
dam−influenced
elev.
soil perm.
% ice cover
imperv.
% area > 1000 m elev.
slope
runoff
Principal axis 2 (28.6%)
Principal axis 1 (50.8%)

Figure 3 (a-c) Coupling between watershed elevation and climatic effects on T_{water}, obtained from full model fit. Coupling = effect size, based on proportionality at each time point. (d-e) Relationships between watershed features and factor loadings on shared trends, from constrained model fit. Regression lines indicate slopes significant at $\alpha = 0.1$. (f) Ordination of landscape predictors by principal coordinates analysis. Length and direction of arrows are proportional to loading of landscape predictors onto each principal axis of their variation. "Imperv." refers to artificial impervious surfaces and "% area > 1000 m" is a proxy for snow load. Vertical bars indicate sites with upstream dams.

The full DFA fit, comprised of the effects of all three climate covariates and five shared trends, accounted for 96% of variation among response time series (mean $R^2 = 0.964$, SD = 0.036). The effects of shared trends alone accounted for 10% of variation (mean $R^2 = 0.103$, SD = 0.042). DFA results, aggregated across months and years for each site, revealed a trend toward reduced $T_{air} \rightarrow T_{water}$ coupling with increasing loading onto principal axis 1 (marginal significance: $p = 0.08$, mult. R^2=0.13; Figure 3a). On average, a 1°C change in T_{air} corresponded to a 0.53 ± 0.03°C change in T_{water} at RD, a 0.51 ± 0.08°C change at RS, and a 0.45 ± 0.17°C change at SD sites. A similar trend was observed with respect to precip $\rightarrow T_{water}$ coupling when SD sites were excluded ($p < 0.01$, mult. $R^2 = 0.39$), but not when they were included ($p = 0.13$, mult. $R^2 = 0.10$; Figure 3b). Coupling between snowmelt and T_{water} increased with greater loading onto principal axis 2 ($p < 0.01$, mult. $R^2 = 0.30$; Figure 3c). The most parsimonious model chosen via AIC and R^2 is detailed in Appendix A.

The strongest examples of $T_{air} \rightarrow T_{water}$ and precip $\rightarrow T_{water}$ coupling were observed in the Duckabush River, while the weakest examples are from the Elwha River. Both rivers drain glaciers of the Olympic Mountain Range, and both are SD. Among SD rivers, those influenced by dams appear to couple less strongly with T_{air} and precip, but more so with snowmelt.

The reduced DFA fit accounted for 93% of variation among response time series (mean R^2 = 0.934, SD = 0.053). The effects of shared trends alone accounted for 20% of variation (mean $R^2 = 0.199$, SD = 0.059). Factor loadings from the reduced, two-trend model each correlated with one of the two principal axes of variation across landscape predictors, determined by PCoA (Figure 3f). The first

principal axis was associated mostly with mean watershed slope, snow (% area > 1000 m) and ice, soil permeability, and other features that vary along elevational gradients, as well as mean elevation itself. Watershed scores along this axis correlated with loadings from one trend, with marginal significance ($p=0.07$, mult. $R^2=0.14$; Figure 3d). The second principal axis was driven by runoff, base flow, and upstream dams, and correlated with the other trend's loadings ($p<0.01$, mult. $R^2=0.35$; Figure 3e). Combined, the first two principal axes accounted for 79.4% of variation across landscape predictors.

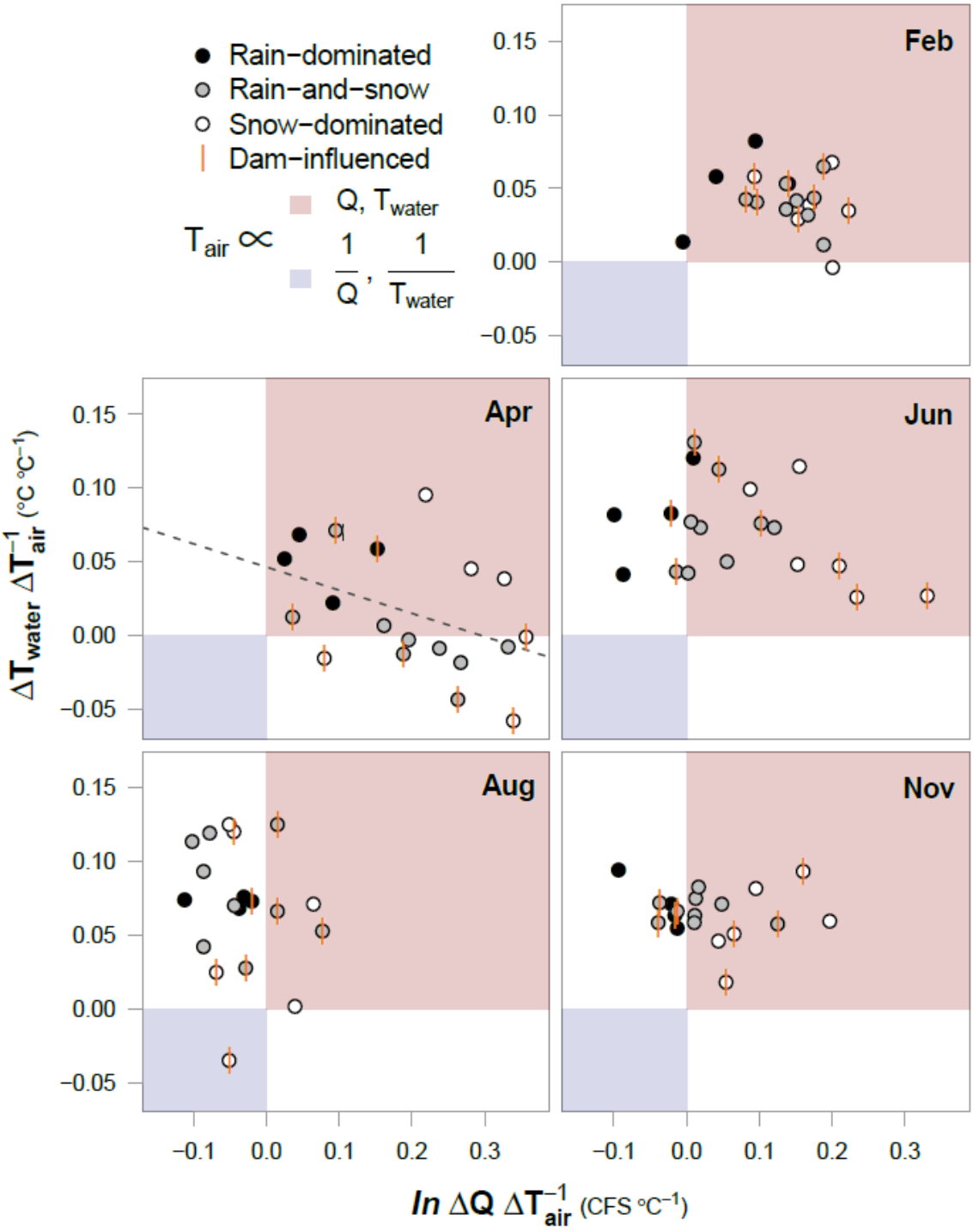

Figure 4 Relationships between $T_{air} \rightarrow T_{water}$ and $T_{air} \rightarrow Q$ coupling per month. The red quadrant designates proportionality between all three variables, the blue inverse proportionality between each response and T_{air}. Coupling = effect size, based on proportionality at each time point. Regression line indicates slope significant at alpha=0.05.

To examine possible sub-season interactions between T_{air}, T_{water} and Q, we performed an additional DFA with Q as the response. T_{air} was allowed to have unique monthly effects with respect to each response variable. These effects, taken together, can be conceptualized in relation to the four quadrants of the Cartesian coordinate system (increasing clockwise from upper right; Figure 4).

In mid-winter (exemplified by February), all river classes primarily occupy the first quadrant, signifying that T_{water} and Q both vary in proportion to T_{air}. In other words, warmer Februaries yield warmer water and higher discharge. RD shows the weakest Q response. By April, many RS and SD sites develop an inverse relationship between T_{air} and T_{water}, while RD sites change little from their winter state. There is an overall inverse relationship between $T_{air} \rightarrow Q$ and $T_{air} \rightarrow T_{water}$ coupling, with sites showing strong positive discharge responses to higher T_{air} showing correspondingly weak T_{water} responses. Early and late summer months (June and August) see a procession of most sites into the near fourth quadrant, with SD trailing. This quadrant signifies a general pattern of lower discharge and higher water T with increased air T. One stark exception is again the Elwha river, which occupies quadrant three. By autumn, RS and SD have begun progress back toward their winter states, led by SD. RD, meanwhile, remain essentially unmoved from summer.

Rivers influenced by dams do not appear to deviate appreciably from undammed systems in February, August, or November. However, SD rivers in April divide across the x-axis according to whether they are dammed. Those with dams exhibit inverse $T_{air} \rightarrow T_{water}$ coupling, while T_{air} fluctuates proportionately to T_{water} for those without. Similarly, in June, dammed SD rivers display stronger coupling between T_{air} and Q than those without dams.

Discussion

We did not detect any long-term trends in coupling between T_{air} and T_{water}; i.e. the sensitivity of T_{water} to variation in T_{air} did not change consistently across 38 years of data (Appendix B) despite trends in T_{air}, precipitation, and several rivers' individual water temperatures over the same period (Appendix D). Nonetheless, dynamic factor analysis did reveal variation among rivers and river classes in terms of T_{water} and Q sensitivity to climatic variation.

The effects of climate on T_{water} suggest that nearly all rivers included in our dataset were influenced strongly by air temperature, precipitation, and/or snowmelt across seasons (Figure 3a-c). At most monitoring sites, T_{water} closely tracked changes in T_{air}, on average responding to increases and decreases with proportional movements of 66% magnitude. However, some rivers only weakly tracked T_{air}, and patterns in the intensity of this coupling relate primarily to changing landscape features along elevational and flow-source gradients (Figure 3).

Changes in elevation coincided with variation in snow load, glaciation, and watershed slope (Figure 3f), as well as the strengths of climatic forces, resulting in a range of mean temperatures of 2.2°C across river classes, averaged over all time points. Flow also varied widely across classes, with mean discharge in SD rivers exceeding that of RD by 4673 CFS (see Figure 2). This owes largely to the fact that RD rivers must necessarily be confined to relatively small, lowland areas. One result of increased discharge and snow/ice melt, particularly in the SD rivers, is a "buffering" effect (the inverse of coupling), whereby a greater volume of flow, contributed in part by frozen stores, reduces the sensitivity of T_{water} to climatic variation in spring and early summer. Where glacial influence is high, this effect can remain throughout the summer months. In an extreme case, the Elwha River was actually cooler in August during those years in which air temperature was higher, probably due to runoff from Carrie and Eel glaciers. The buffering effect of ice on river temperature is therefore two-fold, acting first on all snowmelt-influenced rivers through a cold-water pulse in spring, and then on a subset of those rivers throughout summer and autumn, by way of glacial runoff. For RD rivers, which receive little to no input from snow or ice, summer temperature is entirely dictated by that of the surrounding air, and any rain falling through it.

Temperature buffering during warmer parts of the year by snow and ice appears to be enhanced by the action of dams. Eight sites on five rivers included in this study are (or were until 2014, in the case of the Elwha River) interrupted by dams or embankments, all of which release stored water from the bases of their reservoirs (hypolimnial release). At 33 m, even the shallowest of these reservoirs is deep enough to stratify in summer, meaning released water is delivered from a relatively cold hypolimnion (Olden & Naiman 2010). This certainly would have affected temperature readings for the Green, Elwha, Cedar and upper Skagit River sites, whose mainstems are or were dammed upstream of the sample

location. The impact of damming on temperature at the Skokomish and the lower Skagit River sites should be lesser, as major, unobstructed river forks intercede between sample location and dam, resetting or partially resetting natural conditions (Stanford & Ward 2001). These sites are RS and SD, respectively, and both fall very close to the regression line in Figure 3a. The lower Skagit site therefore occupies a middling space of $T_{air} \rightarrow T_{water}$ coupling between "fully" obstructed and unobstructed SD sites.

The role of reservoirs in restructuring natural temperature coupling relationships is complex (Webb & Walling 1997, Gooseff et al. 2005), and here confounded with many additional variables. Omitting all obstructed sites from Figure 3a, it would appear that no trend exists, yet we believe such omission is unwarranted. If the presence of reservoirs negated the influence of other factors, there would be no separation in coupling between obstructed sites of different river classes. Furthermore, though cold, hypolimnial outflow should be expected to buffer T_{water} in summer, it alone cannot explain an *inverse* relationship between T_{air} and T_{water}. Instead, reservoirs may serve to enhance the decoupling of $T_{air} \rightarrow T_{water}$ and precip. $\rightarrow T_{water}$ brought on by snowmelt and glacial runoff, by selectively withholding warm water in their epilimnia and admitting cold water through their hypolimnia. Evidence for this phenomenon can be seen in the coupling of snowmelt and T_{water}, which is generally greater in RS and SD sites downstream of obstructions (Figure 3c). The Elwha River, which was cleared of its two dams between 2011 and 2014, will provide an excellent opportunity to compare each form of coupling with and without reservoirs, using the same dataset, once enough time has passed for signals to overcome inter-annual variability.

Water temperature in the unobstructed SD sites appears to couple more strongly with both air temperature and precipitation than in the sites with upstream dams (Figure 3a, b). In particular, the Duckabush and Puyallup Rivers (uppermost white circles in Figures 3a, 3b, and 4-Apr.) show stronger coupling relationships even than many of the RD rivers. Compared to all RS and RD rivers, and many SD, these stand out in terms of mean water table depth (Appendix C), suggesting they receive little flow from groundwater, which would otherwise serve to decouple T_{air} and T_{water}. They also occupy smaller watersheds than most of the other SD rivers, which correspond with lower overall discharge and heat capacity, and thus greater susceptibility to temperature change (caissie2006thermal). There may be additional factors at work in the SD rivers that account for the surprisingly high coupling seen in some

unobstructed SD rivers. Another potential candidate is watershed slope, which increases with elevation and affects T_{water} by influencing residence time and evaporative cooling (via greater turbulence; Caissie 2006). High slope and elevation are also associated with lower-order tributaries, and thus lower heat capacity.

As regional temperatures rise and glacial ice declines (Pelto 2010, Mauger et al. 2015), currently snow-influenced rivers may take on characteristics of RD rivers in terms of both climate coupling and absolute temperature and discharge regime. This may mean greater or lesser coupling between T_{air} and T_{water} depending on the presence or absence of major dams (Figures 3a, 4-Apr.). The buffering effect of melt, and its ability to invert this coupling relationship, would be expected to decline in any case. SD rivers may see little change in the near term, as their upper reaches will still receive snow and harbor glacial ice even under mildly warmer conditions. Change may be more rapid in RS rivers, where any shift in average temperature or precipitation could substantially alter the relative contribution of rain and snow to discharge, altering both flow regime and temperature buffering capacity. Regardless of how coupling changes, we expect absolute temperature to increase for snow-influenced rivers, particularly in spring and early summer.

In addition to the most parsimonious DFA, we fit a reduced model, designed to focus on whatever variation in T_{water} could be explained by landscape predictors. The two trends of this model represent additional drivers responsible for structuring water temperature across some or all of the 24 sites included in the analysis (Figure A6). Higher loading on shared trend 1 is associated with systems with higher elevation, snow and ice melt, and slope, as well as lower permeability of soils (Figure 3f). Dams (reservoirs) and BFI (essentially groundwater and reservoir contribution) were also major components of variation in coupling, along with water table depth. Groundwater, being insulated from the air, maintains relatively constant temperatures throughout the year, particular if it is deep underground, and so reduces coupling between T_{water} and climate. These additional sources of flow are expressed by shared trend 2, which wavelet analysis revealed to contain strong 12-month periodicity (Figure E2). The trough of this periodic component occurred in spring, when dam release tends to be highest for snow-influenced rivers (Figure E3). The peak occurred in autumn, when dam release is lowest.

The relationship between climate and river temperature is further influenced by the interaction of discharge, and the fates of rivers in the Puget Sound watershed can be best understood by examining these factors in combination (Figure 4). Whether rain-, snow-, or both-dominated, all rivers appear to take on RD characteristics in winter, when the effects of ice lay dormant. As a result, warmer winters should on average yield warmer rivers and higher flow (less precipitation bound in ice). The critical differences between river classes play out in spring and summer, and it's during these months that future perturbations due to changing climate may be felt most acutely. For example, warmer Aprils on average produced colder water at 9 out of 15 RS and SD sites. Projected reductions in snowpack for the Puget Sound region (Stewart et al. 2005, Hamlet 2013) can therefore be expected to fundamentally alter the responses of currently snow-influenced rivers to yearly variation in spring temperature over the long term. In the next 100 years, changes can be expected for rivers that now receive the temperature-buffering effect of glacial runoff. Glaciers continue to decline across North America, with glacial ice across Western Canada projected to decline by 70% from 2005 to 2100 (Clarke et al. 2015), and only 3 of 13 examined North Cascades glaciers expected to survive the current climate (Pelto 2010).

Conclusion

Temperature regimes across the rivers of the Puget Sound watershed are structured by a combination of climatic drivers at the regional scale, and geophysical drivers at watershed scales. In the absence of snow and ice, river temperature is closely coupled to that of the surrounding air, while discharge contributions from snowmelt and glacial runoff can dampen or even reverse this coupling in spring and summer, particularly where hypolimnial-release reservoirs augment downstream cooling. In some cases, icemelt-influenced rivers exhibit stronger positive responses to climate patterns than their rain-driven counterparts. Our results suggest elevational variations in groundwater influx and total discharge may account for these patterns. However, while these factors and artificial reservoirs may influence the degree of coupling between climatic drivers and water temperature, only snow and ice can reverse it. Since 1978, such reversals have been widespread and commonplace, particularly during spring melt. Though we did not detect changes in this effect across historical observations, future reductions in snowpack and glacial

mass are projected. Consequently, many rivers that now undergo the mildest seasonal temperature changes may be impacted most strongly.

Acknowledgements

We thank Timothy Cline for the use of his TMB script, and Mark Scheuerell, Eric Ward, Eli Holmes, Jan Ohlberger, and Adrianne Smits for technical advice. Daniel Schindler and Michael Brett provided additional suggestions and guidance.

References

ArcMap. (2016). Environmental Systems Research Institute (ESRI). Redlands, CA: http://www.esri.com.

Beechie, T. J., Moir, H., & Pess, G. (2008). Hierarchical Physical Controls on Salmonid Spawning Location and Timing. In American Fisheries Society Symposium (Vol. 65, pp. 83–101).

Berman, C. H., & Quinn, T. P. (1991). Behavioural thermoregulation and homing by spring chinook salmon, Oncorhynchus tshawytscha (Walbaum), in the Yakima River. Journal of Fish Biology, 39(3), 301–312.

Boisneau, C., Moatar, F., Bodin, M., & Boisneau, P. (2008). Does global warming impact on migration patterns and recruitment of Allis shad (Alosa alosa L.) young of the year in the Loire River, France? Hydrobiologia, 602(1), 179–186. http://doi.org/10.1007/s10750-008-9291-6

Boscarino, B. T., Rudstam, L. G., Mata, S., Gal, G., Johannsson, O. E., & Mills, E. L. (2007). The effects of temperature and predator-prey interactions on the migration behavior and vertical distribution of Mysis relicta. Limnology and Oceanography, 52(4), 1599–1613. http://doi.org/10.4319/lo.2007.52.4.1599

Brutsaert, W. (1975). A theory for local evaporation (or heat transfer) from rough and smooth surfaces at ground level. Water Resources Research, 11(4), 543–550.

Bunn, S. E., & Arthington, a H. (2002). Basic Principles and Ecological Consequences of Altered Flow Regimes for Aqatic Biodiversity. Environmental Management, 30(4), 492–507. http://doi.org/10.1007/s00267-002-2737-0

Burnham, K. P., & Anderson, D. R. (2003). Model selection and multimodel inference: a practical information-theoretic approach. Springer Science & Business Media.

Caissie, D. (2006). The thermal regime of rivers: a review. Freshwater Biology, 51(8), 1389–1406.

Carter, K. (2005). The effects of temperature on steelhead trout, coho salmon, and Chinook salmon biology and function by life stage. Implications for the Klamath River Total Maximum Daily Loads. California Regional Water Quality Control Board. North Coast Region, Santa Rosa, California.

Clarke, G. K. C., Jarosch, A. H., Anslow, F. S., Radić, V., & Menounos, B. (2015). Projected deglaciation of western Canada in the twenty-first century. Nature Geoscience, 8(5), 372–377. http://doi.org/10.1038/ngeo2407

Eldridge, E. F. (1967). Water temperature: influences, effects, and control.

Garner, G., Hannah, D. M., Sadler, J. P., & Orr, H. G. (2014). River temperature regimes of England and Wales: Spatial patterns, inter-annual variability and climatic sensitivity. Hydrological Processes, 28(22), 5583–5598. http://doi.org/10.1002/hyp.9992

Gooseff, M. N., Strzepek, K., & Chapra, S. C. (2005). Modeling the potential effects of climate change on water temperature downstream of a shallow reservoir, Lower Madison River, MT. Climatic Change, 68(3), 331–353.

Gower, J. C. (1966). Some distance properties of latent root and vector methods used in multivariate analysis. Biometrika, 53(3–4), 325–338. http://doi.org/10.1093/biomet/53.3-4.325

Hamlet, A. F., Elsner, M. M., Mauger, G. S., Lee, S.-Y., Tohver, I., & Norheim, R. A. (2013). An Overview of the Columbia Basin Climate Change Scenarios Project: Approach, Methods, and Summary of Key Results. Atmosphere-Ocean, 51(4), 392–415. http://doi.org/10.1080/07055900.2013.819555

Harvey, A. C. (1990). Forecasting, structural time series models and the Kalman filter. Cambridge university press.

Hill, R. A., Weber, M. H., Leibowitz, S. G., Olsen, A. R., & Thornbrugh, D. J. (2016). The Stream-Catchment (StreamCat) Dataset: A Database of Watershed Metrics for the Conterminous United States. JAWRA Journal of the American Water Resources Association, 52(1), 120–128.

Holmes, E. E., Ward, E. J., & Wills, K. (2012). MARSS: Multivariate Autoregressive State-space Models for Analyzing Time-series Data. The R Journal, 4(1), 11–19. Retrieved from https://journal.r-project.org/archive/2012-1/RJournal_2012-1_Holmes~et~al.pdf

Huryn, A. D., & Wallace, J. B. (2000). Life History and Production of Stream Insects. Annual Review of Entomology, 45(1), 83–110. http://doi.org/10.1146/annurev.ento.45.1.83

Kristensen, K., Nielsen, A., Berg, C. W., Skaug, H., & Bell, B. (2015). TMB: Automatic Differentiation and Laplace Approximation. arXiv Preprint arXiv:1509.00660. http://doi.org/10.18637/jss.v070.i05

Kristensen, K., Nielsen, A., Berg, C. W., Skaug, H., & Bell, B. M. (2016). {TMB}: Automatic Differentiation and {L}aplace Approximation. Journal of Statistical Software, 70(5), 1–21. http://doi.org/10.18637/jss.v070.i05

Lehmkuhl, D. (1974). Thermal regime alteration and vital environmental physiological signals in aquatic organisms. In Thermal ecology. INTIS [National Technical Information … (Vol. 730505, pp. 116–222). Retrieved from http://www.famu.org/mayfly/pubs/pub_l/publehmkuhld1974p216.pdf%5Cnpapers2://publication/uuid/40173C8E-BE69-4C58-B258-31A965B8C94F

Lisi, P. J., Schindler, D. E., Bentley, K. T., & Pess, G. R. (2013). Association between geomorphic attributes of watersheds, water temperature, and salmon spawn timing in Alaskan streams. Geomorphology, 185, 78–86. http://doi.org/10.1016/j.geomorph.2012.12.013

Lisi, P. J., Schindler, D. E., Cline, T. J., Scheuerell, M. D., & Walsh, P. B. (2015). Watershed geomorphology and snowmelt control stream thermal sensitivity to air temperature. Geophysical Research Letters, 42(9), 3380–3388.

Mauger, G. S., Casola, J. H., Morgan, H. A., Strauch, R. L., Jones, B., Curry, B., Isaksen Busch, TM, … . (2015). State of Knowledge: Climate Change in Puget Sound. Climate Impacts Group, University of Washington, Seattle. http://doi.org/10.7915/CIG93777D

McCullough, D. a. (1999). A Review and Synthesis of Effects of Alterations to the Water Temperature Regime on Freshwater Life Stages of Salmonids, with Special Reference to Chinook Salmon. Environmental Protection Agency. US Environmental Protection Agency, Region 10. http://doi.org/10.1017/CBO9781107415324.004

McKay, L., Bondelid, T., Dewald, T., Johnston, J., Moore, R., & Reah, A. (2012). NHDPlus Version 2 User Guide. National Operational Hydrologic Remote Sensing Center, Washington, DC, accessed October 2015. Retrieved from ftp://ftp.horizonsystems.com/NHDPlus/NHDPlusV21/Documentation/NHDPlus-V2_User_Guide.pdf

Mote, P. W., & Salathe Eric P., J. (2010). Future climate in the Pacific Northwest. Climate Change, 102(1–2), 29–50.

Munn, M. D., & Brusven, M. A. (1991). Benthic macroinvertebrate communities in nonregulated and regulated waters of the Clearwater River, Idaho, USA. River Research and Applications, 6(1), 1–11.

NOAA. (2017). National Centers for Environmental Information, Climate at a Glance: U.S. Time Series.

Olden, J. D., & Naiman, R. J. (2010). Incorporating thermal regimes into environmental flows assessments: Modifying dam operations to restore freshwater ecosystem integrity. Freshwater Biology, 55(1), 86–107. http://doi.org/10.1111/j.1365-2427.2009.02179.x

Pelto, M. S. (2010). Forecasting temperate alpine glacier survival from accumulation zone observations. The Cryosphere, 4(1), 67–75. http://doi.org/10.5194/tc-4-67-2010

Peterson, J. T., & Rabeni, C. F. (1996). Natural thermal refugia for temperate warmwater stream fishes. North American Journal of Fisheries Management, 16(4), 738–746. http://doi.org/10.1577/1548-8675(1996)016<0738:NTRFTW>2.3.CO;2

Poole, G. C., & Berman, C. H. (2001). An ecological perspective on in-stream temperature: natural heat dynamics and mechanisms of human-causedthermal degradation. Environmental Management, 27(6), 787–802.

R Core Team. (2017). R: A Language and Environment for Statistical Computing. Vienna, Austria. Retrieved from https://www.r-project.org/

Radeloff, V. C., Nelson, E. J., Plantinga, A., Lewis, D. J., Helmers, D. P., Lawler, J. J., … Polasky, S. (2012). Economic-based projections of future land use in the conterminous United States under alternative policy scenarios. Ecological Applications, 22(3), 1036–1049. http://doi.org/10.1890/11-0306.1

Reidy Liermann, C. A., Olden, J. D., Beechie, T. J., Kennard, M. J., Skidmore, P. B., Konrad, C. P., & Imaki, H. (2012). Hydrogeomorphic classification of Washington State River to support emerging environmental flow management strategies. River Research and Applications, 28(9), 1340–1358. http://doi.org/10.1002/rra.1541

Roesch, A., & Schmidbauer, H. (2014). WaveletComp: Computational Wavelet Analysis. Retrieved from https://cran.r-project.org/package=WaveletComp

Rørslett, B., Mjelde, M., & Johansen, S. W. (1989). Effects of hydropower development on aquatic macrophytes in Norwegian rivers: present state of knowledge and some case studies. River Research and Applications, 3(1), 19–28.

Sanders, J. E., Pilcher, K. S., & Fryer, J. L. (1978). Relation of water temperature to bacterial kidney disease in coho salmon (Oncorhynchus kisutch), sockeye salmon (O. nerka), and steelhead trout

(Salmo gairdneri). Journal of the Fisheries Research Board of Canada, 35(1954), 8–11. Retrieved from files
Smith, K. (1972). River water temperatures - an environmental review. Scottish Geographical Magazine, 88(3), 211–220. http://doi.org/10.1080/00369227208736229
Stanford, J. A., & Ward, J. V. (2001). Revisiting the serial discontinuity concept. Regulated Rivers: Research & Management, 17(4–5), 303–310. http://doi.org/10.1002/rrr.659
Stewart, I. T., Cayan, D. R., & Dettinger, M. D. (2005). Changes toward earlier streamflow timing across western North America. Journal of Climate, 18(8), 1136–1155. http://doi.org/10.1175/JCLI3321.1
USDA. (2017). National Resources Conservation Service.
USGS. (2017). National Water Information System.
van Vliet, M. T. H., Franssen, W. H. P., Yearsley, J. R., Ludwig, F., Haddeland, I., Lettenmaier, D. P., & Kabat, P. (2013). Global river discharge and water temperature under climate change. Global Environmental Change-Human and Policy Dimensions, 23(2), 450–464. http://doi.org/10.1016/j.gloenvcha.2012.11.002
Vinson, M. R., & Hawkins, C. P. (1998). Biodiversity of Stream Insects: Variation at Local, Basin, and Regional Scales. Annual Review of Entomology, 43(1), 271–293. http://doi.org/10.1146/annurev.ento.43.1.271
Von Prause, M. (2017). River and Stream Water Quality Monitoring program.
Ward, E. (2017, March). nwfsc-timeseries/statss: Initial release for time series class. http://doi.org/10.5281/zenodo.375646
Ward, J. (1985). Thermal characteristics of running waters. In Hydrobiologia (Vol. 125, pp. 31–46). Springer.
Webb, B. W., & Walling, D. E. (1997). Complex summer water temperature behaviour below a UK regulating reservoir. Regulated Rivers: Research & Management, 13(5), 463–477. http://doi.org/10.1002/(SICI)1099-1646(199709/10)13:5<463::AID-RRR470>3.0.CO;2-1
Wulf, H., Bookhagen, B., & Scherler, D. (2016). Differentiating between rain, snow, and glacier contributions to river discharge in the western Himalaya using remote-sensing data and distributed hydrological modeling. Advances in Water Resources, 88, 152–169.
Zhong, Y., & Power, G. (1996). Environmental impacts of hydroelectric projects on fish resources in China. River Research and Applications, 12(1), 81–98.
Zuur, A. F., Tuck, I. D., & Bailey, N. (2003a). Dynamic factor analysis to estimate common trends in fisheries time series. Canadian Journal of Fisheries and Aquatic Sciences, 60(5), 542–552. http://doi.org/10.1139/f03-030
Zuur, A. F., Fryer, R. J., Jolliffe, I. T., Dekker, R., & Beukema, J. J. (2003b). Estimating common trends in multivariate time series using dynamic factor analysis. Environmetrics, 14(7), 665–685. http://doi.org/10.1002/env.611

Appendix A

Temperature DFA output and diagnostics

The process of selecting the best T_{water} and discharge models involved three climate covariates (air temperature, precipitation, and snowmelt), between 1 and 15 shared trends, four within-and-among-site error structures (see methods), and two expressions of unknown seasonal variation (fixed monthly factors and Fourier series). The most parsimonious models were selected using the Akaike Information Criterion (AIC) in tandem with R^2 (required increase of 0.01 for each additional parameter), and in each case included air temperature, precipitation, and snowmelt as covariates, as well as five shared trends. Both models included an independent and unequally distributed error structure among rivers (i.e. diagonal and unequal variance-covariance matrix). All subsequent plots relate to the T_{water} model, and alphabetic names correspond to sampling sites (Figure 1, Table C1).

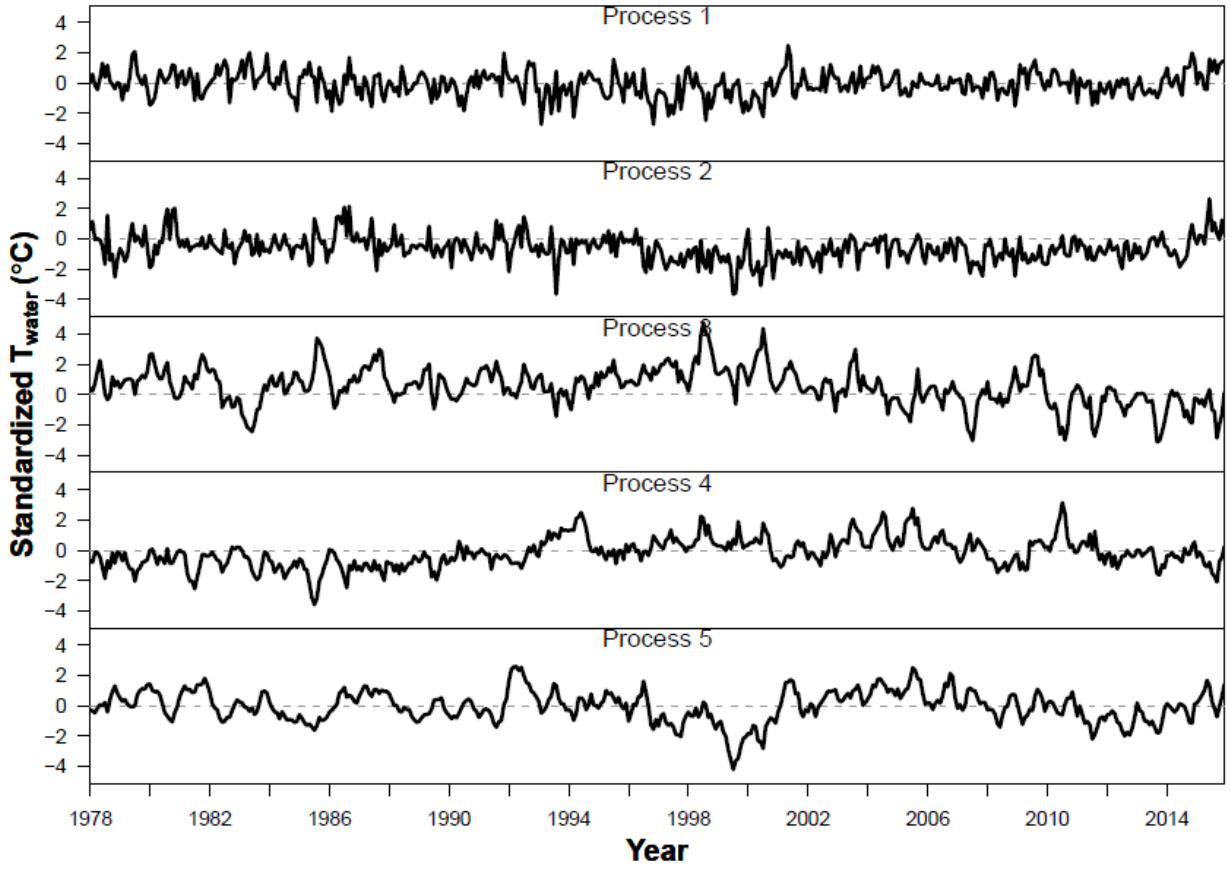

Figure A1 Shared trends from full T_{water} model.

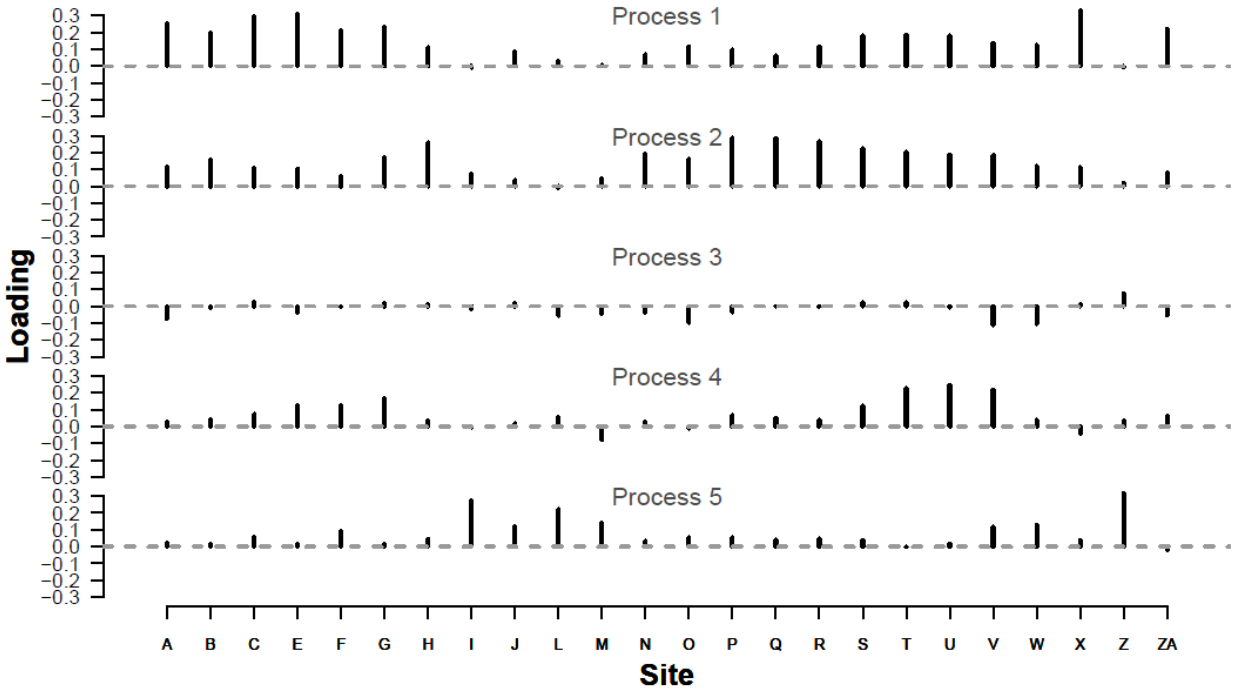

Figure A2 Factor loadings on shared trends from full T_{water} model.

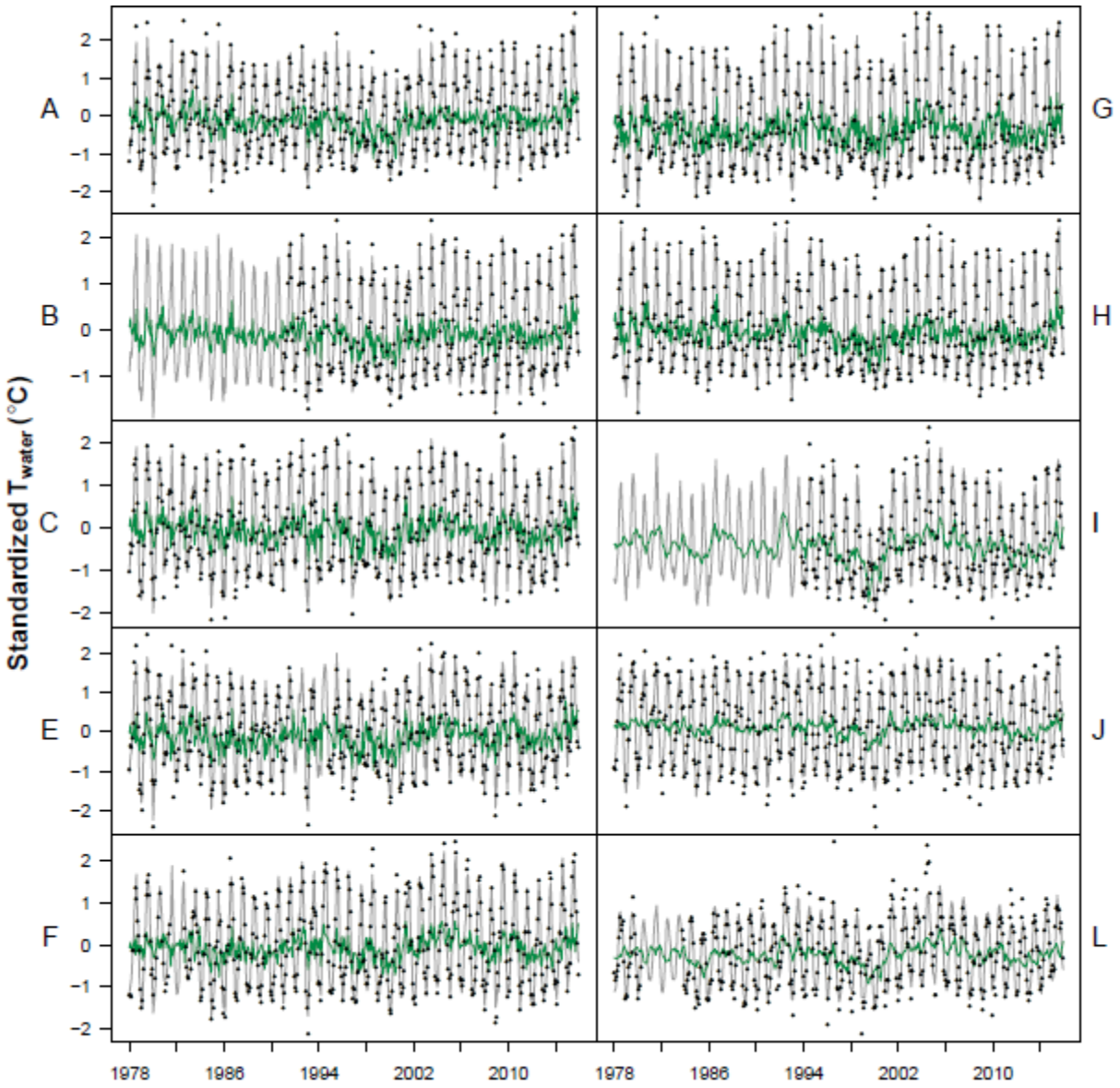
Standardized T_{water} (°C)
A
B
C
E
F
G
H
I
J
L
2
1
0
−1
−2
1978
1986
1994
2002
2010

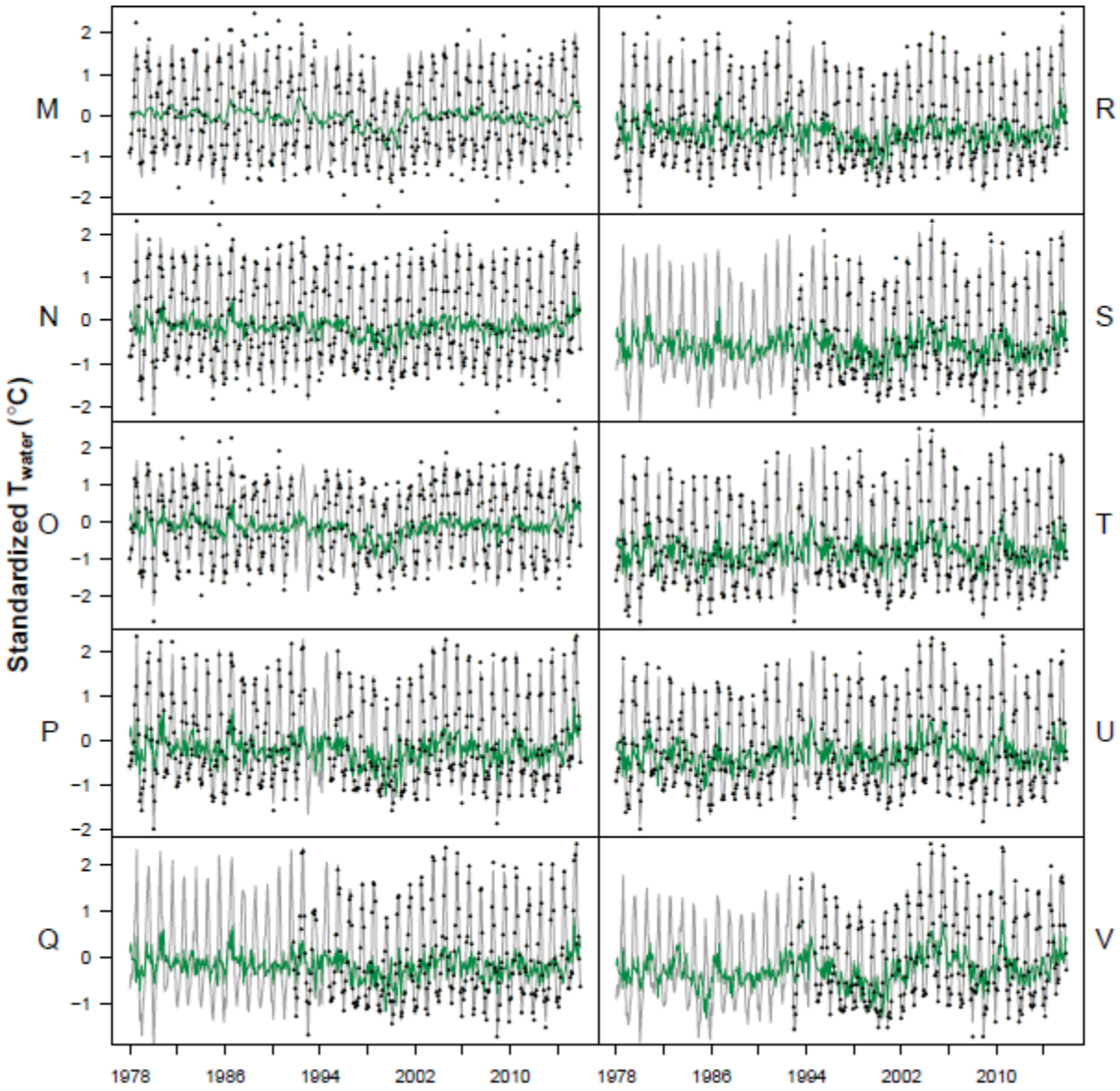
Standardized T_{water} (°C)
M
N
O
P
Q
R
S
T
U
V
2
1
0
−1
−2
1978
1986
1994
2002
2010

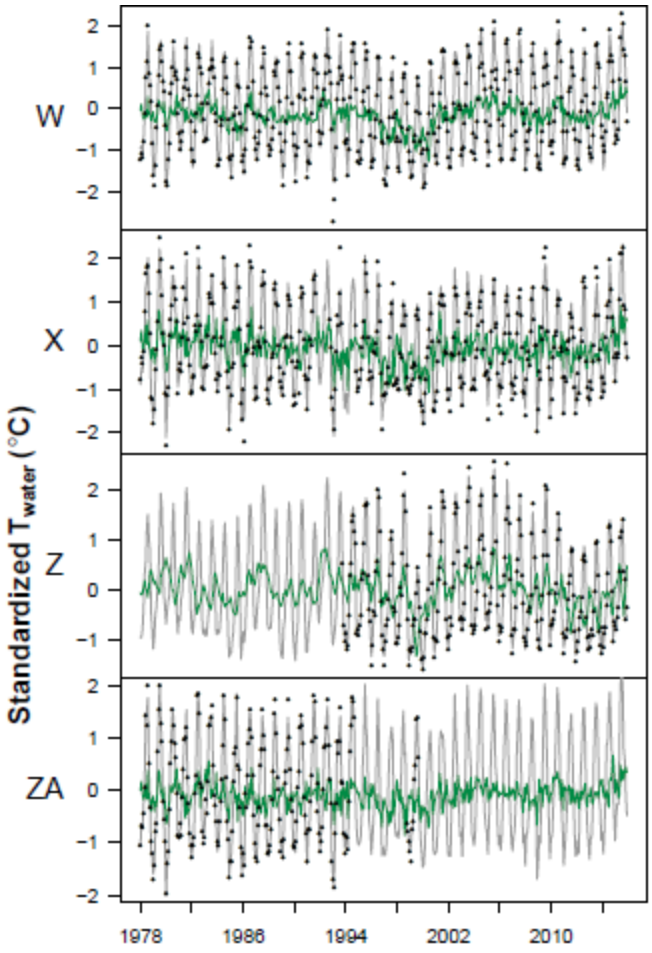

Figure A3 Full T_{water} model fits (gray line = overall fit; green line = shared-trend-only fit).

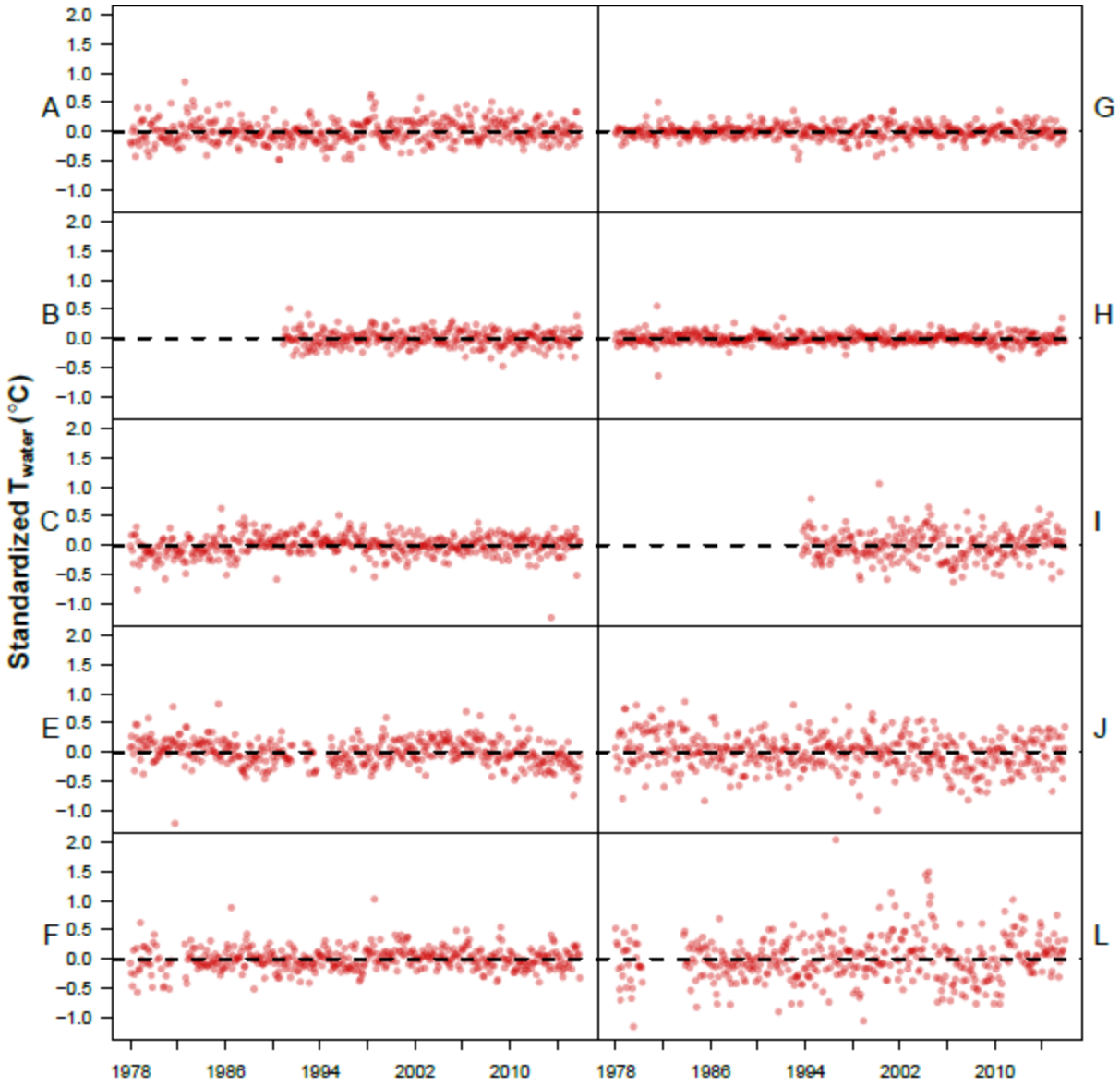
Standardized T_{water} (°C)
A
B
C
E
F
G
H
I
J
L
2.0
1.5
1.0
0.5
0.0
−0.5
−1.0
1978
1986
1994
2002
2010

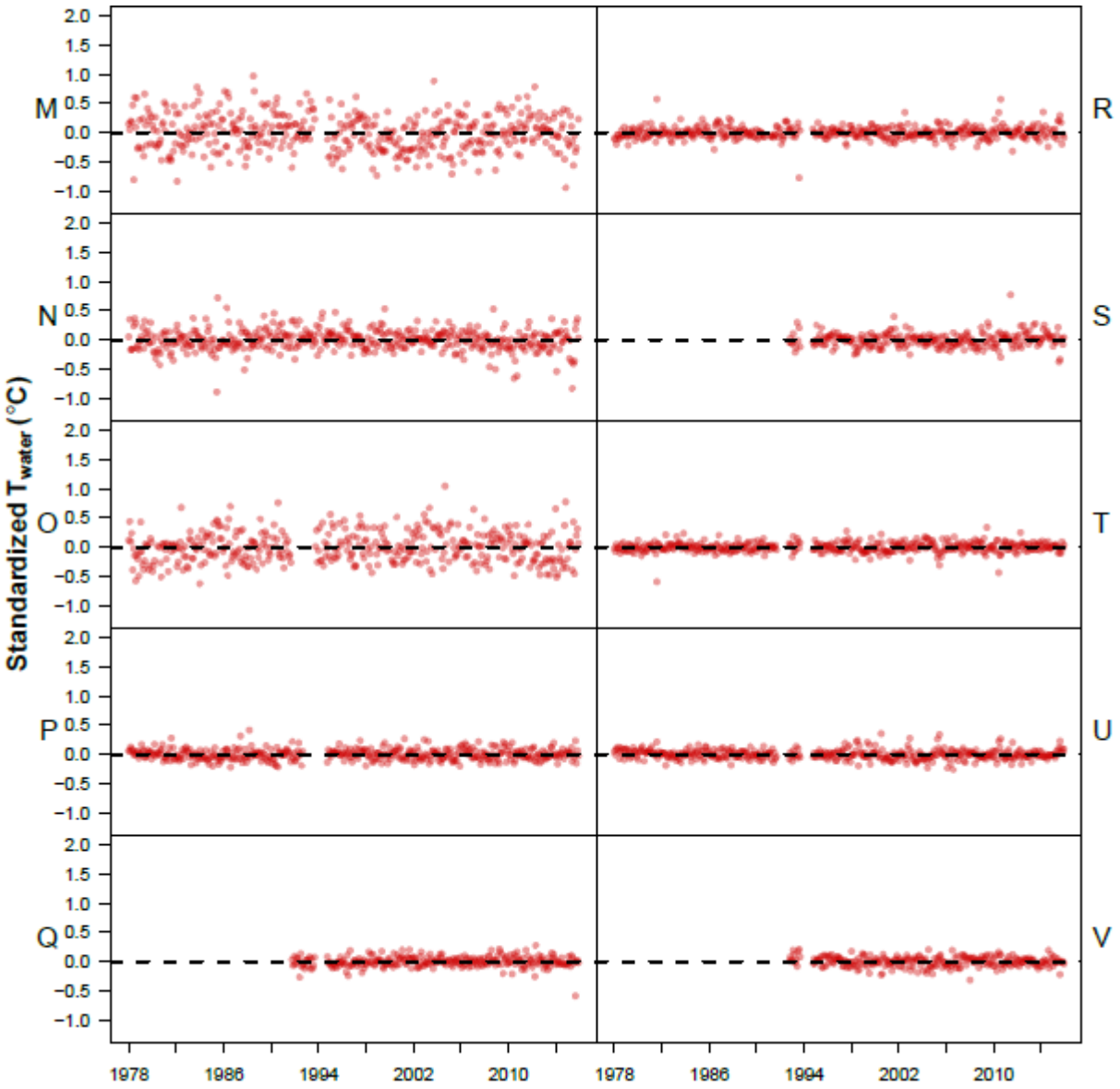
Standardized T_{water} (°C)
M
N
O
P
Q
R
S
T
U
V
2.0
1.5
1.0
0.5
0.0
−0.5
−1.0
1978
1986
1994
2002
2010

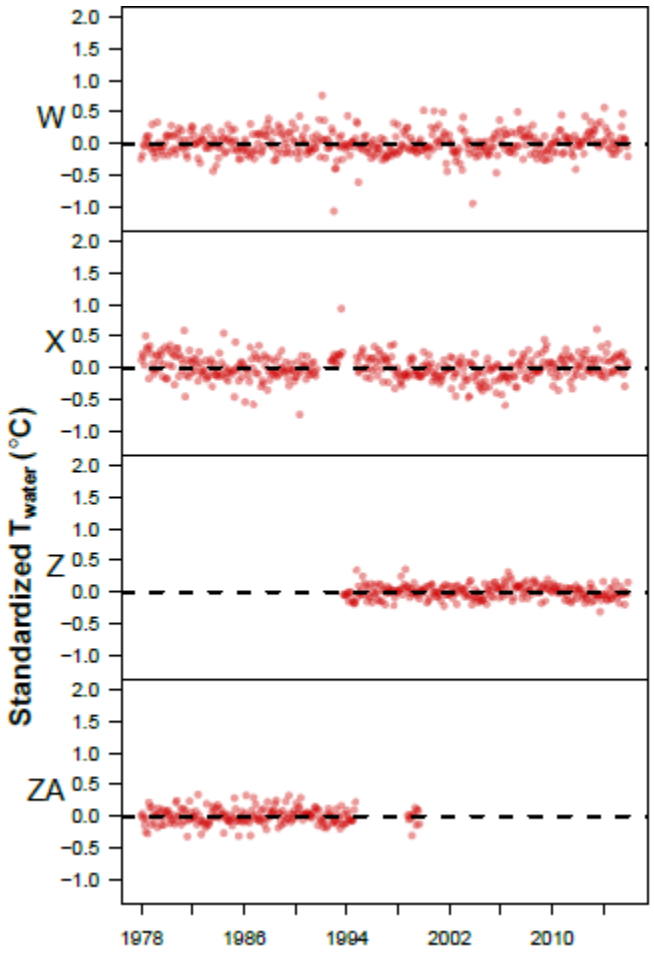

Figure A4: Full T_{water} model residuals.

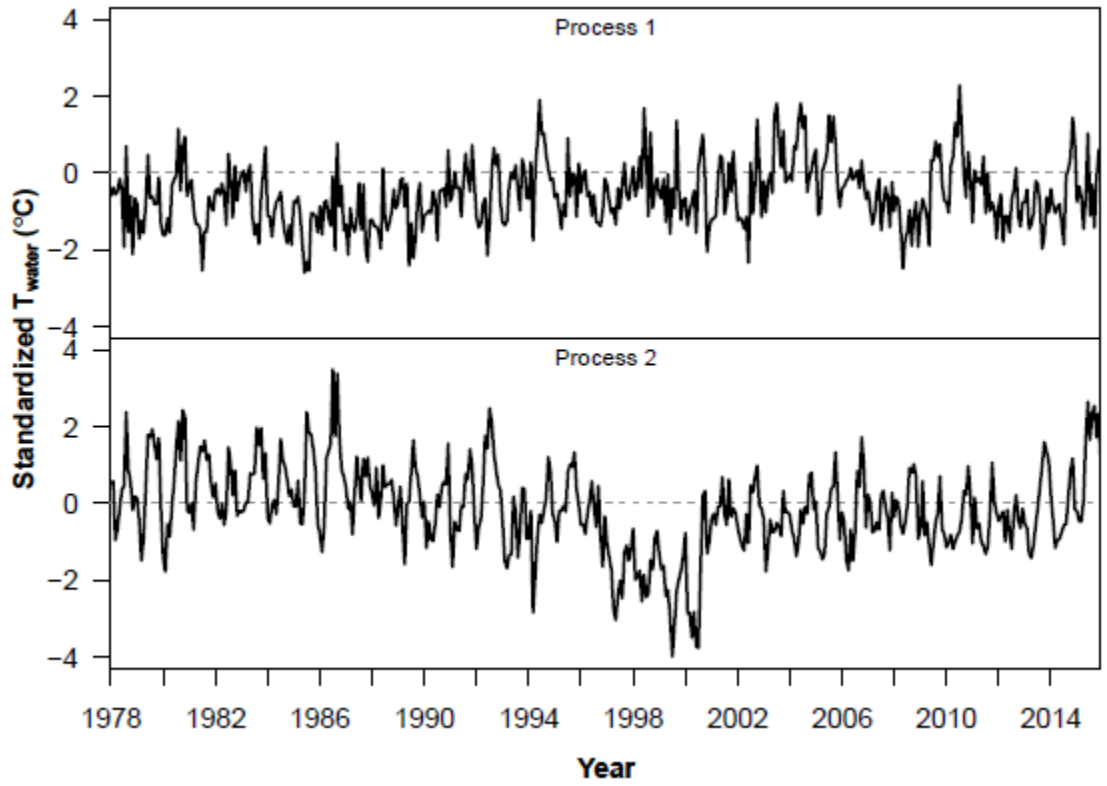

Figure A5 Shared trends from reduced T_{water} model.

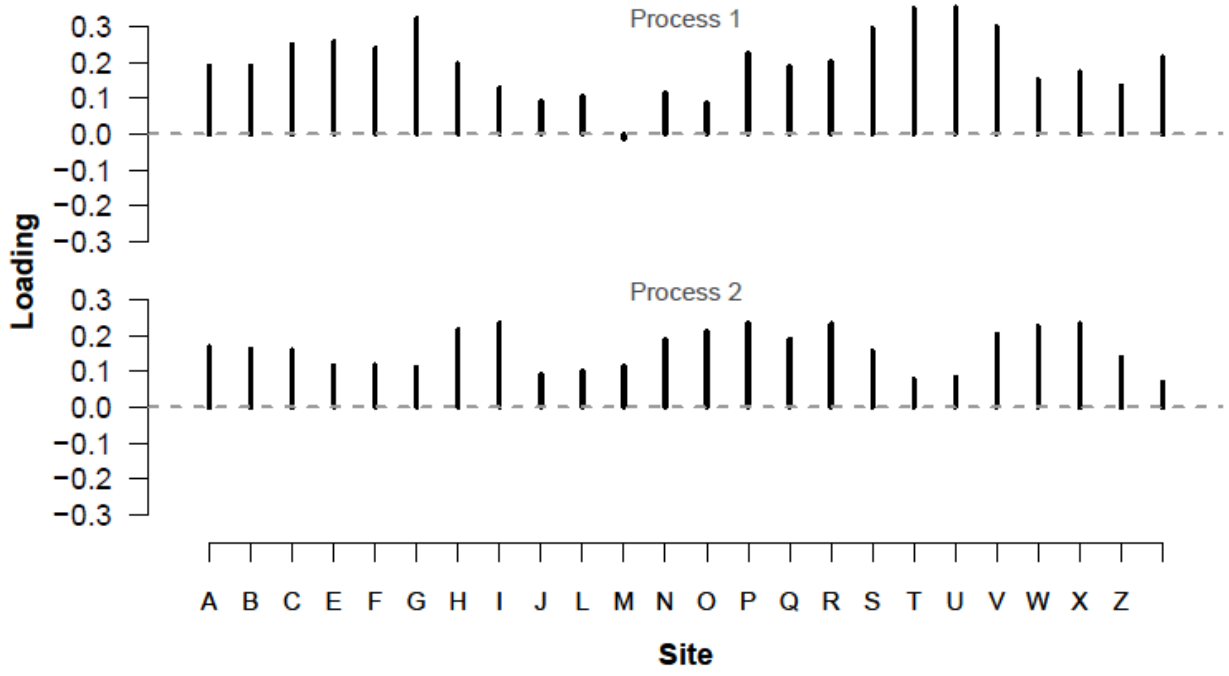

Figure A6 Factor loadings on shared trends from reduced T_{water} model.

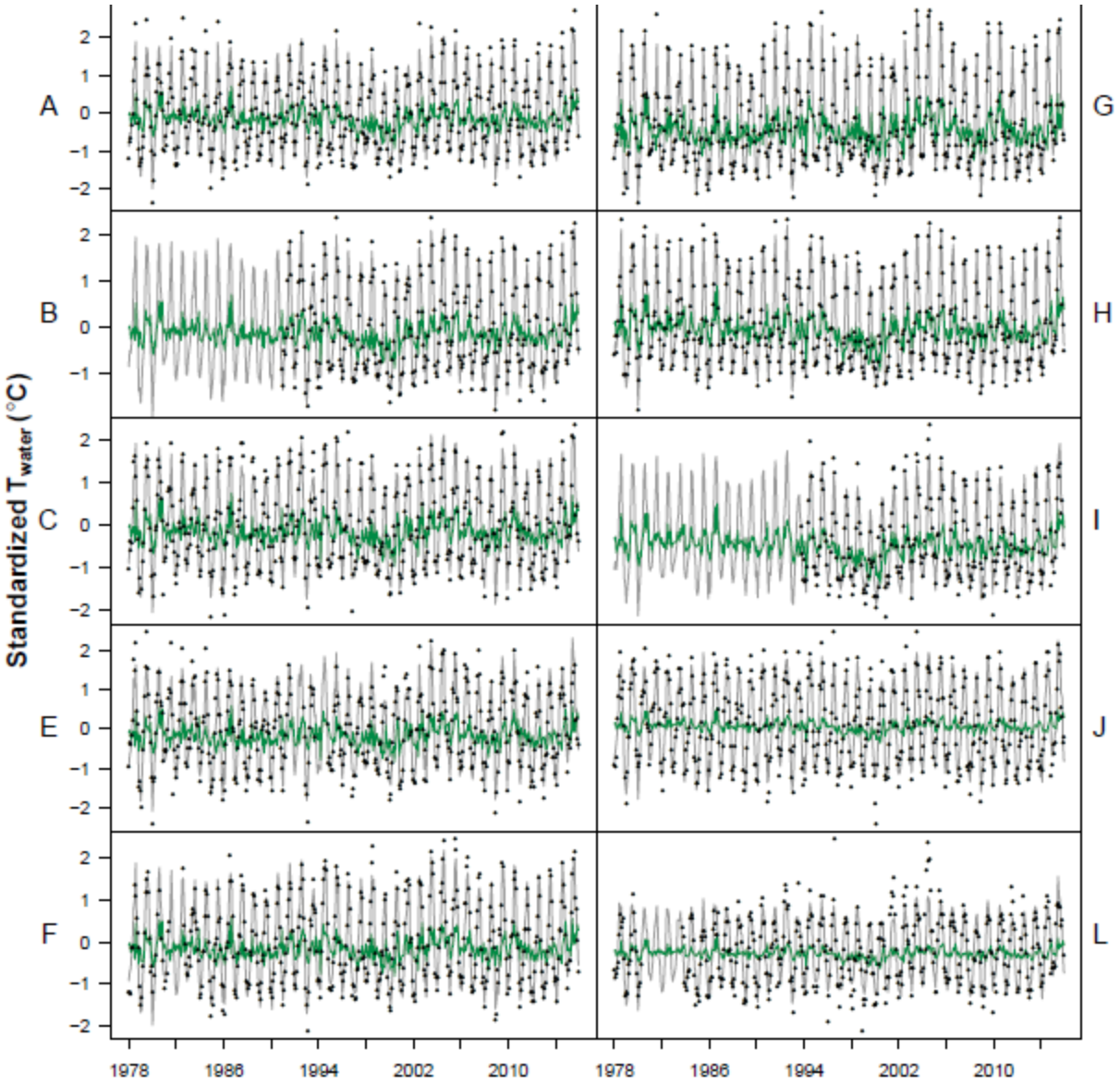
Standardized T_{water} (°C)
A
B
C
E
F
G
H
I
J
L
2
1
0
−1
−2
1978
1986
1994
2002
2010

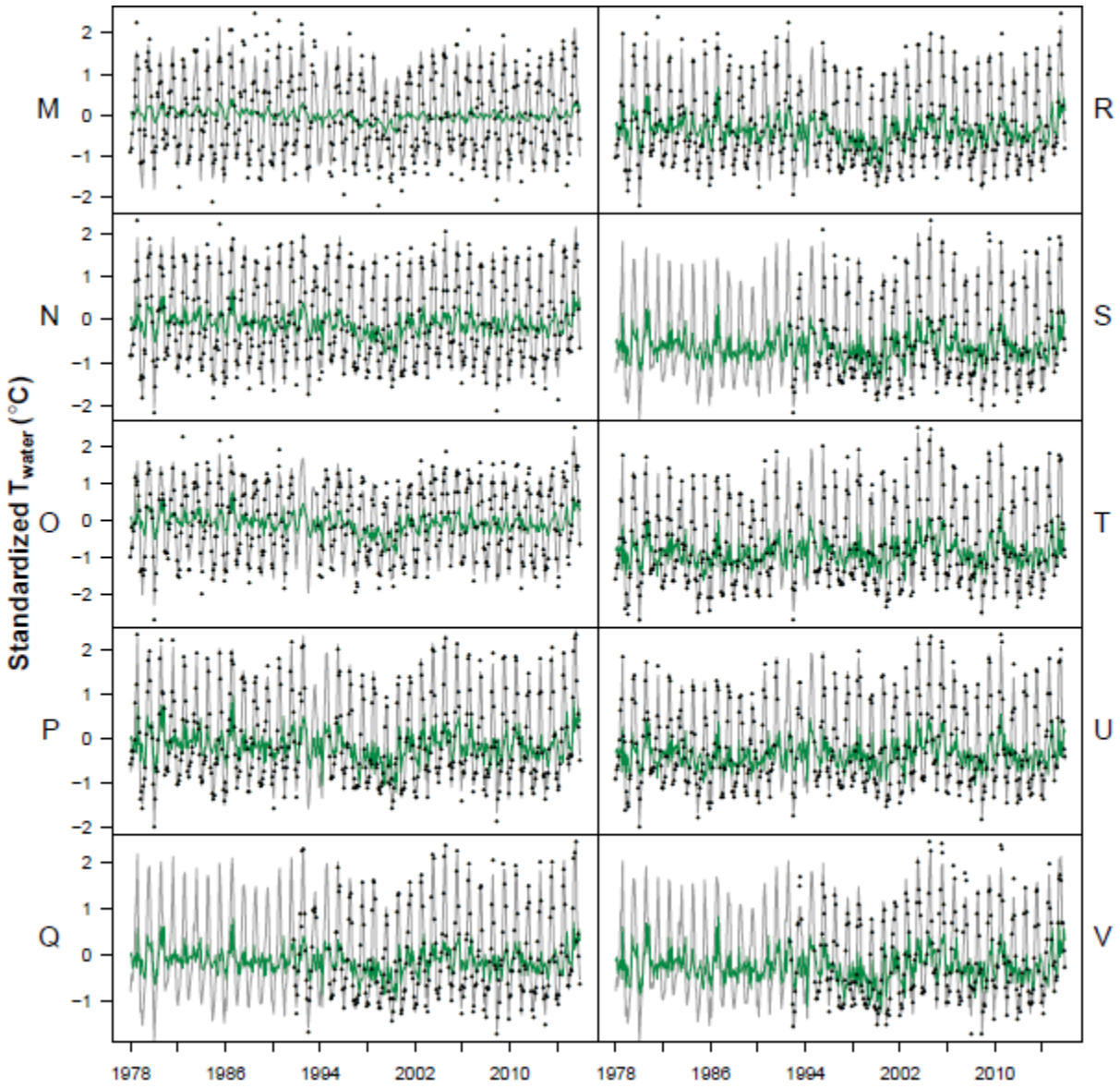
Standardized T_{water} (°C)
M
N
O
P
Q
R
S
T
U
V
2
1
0
−1
−2
1978
1986
1994
2002
2010

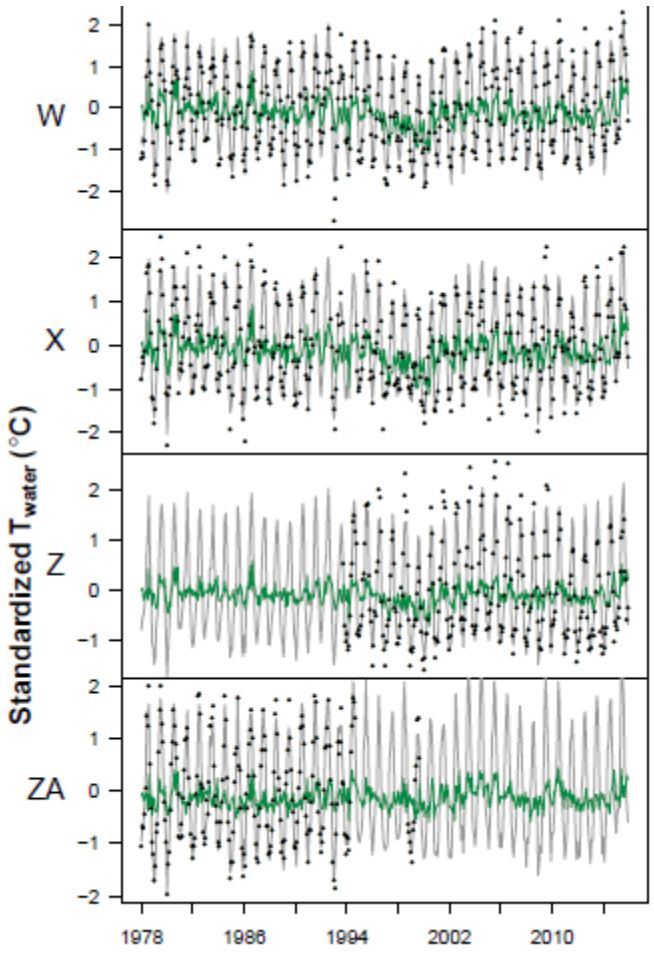

Figure A7 Reduced T_{water} model fits (gray line = overall fit; green line = shared-trend-only fit).

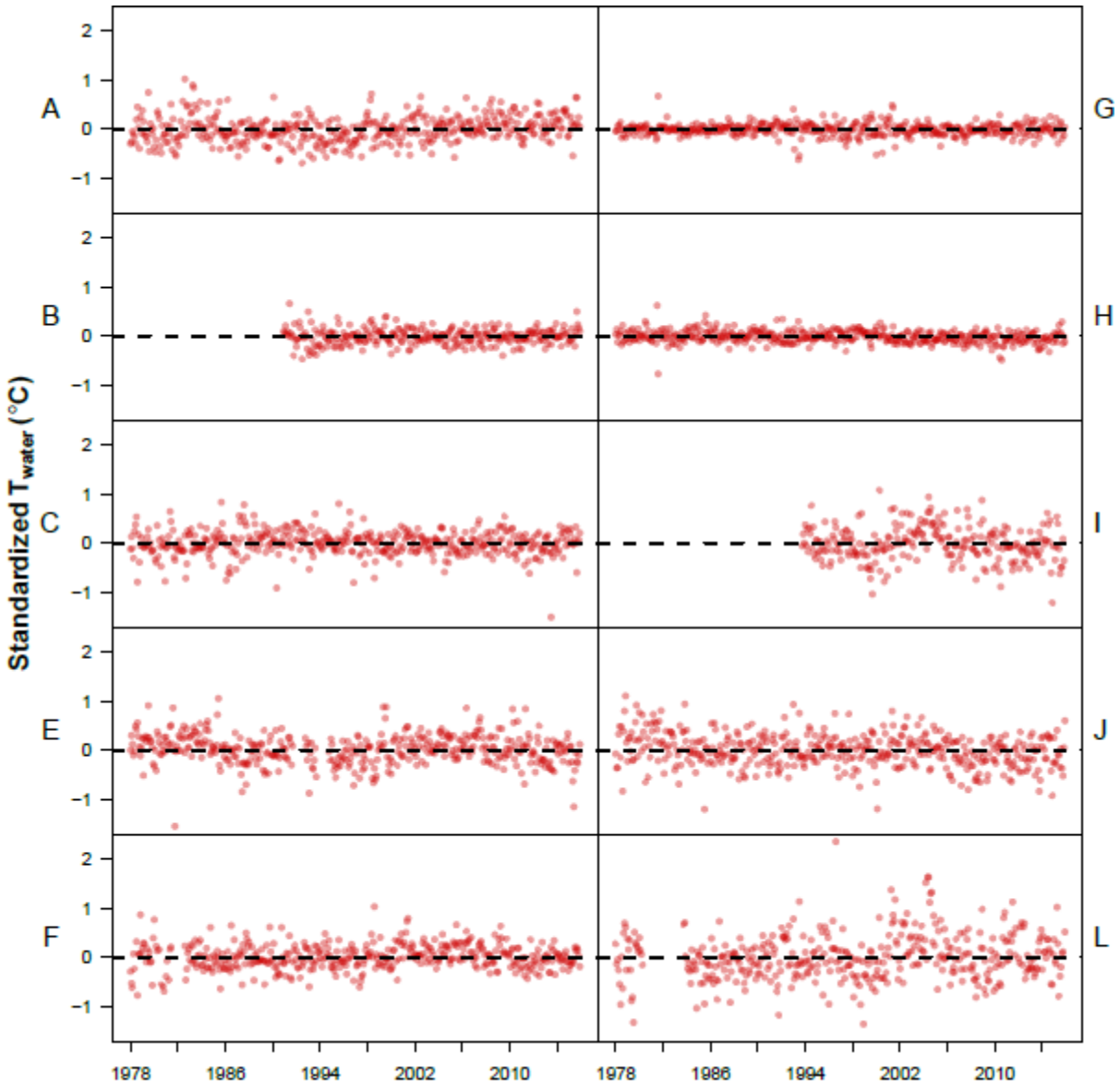
Standardized T_{water} (°C)
A
B
C
E
F
G
H
I
J
L
2
1
0
−1
1978
1986
1994
2002
2010

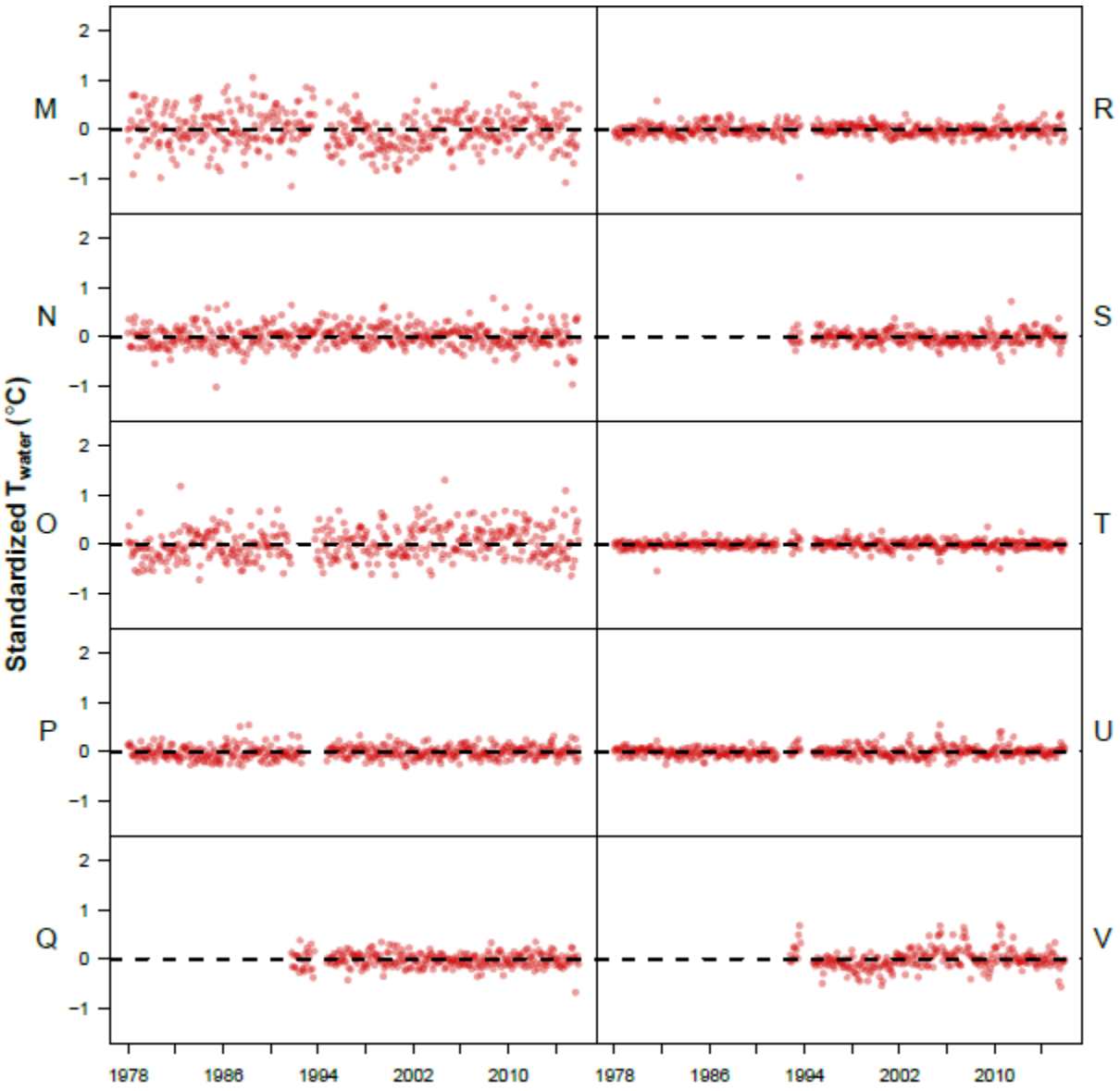
Standardized T_{water} (°C)
M
N
O
P
Q
R
S
T
U
V
2
1
0
−1
1978
1986
1994
2002
2010

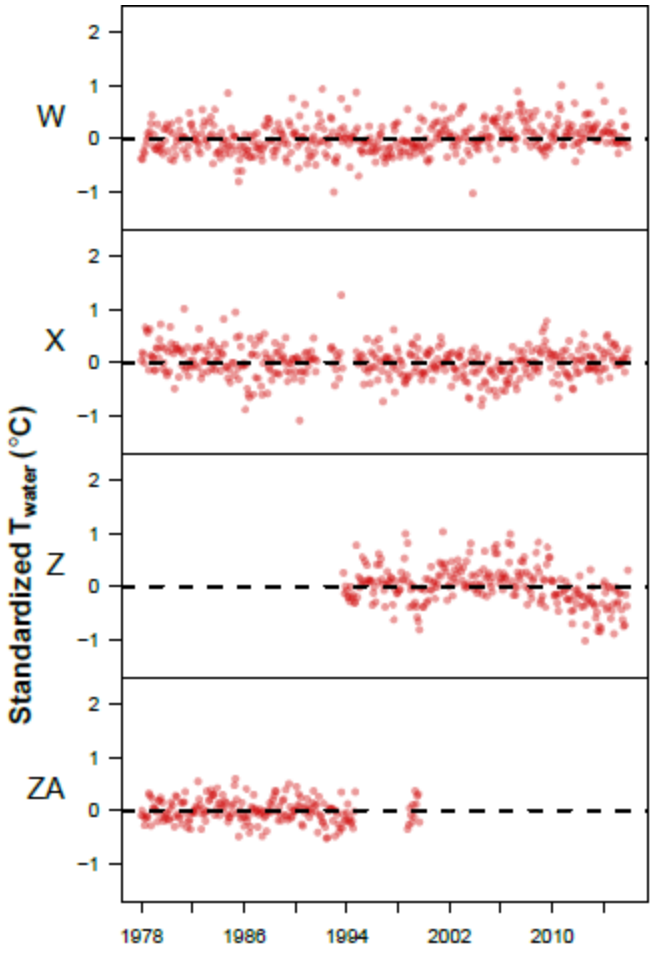

Figure A8 Reduced T_{water} model residuals.

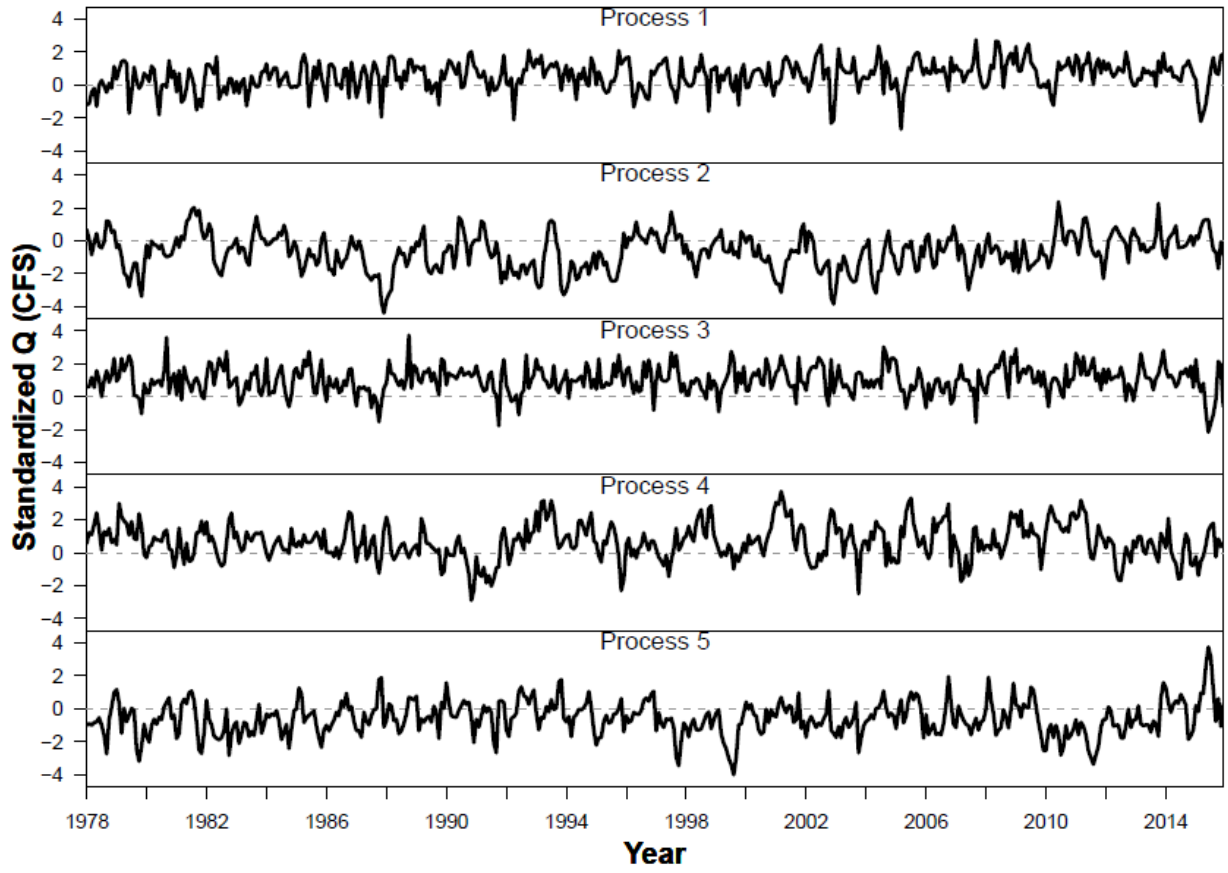

Figure A9 Shared trends from Q model.

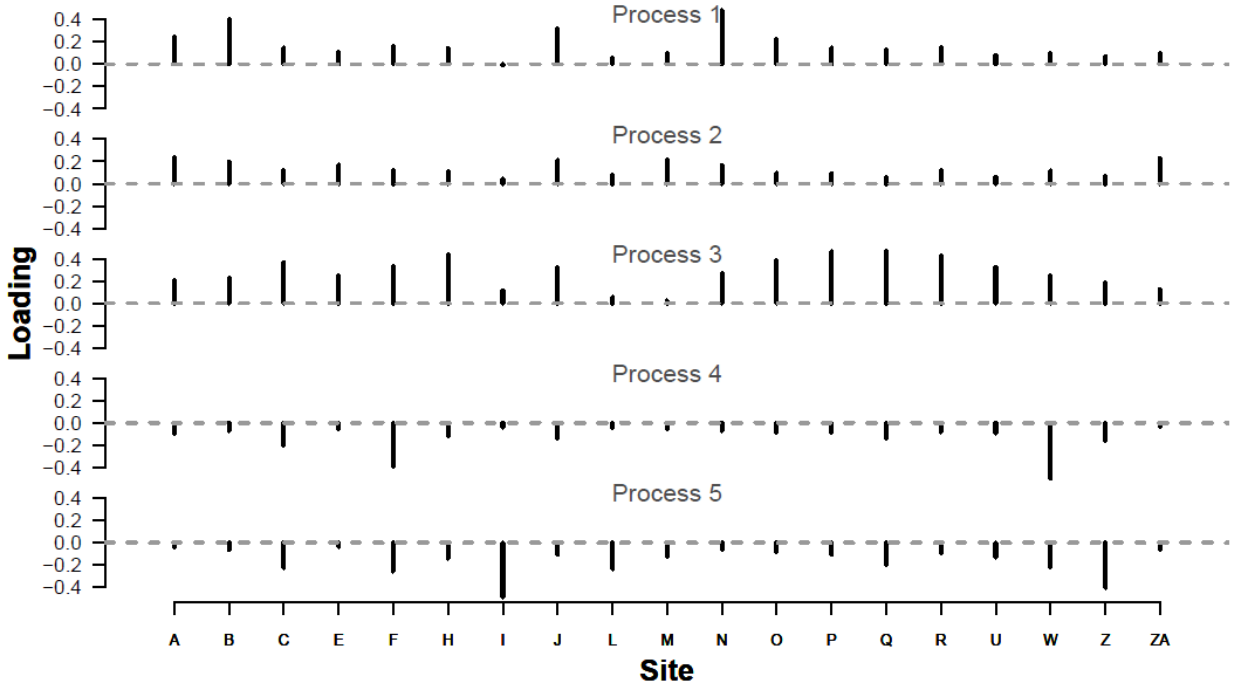

Figure A10 Factor loadings on shared trends from Q model.

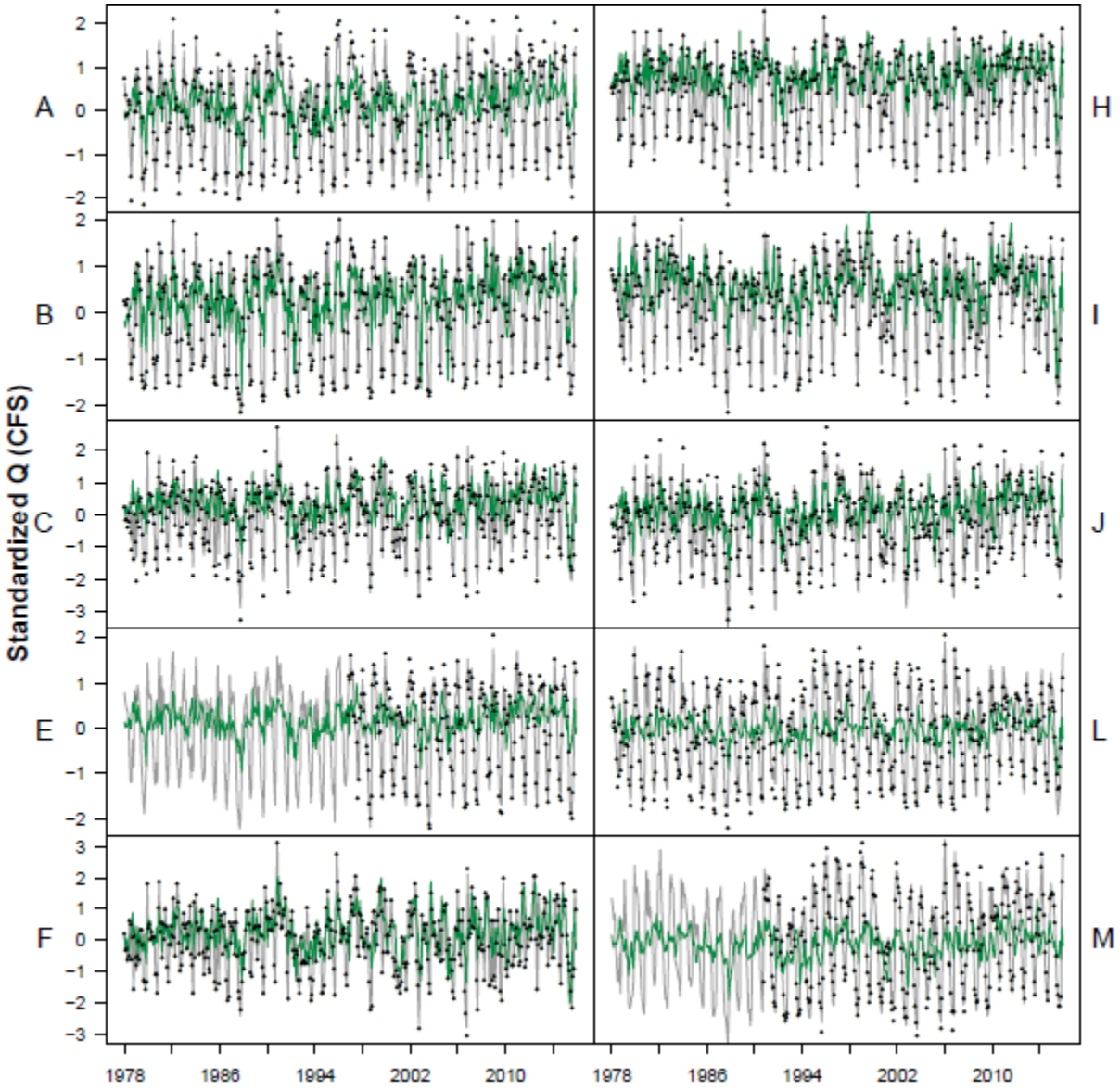

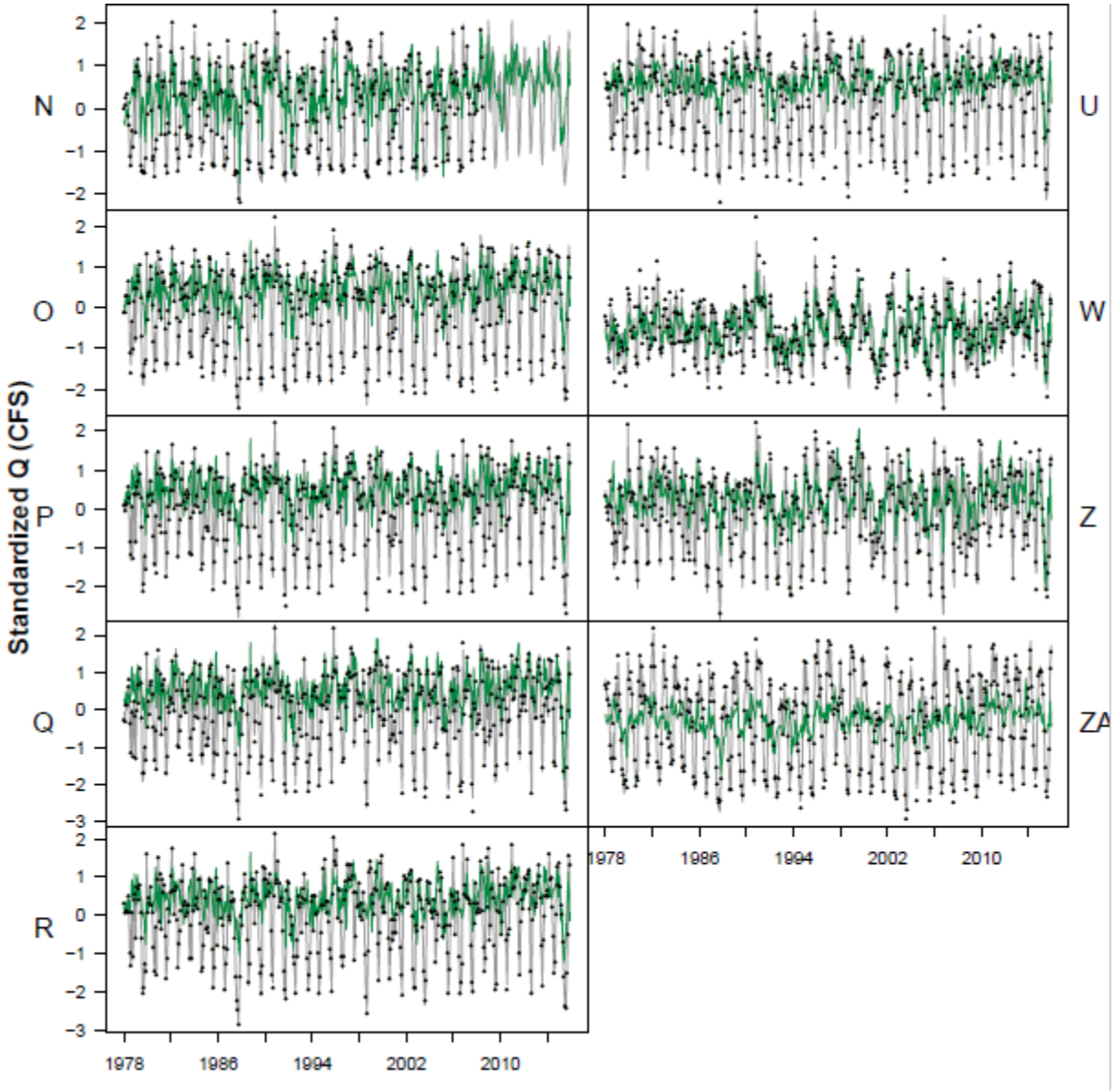

Figure A11 Q model fits (gray line = overall fit; green line = shared-trend-only fit).

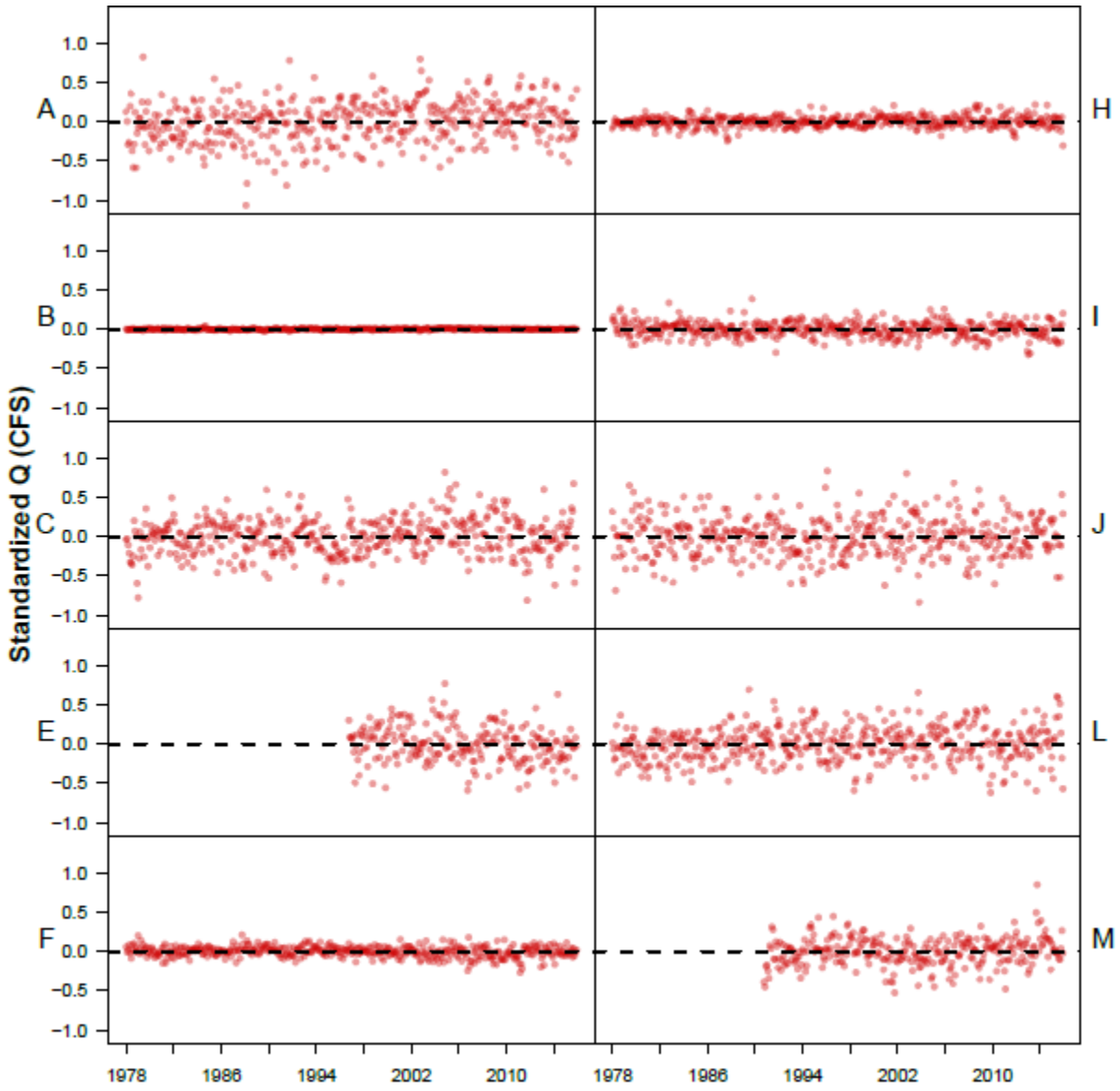
Standardized Q (CFS)
A
B
C
E
F
H
I
J
L
M
1.0
0.5
0.0
−0.5
−1.0
1978
1986
1994
2002
2010

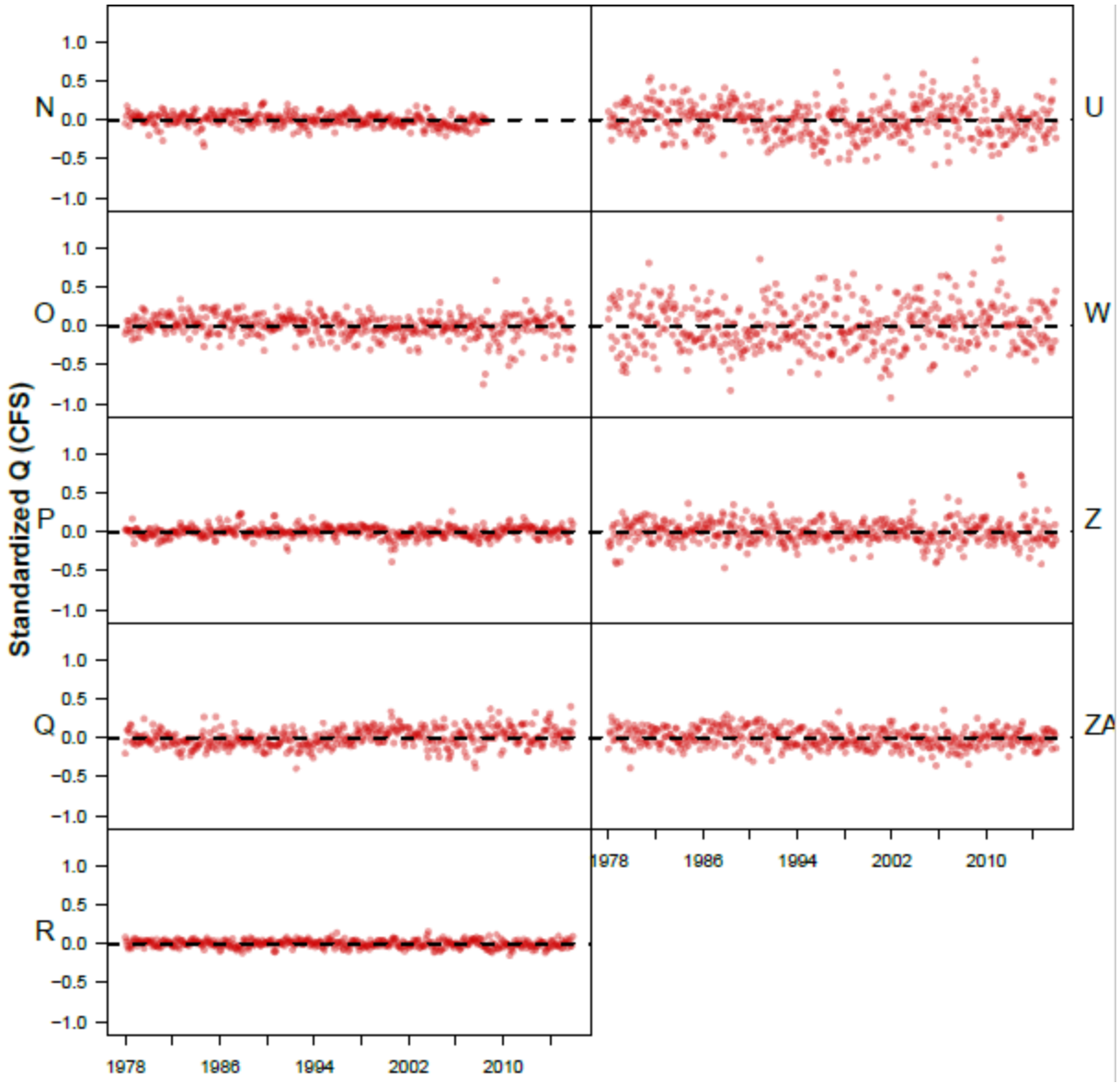

Figure A12 Q model residuals.

Appendix B

Testing for change in coupling over time

We used an additional DFA model to test for changes in $T_{air} \rightarrow T_{water}$ coupling over time, by dividing the 1978-2015 time series into 5 intervals and comparing central tendency and variance of effect sizes for each interval. Figures B1-B3 show mean $T_{air} \rightarrow T_{water}$ coupling for each river.

To approximate estimates of variability over time, we performed the same analyses within a Bayesian framework, and obtained uncertainty estimates from the credible intervals of the effect size (i.e. degree of coupling) posteriors. This approach yielded no trends in variation over time, and is not visualized here. For Bayesian analyses, we used R package “statss” (eric_ward_2017_375646).

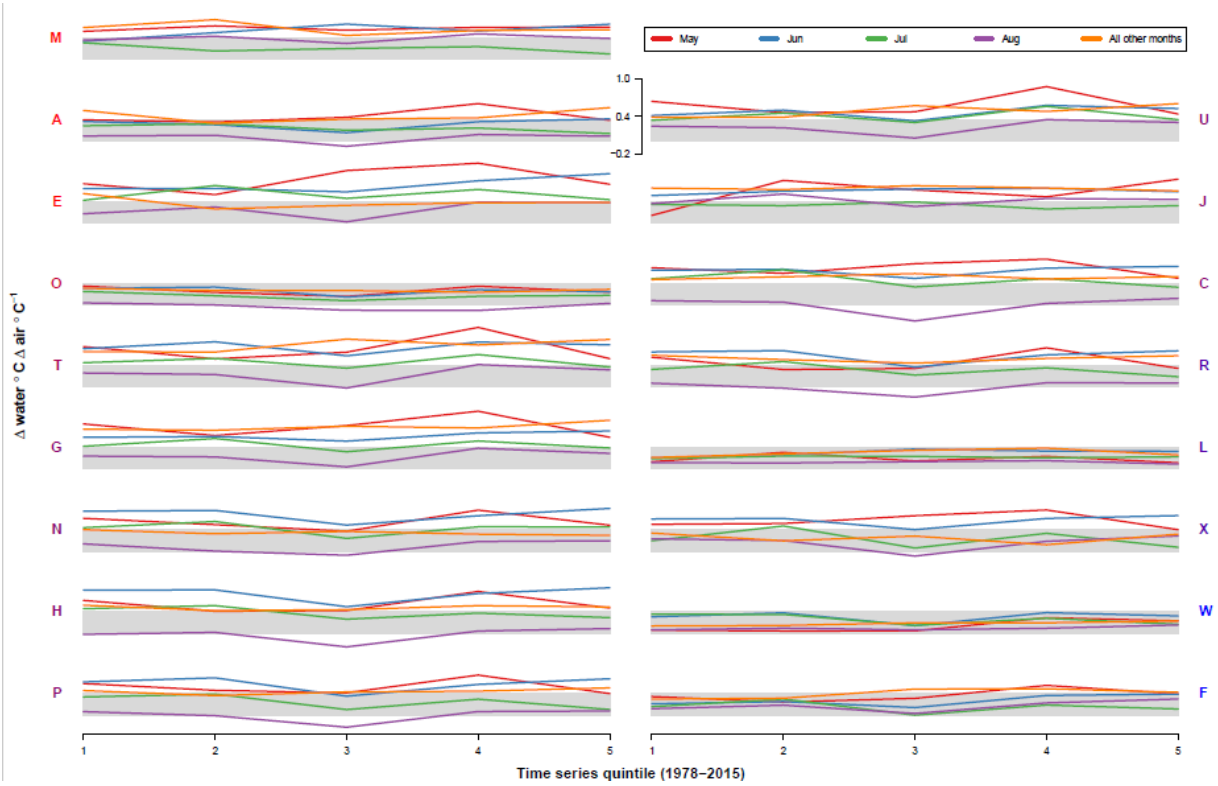

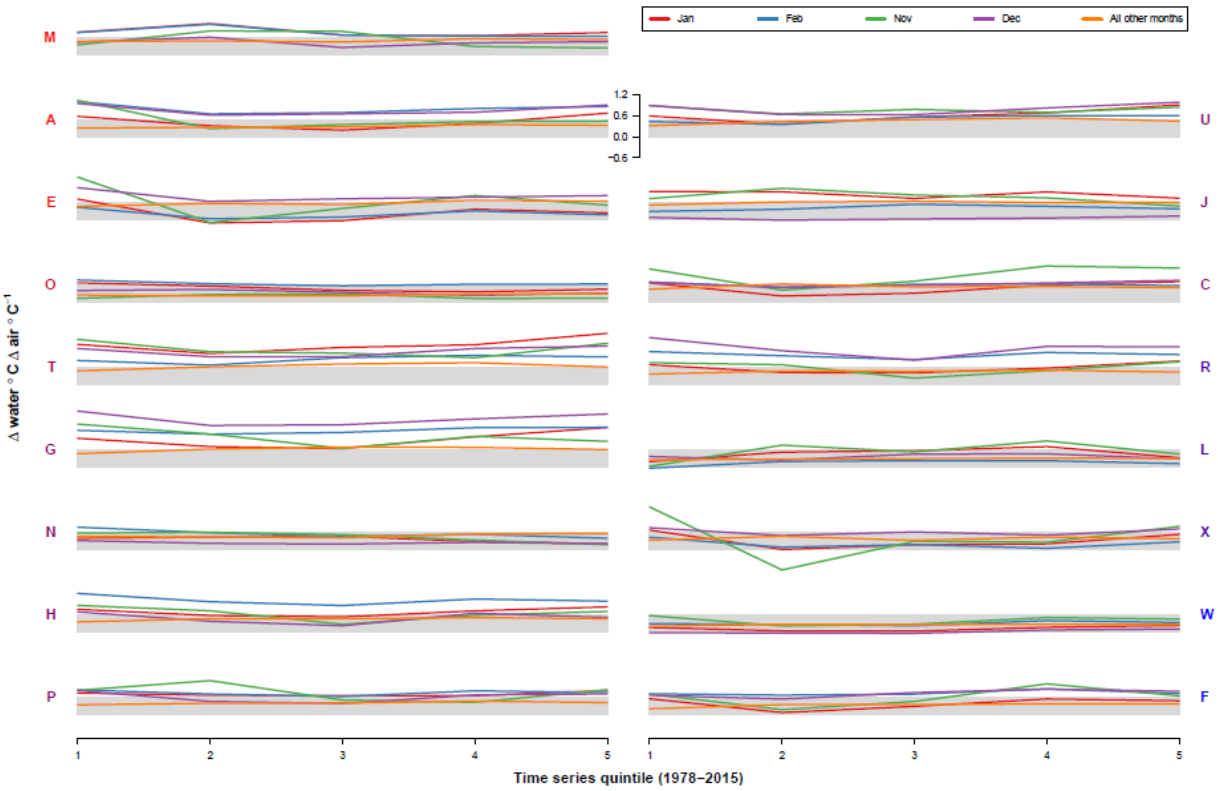
Jan
Feb
Nov
Dec
All other months
M
A
E
O
T
G
N
H
P
U
J
C
R
L
X
W
F
1.2
0.6
0.0
−0.6
Δ water °C Δ air °C⁻¹
1
2
3
4
5
Time series quintile (1978–2015)

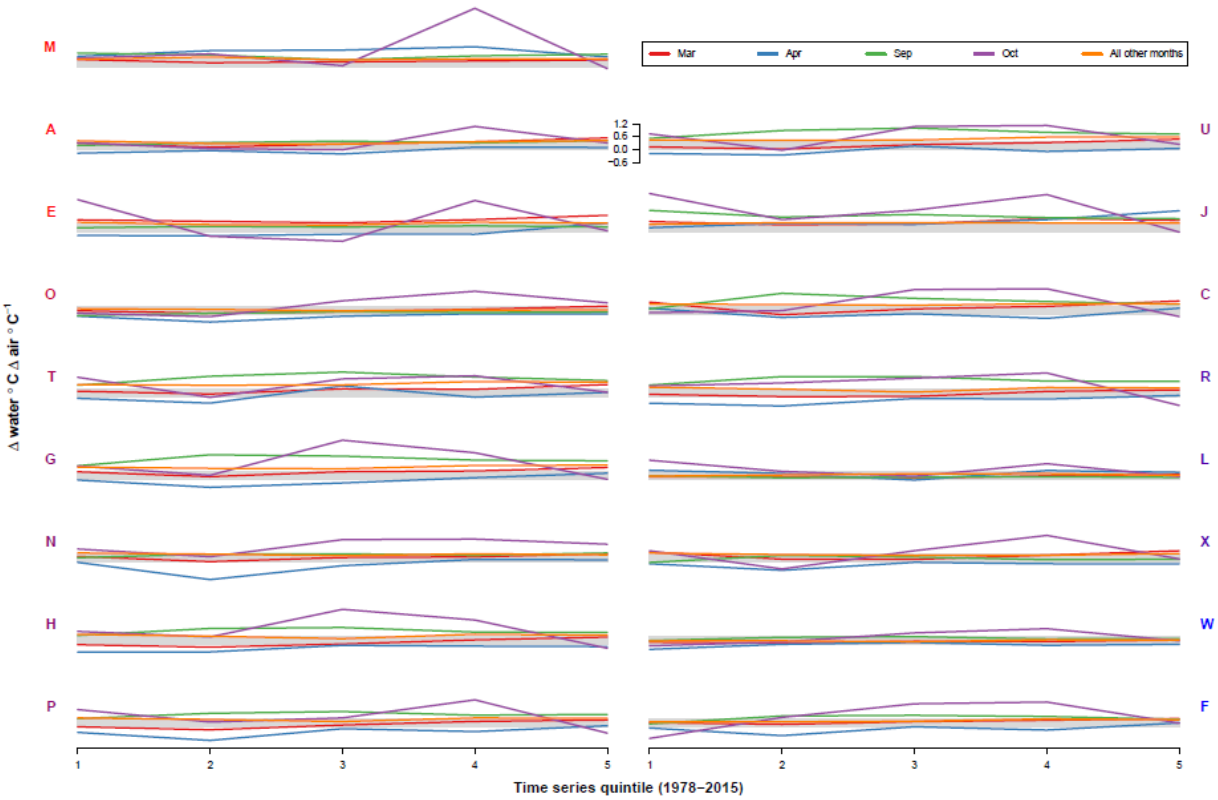
Mar
Apr
Sep
Oct
All other months
M
A
E
O
T
G
N
H
P
U
J
C
R
L
X
W
F
1.2
0.6
0.0
−0.6
Δ water °C Δ air °C⁻¹
1
2
3
4
5
Time series quintile (1978–2015)

Figure B1 Mean $T_{air} \rightarrow T_{water}$ coupling over time. Panel labels correspond to site IDs, and are colored by loading on PCoA axis 1, where bluer = stronger positive loading. Gray bars are for visual reference, and represent the vertical span between zero and overall mean.

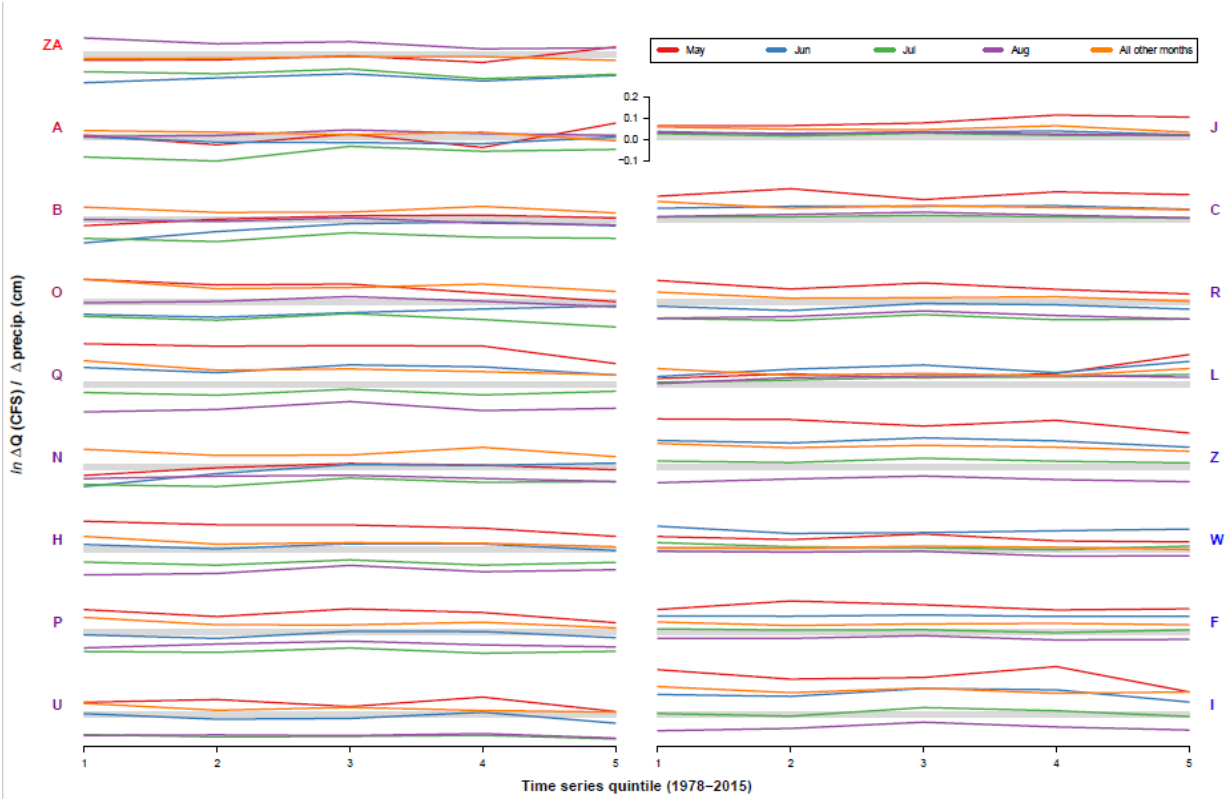

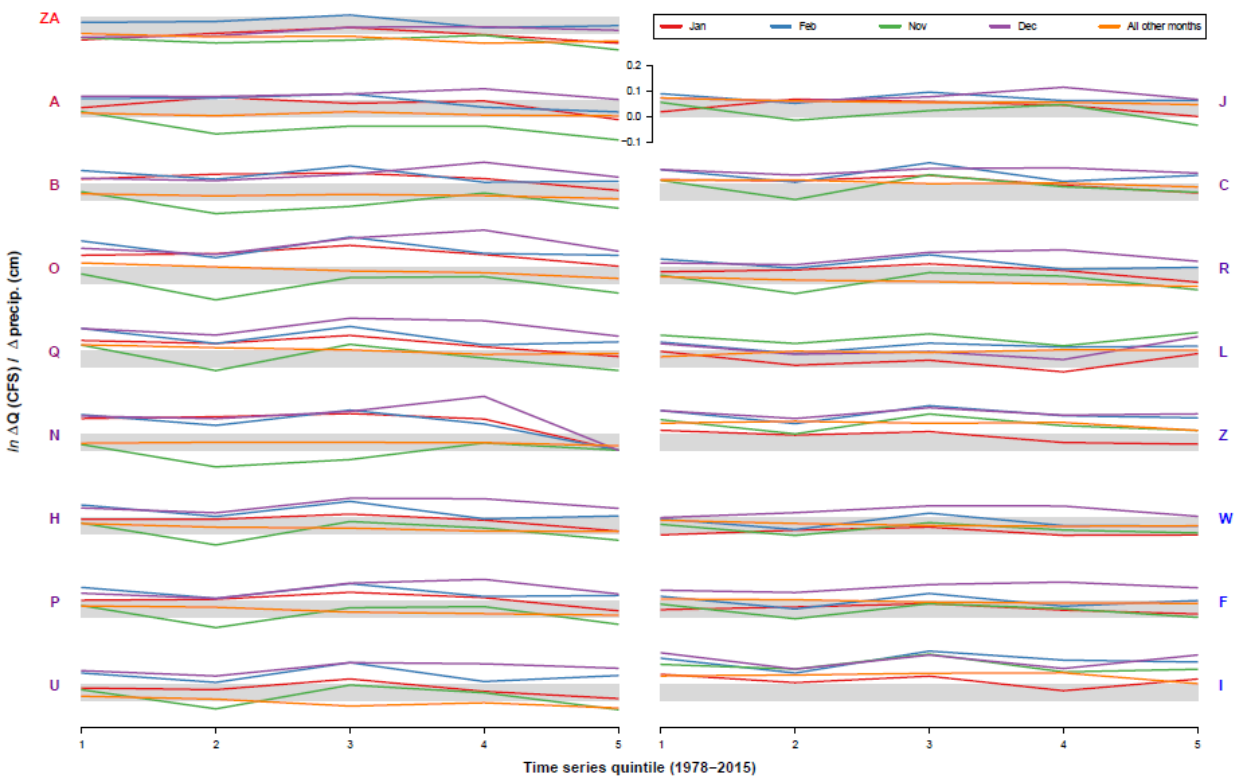
Jan
Feb
Nov
Dec
All other months
ZA
A
B
O
Q
N
H
P
U
J
C
R
L
Z
W
F
I
0.2
0.1
0.0
−0.1
1
2
3
4
5
ln ΔQ (CFS) / Δ precip. (cm)
Time series quintile (1978–2015)

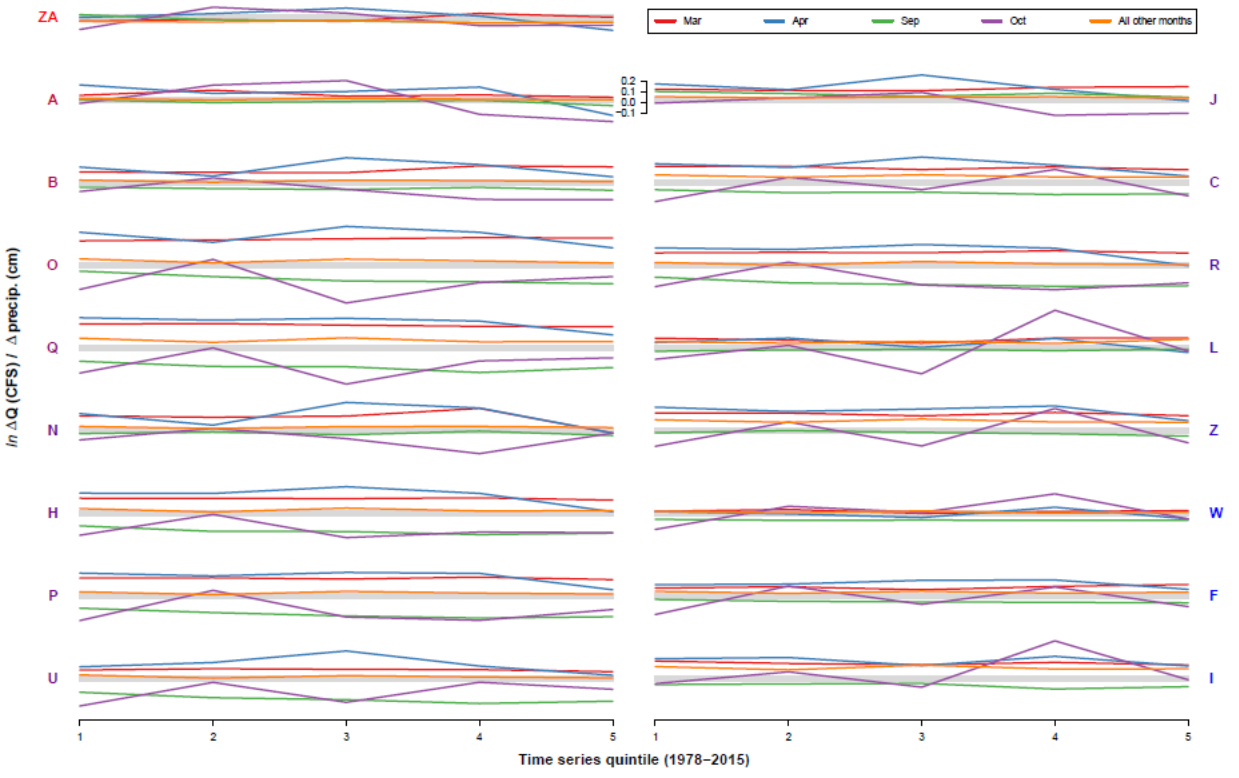
Mar
Apr
Sep
Oct
All other months
ZA
A
B
O
Q
N
H
P
U
J
C
R
L
Z
W
F
I
0.2
0.1
0.0
−0.1
1
2
3
4
5
ln ΔQ (CFS) / Δ precip. (cm)
Time series quintile (1978–2015)

Figure B2 Mean $T_{air} \rightarrow Q$ coupling over time. Panel labels correspond to site IDs, and are colored by loading on PCoA axis 1, where bluer = stronger positive loading. Gray bars are for visual reference, and represent the vertical span between zero and overall mean.

Appendix C

Table C1 Site attributes. See methods for details. See Figure 1 for map locations.

Site code	DoE ID	Class	Description	Lat.	Long.	Site elev.	Elev.	Area	Area over 1000 m	Slope	Dammed
A	08C070	RD	Cedar R @ Logan St/Renton	47.5	-122.2	4.6	611.3	457.1	0.3	18.1	yes
B	09A080	SD	Green R @ Tukwila	47.5	-122.2	1.2	546.2	1115.7	0.6	23.5	yes
C	01A050	RD	Nooksack R @ Brennan	48.8	-122.6	3	674.5	2046.2	0	5	no
E	03B050	SD	Samish R nr Burlington	48.5	-122.3	11.6	268	225.3	0.2	16.7	no
F	03A060	RS	Skagit R nr Mount Vernon	48.4	-122.3	4.3	1128.3	8035.1	0.2	15.4	partial
G	05A070	RS	Stillaguamish R nr Silvana	48.2	-122.2	10.7	604.1	1456.7	0	6.8	no
H	07A090	SD	Snohomish R @ Snohomish	47.9	-122.1	2.4	688.4	4449.9	0.5	19.2	no
I	16C090	SD	Duckabush R nr Brinnon	47.7	-123	91.4	1047.5	178.6	0.2	13.5	no
J	10A070	RS	Puyallup R @ Meridian	47.2	-122.3	9.1	921	2439.4	0.2	14.1	no
L	16A070	RD	Skokomish R nr Potlatch	47.3	-123.2	18.3	608.8	591.7	0.2	17.1	partial
M	13A060	RS	Deschutes R @ E St Bridge	47	-122.9	28.3	288.2	408.5	0.3	15.7	no
N	09A190	RS	Green R @ Kanaskat	47.3	-121.9	236.2	822.2	659.1	0	5.3	yes
O	08C110	RS	Cedar R nr Landsburg	47.4	-121.9	187.8	808.3	310.3	0.8	25.7	yes
P	07D130	RS	Snoqualmie R @ Snoqualmie	47.5	-121.8	121.9	897.8	946.6	0	11.9	no
Q	07D050	RS	Snoqualmie R @ Monroe	47.8	-122	4.6	638.1	1779.7	0.2	22.8	no
R	07C070	RS	Skykomish R @ Monroe	47.9	-122	13.1	904.6	1986.9	0.3	14.5	no
S	05A110	RS	SF Stillaguamish R nr Granite Falls	48.1	-122	88.4	768.7	308.1	0	8.1	no
T	05A090	RS	SF Stillaguamish R @ Arlington	48.2	-122.1	16.8	625.2	657	0.4	15.7	no
U	05B070	RS	NF Stillaguamish R @ Cicero	48.3	-122	33.5	665.5	667.4	0.4	18.3	no
V	05B110	SD	NF Stillaguamish R nr Darrington	48.3	-121.7	132.6	714.2	222.5	0.3	15.6	no
W	04A100	SD	Skagit R @ Marblemount	48.5	-121.4	109.7	1349.2	3601.1	0.4	14.6	yes
X	01A120	SD	Nooksack R @ No Cedarville	48.8	-122.3	42.7	868.2	1542.7	0.2	9.9	no
Z	18B070	RD	Elwha @ Port Angeles	48.1	-123.6	67.1	1088.6	757.1	0.6	27.5	yes
ZA	08B070	RS	Sammamish R @ Bothell	47.8	-122.2	4.6	147.2	559.8	0.4	19.2	no

Site code	Perenn. ice	Runoff	Bedrock dep.	Water tbl. dep.	Soil perm.	Aspect	BFI	Rip. pop. dens.	Imp. surf.	Urb.	Road dens.
A	0.3	1238.8	143	135.1	14.2	290.6	61.3	81.6	2.9	5.5	3.4
B	2.2	1169.4	140.8	134.6	12.3	295.6	61.1	148.8	4.3	8.2	3.9
C	0	1714.2	139.3	127.2	9	269.1	58.4	26.9	1.2	2.2	1.4
E	0.2	1546	143.2	118.4	12	252.7	52.8	29.2	2.4	5.3	1.8
F	0.6	1998.6	133.5	145.3	7.5	260.8	61.3	5.6	0.6	1.2	0.6
G	0	2563.9	139.8	126.9	7.4	261.5	52	19.6	0.9	1.6	1.3
H	0.3	2255.7	137.2	135	10.9	277.8	57.2	38	1.7	3.5	1.9
I	0.1	1993.8	95.7	172.8	4.7	87.4	54.3	1	0.1	0	0.2
J	0.1	1204.2	145.8	144.4	12.2	295.1	61.5	48.2	2.3	4.5	1.7
L	0.1	1900	112.6	143	7.3	139.2	52.3	2.7	0.5	0.3	1.4
M	0.2	1261.1	139.8	157	17.1	317.2	59.4	70.4	2.1	3.5	2.9
N	0	1165	135.5	152.4	7.7	284.9	59.4	5	0.8	0.9	3.1
O	2.5	1239.9	141.1	139.2	10.4	271.3	59	4.3	0.7	0.5	2.6
P	0	2087.7	135.8	153.4	16.5	243	58.3	18.3	1.4	2.5	2
Q	4	2097.9	139.4	136.8	13.8	270.5	58.6	33.1	1.6	3.1	2.6
R	1.8	2605.6	133.1	143.8	9.3	277.5	56.4	11.1	1	2.1	1.1
S	0	2545	134.5	137.1	6.8	276	54.9	9.4	0.7	1.1	1
T	0	2557.2	137.6	129.5	6.9	280.1	52	23.4	1.1	1.9	1.4
U	0.1	2568.8	140.5	127.9	7.2	272.5	53.1	5.2	0.6	1	1
V	0.1	2562.5	138.2	134.1	6.4	254.4	57.4	3.7	0.5	0.7	1.1
W	3	1806.4	132.1	150.4	6.5	253.8	65.3	0.3	0.5	1.1	0.2
X	0	1715.1	136.6	137.1	7.2	257.9	58.7	5.4	0.6	0.8	1.2
Z	4.4	1599.4	118.3	175	7	323.4	60.4	1	0.1	0	0.2
ZA	2.3	1264.4	143.2	124.1	20.6	339.4	64.2	529.7	14.6	29	6.6

Appendix D

Testing for trends in absolute T_{water}, T_{air}, precipitation, and snowmelt over the entire time series

We performed Kendall's Test for Trend to determine whether T_{water} or any of the climate predictors showed significant, monotonic positive or negative slopes over the 38-year interval. The Seasonal Kendall Test was avoided because of its assumption that any monotonic trends present are the same across all seasons (months, in our case). Instead, each time series was decomposed into trend, seasonal, and noise components, and only the trends (Figure D1) were used in the analyses, with six data points on either end removed during the decomposition process.

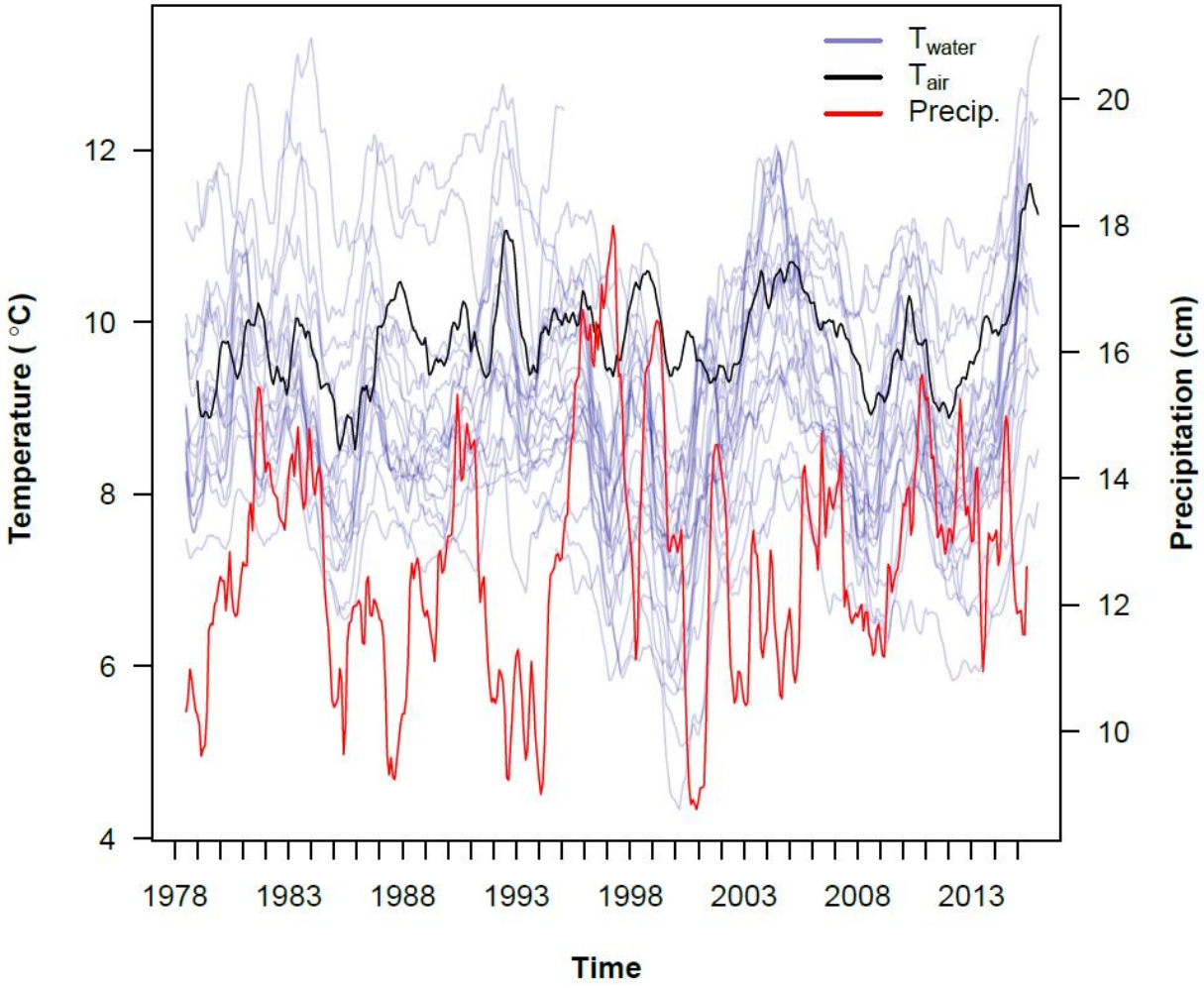

Figure D1 Time series of T_{water} across all sites, and regional T_{air} and precipitation, with seasonality and random noise removed via decomposition.

Kendall's test identified significant positive, monotonic trends in T_{air}, precipitation, and 10 out of 24 T_{water} time series (Tables D1, D2). The same number of T_{water} series was determined to be monotonically decreasing over the 37-year interval from July 1978 to June 2015.

Table D1 Results of Kendall's Test for Trend (with continuity correction) on climate predictor time series with seasonality and random noise removed via decomposition. Slope estimated via Thiel/Sen Estimator; intercept via Conover's Estimator. Confidence intervals (upper and lower 95%) determined via Gilbert's modification to Thiel/Sen method.

Predictor	Kendall's Tau	Slope	Lower 95	Upper 95	Intercept	z	*p*
T_{air}	0.128	0.001	0	0.001	9.613	4.015	0
Precip	0.101	0.002	0.001	0.004	12.136	3.167	0.002
Snowmelt	0.043	0	0	0.001	2.658	1.355	0.175

Table D2 Results of Kendall's Test for Trend (with continuity correction) on T_{water} time series with seasonality and random noise removed via decomposition. Specifications same as above. Slopes significant at α = 0.05 are bolded. Significant negative slopes are italicized.

Site	Kendall's Tau	Slope	Lower 95	Upper 95	Intercept	z	*p*
A	**0.150**	**0.001**	**0.001**	**0.002**	**9.870**	**4.721**	**0.000**
B	*-0.293*	*-0.002*	*-0.002*	*-0.001*	*11.649*	*-9.270*	*0.000*
C	0.003	0.000	-0.001	0.001	9.177	0.084	0.933
E	0.011	0.000	-0.001	0.001	9.325	0.358	0.720
F	**0.088**	**0.001**	**0.000**	**0.001**	**8.675**	**2.780**	**0.005**
G	**0.094**	**0.001**	**0.000**	**0.002**	**8.966**	**2.975**	**0.003**
H	*-0.208*	*-0.002*	*-0.002*	*-0.001*	*10.090*	*-6.564*	*0.000*
I	*-0.326*	*-0.002*	*-0.002*	*-0.001*	*7.763*	*-10.321*	*0.000*
J	*-0.221*	*-0.002*	*-0.003*	*-0.002*	*9.836*	*-6.945*	*0.000*
L	**0.224**	**0.001**	**0.001**	**0.002**	**8.077**	**7.060**	**0.000**
M	*-0.147*	*-0.001*	*-0.001*	*-0.001*	*11.055*	*-4.635*	*0.000*
N	-0.061	-0.000	-0.001	0.000	8.572	-1.928	0.054
O	**0.096**	**0.001**	**0.000**	**0.001**	**8.297**	**3.029**	**0.002**
P	-0.060	-0.001	-0.001	0.000	8.328	-1.877	0.061
Q	*-0.416*	*-0.004*	*-0.005*	*-0.004*	*11.417*	*-13.195*	*0.000*
R	*-0.127*	*-0.001*	*-0.002*	*-0.001*	*9.085*	*-3.991*	*0.000*
S	**0.235**	**0.001**	**0.000**	**0.002**	**7.365**	**7.413**	**0.000**
T	**0.183**	**0.002**	**0.001**	**0.003**	**8.436**	**5.759**	**0.000**
U	**0.175**	**0.002**	**0.001**	**0.003**	**7.846**	**5.505**	**0.000**
V	*-0.107*	*-0.000*	*-0.000*	*0.000*	*7.942*	*-3.392*	*0.001*
W	**0.098**	**0.001**	**0.000**	**0.001**	**7.333**	**3.100**	**0.002**
X	*-0.242*	*-0.002*	*-0.002*	*-0.002*	*8.550*	*-7.615*	*0.000*
Z	**0.071**	**0.000**	**-0.000**	**0.000**	**8.167**	**2.288**	**0.022**
ZA	*-0.466*	*-0.002*	*-0.003*	*-0.002*	*11.624*	*-14.788*	*0.000*

Appendix E

Wavelet analysis of shared trends

To identify potential sub-seasonal periodic structure in the two shared trends from the reduced fit model, we conducted a wavelet power spectrum analysis using the Morlet wavelet (RoeschWavelet). Shared trends were detrended using a Loess span of 0.75. Power spectra revealed a continuous ridge of strong 12-month periodicity in shared trend 2 (Figure E2).

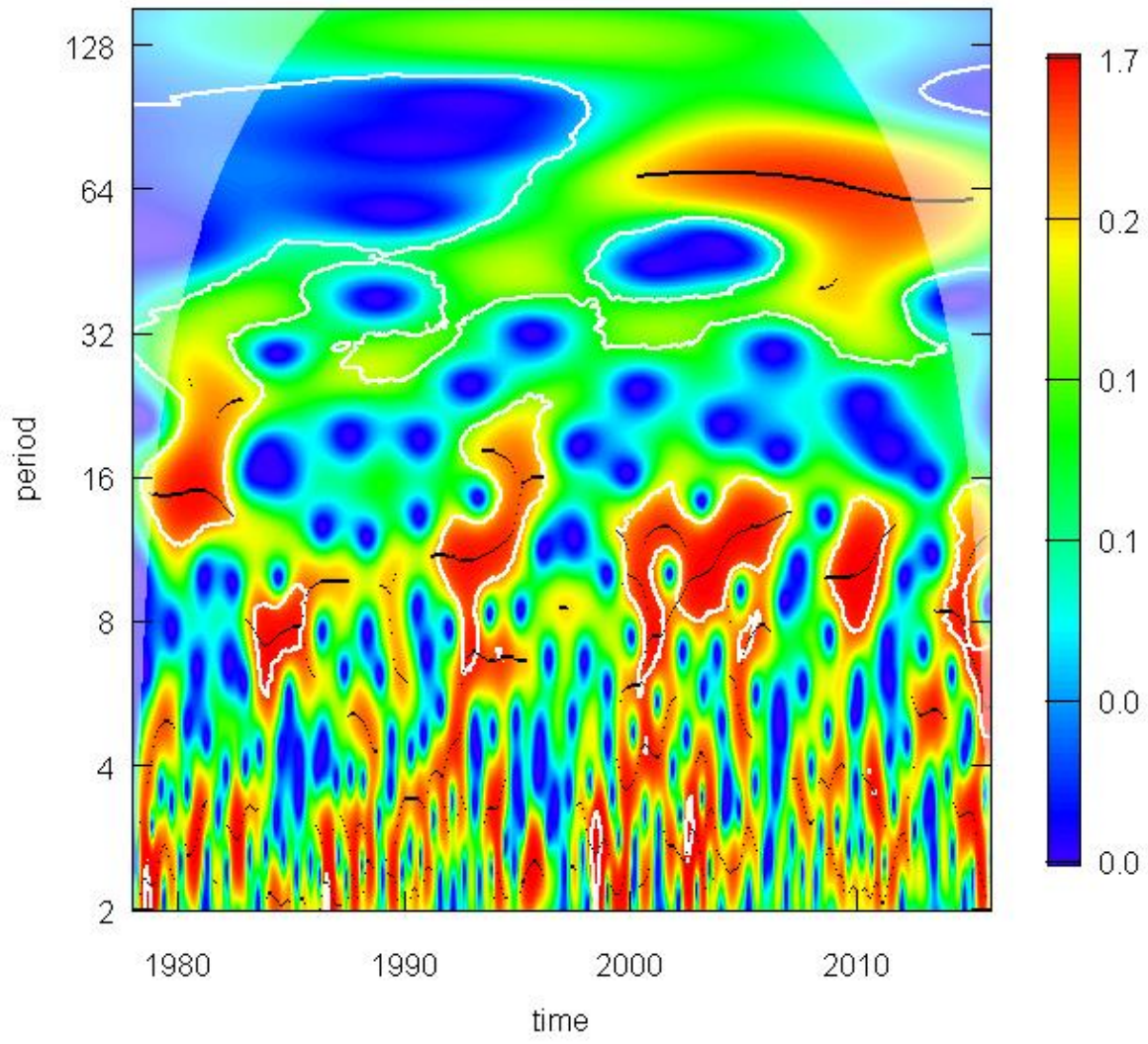

Figure E1 Wavelet power spectrum for shared trend 1. Period refers to Fourier period. Warmer colors denote greater strength of periodicity. White polygons encompass areas of significant periodicity at α = 0.10, based on comparison with a white noise surrogate time series. Black lines correspond to "ridges" of highest power within significant regions.

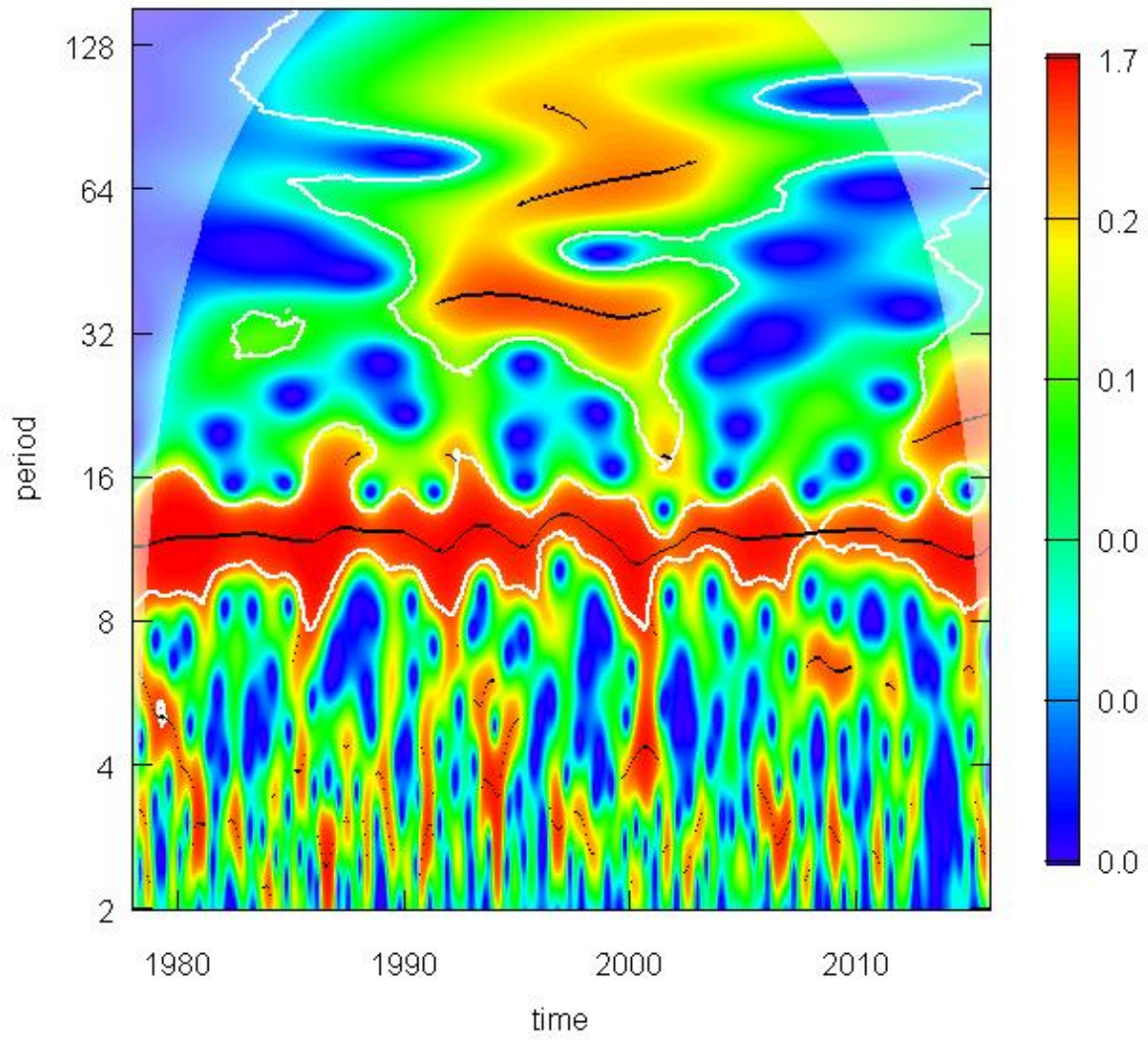

Figure E2 Wavelet power spectrum for shared trend 2. See Figure E1 for details.

Trend 2 was cleaned to remove all but the time series components contributing to the ridge at period=12. The original trend was then reconstructed using only those components, revealing a yearly recurring sinusoid patter of low values in spring and high values in late summer/early fall.

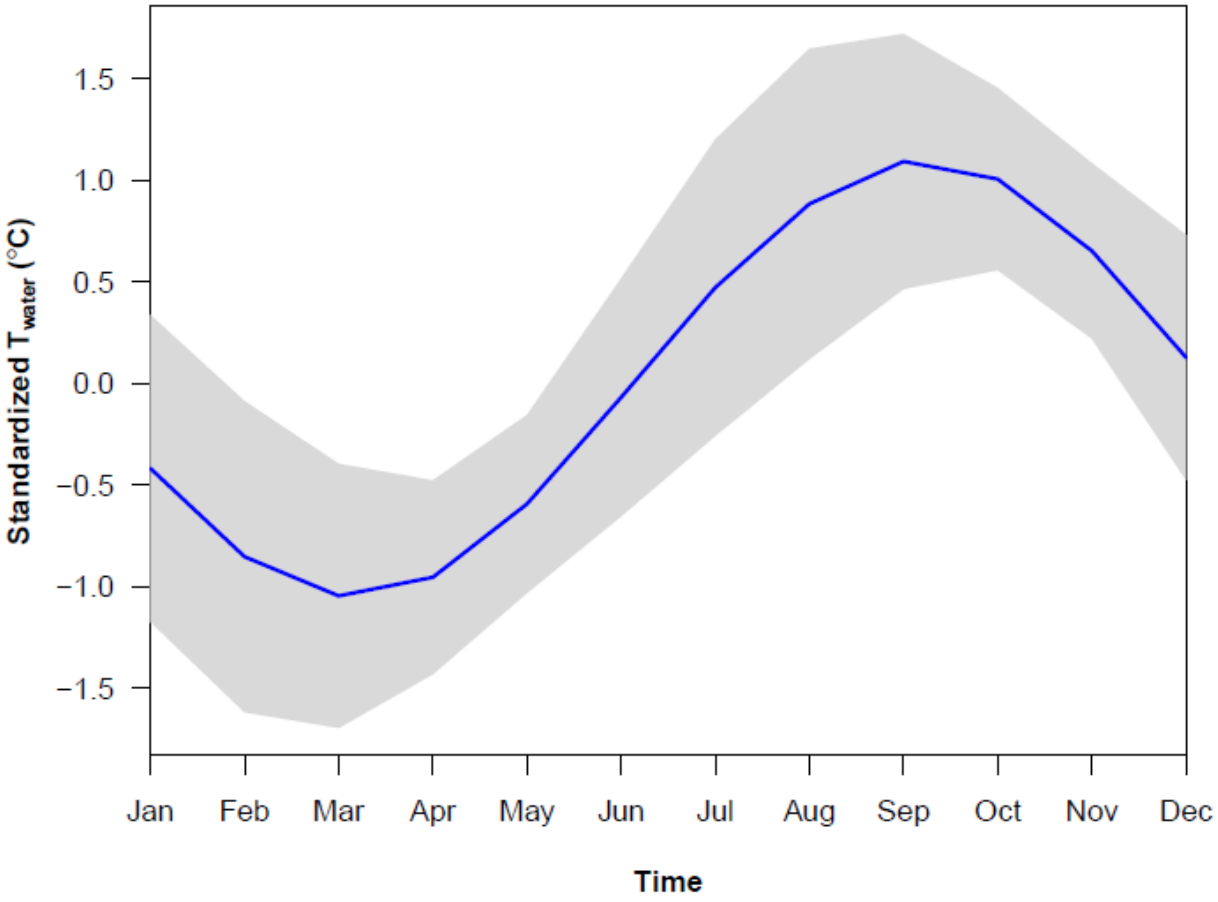

Figure E3 Mean (blue) and standard deviation (gray) of the seasonal component of shared trend 2, averaged across the 38 years between 1978 and 2015.